BEAM ENGINEERING, INC.
ELECTRICAL AND MECHANICAL ENGINEERS
732 NORTH PASTORIA AVENUE P O BOX 60745 SUNNYVALE CALIFORNIA 94086
(408) 738-4573

NASA CR-152082

ACOUSTICAL EFFECTS OF BLADE TIP SHAPE CHANGES ON A FULL SCALE HELICOPTER ROTOR IN A WIND TUNNEL

by

Albert Lee
Senior Research Engineer
Beam Engineering, Inc.
Sunnyvale, California 94086

April 1978

Prepared under NASA Contract NAS2-9399
NASA-Ames Research Center
Moffett Field, California 94035

BEAM ENGINEERING, INC.
ELECTRICAL AND MECHANICAL ENGINEERS
732 NORTH PASTORIA AVENUE P O BOX 60745 SUNNYVALE CALIFORNIA 94086
(408) 738-4573

NASA CR-152082

ACOUSTICAL EFFECTS OF BLADE TIP SHAPE CHANGES ON A FULL SCALE HELICOPTER ROTOR IN A WIND TUNNEL

by

Albert Lee
Senior Research Engineer
Beam Engineering, Inc.
Sunnyvale, California 94086

April 1978

Prepared under NASA Contract NAS2-9399
NASA-Ames Research Center
Moffett Field, California 94035

TABLE OF CONTENTS

Abstract

A full-scale wind tunnel study of the effects of tip shapes on noise radiation was performed in the NASA-Ames Research Center 40- by 80-Foot Wind Tunnel. Four tip shapes were tested. They are rectangular, swept, tapered, and swept-tapered. The measured data covered a wide range of operating conditions. The range of advancing tip Mach numbers were between 0.72 to 0.96, and the advance ratios were from 0.2 to 0.375. At low and moderate advancing tip Mach number, the data in the dbA scale appear to indicate the swept tip is the quietest, swept tapered the second, tapered third and rectangular the most noisy. Above an advancing tip Mach number of about 0.89, a distinct acoustical pulse can be observed, which dominates the acoustical waveform. The pulse shape is symmetric at moderate tip Mach number, changing to a sawtooth shape at high advancing tip Mach numbers. Based on the amplitude of the impulsive noise, it appears the swept-tapered tip is the quietest, tapered tip the second, swept tip third and square tip the most noisy. The data presented in this report should be useful as data bases for the modeling and evaluating helicopter impulsive noise.

Acknowledgements

The author wishes to express his appreciation to Mr. David H. Hickey Mr. John P. Rabbott, Jr., Mr. James C. Biggers, Mr. Robert H. Stroub, and Miss Marianne Mosher for their valuable suggestions and help during the course of this effort.

The work reported here was sponsored by NASA, Ames Research Center under Contract NAS 2-9399. The technical monitor is Mr. John P. Rabbott, Large-Scale Aerodynamics Branch, NASA, Ames Research Center.

1. Introduction

The designs of modern helicopters are challenged by the government noise regulations and community acceptance in addition to the comfort requirements of passengers in civil applications. For military service, reduced noise is desirable to reduce the detectability of vehicles and the fatique of soldiers. External noise of a helicopter is mainly dominated by the aerodynamic noise produced by the main rotor and tail rotor. The mechanisms of noise generation of main rotor and tail rotor are similar.

According to Cox[1] the aerodynamic noise from rotors can be classified into rotational noise and broadband noise. The aerodynamic sources of rotational noise are mean lift and drag forces, harmonic force fluctuations, and blade thickness. The broadband noise is mainly due to random force fluctuations, and wake self-noise. A prominent and impulsive sound occurs when a helicopter operates in certain conditions. When it occurs this sound dominates all other noise sources.

The blade tip is one of the most important noise source regions. The effects of tip shapes on the noise generation are rather complicated because of the complexity of tip aerodynamics. For different tip shapes, the aerodynamic loading distributions are different and the resulting tip vortices are different. Due to the combined effects of tip vortex changes and different aerodynamic response at tip region, the blade vortex interaction noise will be changed. Because of the change in unsteady blade loading, the rotational noise radiation will also be changed. The low frequency broadband noise is believed mainly due to blade/turbulence interaction[2-4]. It, too, will be different for different tip shapes due to the change of rotor wake turbulence and blade aerodynamic response. The high frequency broadband noise which may be due to vortex shedding[5,6] will be altered when the tip shapes are altered. At high speed, blade thickness[7-9] may be significant noise source. The thickness noise is directly related to the tip shapes and their thickness distributions. Different tips may have different compressibility characteristics. The sound radiation due to drag divergence is dependent on the tip compressibility.

Because of the complexity of the tip shape effects on noise generation, no complete analytical method has been developed. There have been many efforts to find a low noise tip shape configurations while trying to keep or improve the helicoter performance. Lyon, Mark and Pyle[10] theoretically studied the rotor tip sound radiation and tried to synthesize rotor tips for less noise. Lowson, Whatmore and Whitfield[11] found that cutting off the corner of fan blade tips of rectangular planform can reduce the high frequency broadband noise. They suggested that this planform change may alter the tip vortex self-interaction and therefore the noise radiation. Farassat[12, 13] studied the effects of thickness distribution in tip region on noise radiation. Some tip shapes

have been experimental tried in wind tunnel and in flight. A full-scale ogee tip helicopter rotor was tested[14]. This tip was found to have a favorable effect on the rotor acoustics.

It is believed that by suitable design of tip shapes, the noise could be reduced while improving the performance. To reach this end, a comprehensive test was undertaken on a rotor having interchangeable tips not only to determine the acoustic effects of the specific tip shapes, but also to establish a data base for the theoretical modeling and predictions.

A 44-foot diameter, four bladed rotor with interchangeable tips was used. The four tip shapes which are shown in Figure 1 were tested. They were rectangular, swept, tapered (trapezoidal) and swept-tapered. The rectangular tip serves as a baseline, and the other three tips were used to systematically evaluate the effects of taper and/or sweep.

The investigation covered a wide range of operating conditions. The range of advancing tip Mach numbers was 0.72 to 0.96, and the advance ratios were from 0.2 to 0.375. For detail rotor configurations, test procedures and rotor performance, see Reference 15.

2. Data Acquisition and Reduction

Seven ½-inch B&K condenser microphone with cathode followers were used for the acoustical measurements. Each microphone was equipped with a nose cone to reduce the wind-induced noise. The microphone locations are given in Table I and shown in Figure 2. A coordinate system is also shown. The origin is at the rotor center, with the x-axis downstream, the y-axis along the advancing side of the disc, and the z-axis up. The microphones were calibrated daily with a B&K pistonphone.

The instrumenation set-up is schematically shown in Figure 3. Standard acoustic power supply and amplifier units were used for data conditioning. An Ampex 1300 A, 14-track FM tape recorder was used for data recording. The recorder setting was IRIG wide-band 1 and 7½ ips, with a FM center frequency of 27 K Hz, and a bandwidth of 5 K Hz. The playback was performed at the same time of recording. By comparing the input and output signal, one can be sure that valid data were recorded on the tape. Tracks 6 to 12 were used to record the acoustic data of Mic 1 to 7. Track 13 and 14 recorded 256/rev and 1/rev signals, respectively. The data were also recorded on an oscillograph for visual inspection.

A home-made acoustical polarity calibration device, named polaritometer, was used to calibrate the polarity of the acoustical data system. The polaritometer generated a strong positive pressure pulse as one pushed its plunge. This pressure pulse was recorded on all channels of the recorder ahead of the acoustical data. A typical trace is shown in Figure 4. The first downward pulse is compression and represents the positive pressure. the sign of helicopter impulsive noise was cailbrated against this polaritometer trace.

The A-weighted SPL were reduced by using a B&K audio frequency analyzer type 2107. The acoustical waveforms were reduced by applying a periodic averaging scheme with the Dynamic Analysis System (DAS). The DAS is a DEC PDP 11/45 mini-computer based data system with two RK-05 disc drives. For detail descriptions of the DAS, see Reference 16. The acoustical data were digitized at a sample rate of 5120 per sec. Triggering with the 1/rev pulses which were generated once per rotor revolution when the red blade was at downstream direction, records of 0.2 sec (1024 samples) were taken. The anti-aliasing filters (low-pass) were set at 2 K Hz. After averaging 50 records in a synchronized fashion, the nonperiodic noise was significantly reduced. A discrete fourier transform was then applied to obtain the amplitude and phase relationship of each frequency component. After zeroing out the frequency components below 25 Hz and applying inverse fourier transform, the averaged, 25 Hz high-passed, phase distortion-free acoustical waveforms were obtained. Thse waveforms are very useful in the study of helicopter impulsive noise. A Kronhite analog filter was tried for the high-pass filtering, but serious distortion of the waveform was found. The method of analog filtering was therefore not used in data reduction.

3. Results and Discussions

The data are presented both in dbA and time-domain waveforms. The tip shape effects on the noise radiation at various operation conditions were examined. Since the noise mechanisms are different in the various tip Mach number regions, the data were organized into three-parts; low speed ($V/\Omega R = .2$, $M_{1,0} = .6$) medium speed ($V/\Omega R = .4$, $M_{1,0} = .6$) and high speed ($V/\Omega R = .375$, $M_{1,0} = .65$).

The background noise in the test section of the 40- by 80-Foot Wind Tunnel is shown in Figure 5. These background noise data are measured at two locations during the present test with rotor hub turning (no blade) and those measured in 1974 with different struts installed. It can be seen that all data collapse into a straight line on a log-log scale. The A-weight SPL is proportional to the 5.6th power of wind tunnel velocity. The dbA data in subsequent figures are corrected for the background noise.

The background noise is assumed to be unrelated to the rotor noise. The following relationship is resulted:

$$P_T = P_R + P_B$$

$$P_T\, A(f) = P_R\, A(f) + P_B\, A(f)$$

$$P_R\, A(f) = P_T\, A(f) - P_B\, A(f)$$

where P_T is the mean square sound pressure measured during the test. P_R and P_B are the mean square sound pressure due to rotor and background noise, respectively. A(f) is the weighting function of dbA.

In terms of dbA, we have:

$$dbA_R = 10 \log \frac{P_T \quad A(f)}{P_{ref}} \quad (1 - \frac{P_B}{P_T})$$

$$dbA_R = dbA_T + 10 \log \left(1 - 10^{\frac{dbA_B - dbA_T}{10}}\right)$$

The above relationship was used for background noise corrections. If the rotor noise is not well above the background noise, the scattering of measured data will be amplified after correction. Table 2 shows the corrections for different signal to noise ratios. If the data are 10 dbA or more above the background noise, no correction is necessary, a scatter of 1 dbA will result in 1.1 db scatter in the corrected data. However, if the measured data is 1 dbA above the background noise, the signal to noise ratio is rather poor. A scatter of 1 dbA will result in about 3.5 dbA scattering after correction. The low speed data presented in this report are those at least 3 dbA scattering results in 1.8 dbA scattering in the final data. The data of medium high speed are those at least 2 dbA above background noise.

The wind tunnel acoustical data were also contaminated by reflections from the hard walls of the wind tunnel. Without a suitable correction, the dbA data should not be considered to be accurate. Nevertheless, these data are useful for the comparison of different tip shapes on the relative bases.

The acoustical waveforms are believed to be more suitable for the study of helicopter impulsive noise. The problems of reflections from tunnel hard surfaces are more easily handled in the time-domain waveform. Since the reflection travels a longer path than the incident wave. The time lag of a reflection behind the incident is directly related to the path difference. If the time lag is equal to or larger than the pulse width of the helicopter implusive noise, the amplitude and waveform of the incident acoustical pulse will not be distorted. In this case, no correction is required. Fortunately, this was true for all of the measurements used herein.

3.1 Low Speed

Figure 6 shows the noise level measured at Mic 3 as a function of $C_{LR/\sigma}$. The rotor was operating at $V/\Omega R = .2$, $M_{1_0} = .6$ (80 knots, 291 RPM), and $\alpha_{TPP} = o$ deg. The dbA level of the swept tip blades is lowest, although the difference is small, typically 1 dbA or less. Figures 7 and 8 show the noise level at $\alpha_{TPP} = 2.5$ deg and -5 deg, respectively. Similar trends are observed. The noise trend is relatively insensitive to $C_{LR/\sigma}$. However, the noise level increases quite rapidly at high $C_{LR/\sigma}$. At low $C_{LR/\sigma}$, the rotor wake is relatively close to the rotor disc. The noise due to the interaction of blade and rotor wake may dominate the noise level. This noise radiation is insensitive to $C_{LR/\sigma}$. At high values of $C_{LR/\sigma}$, blade stall and compressibility effects may become significant and result in the sharp increase of noise level. As shown in Figures 6 and 7 the noise of the swept-tapered tip blades does not increase as fast as other three blades at high $C_{LR/\sigma}$. This is possibly due to the better stall and compressibility characteristics of that blade tip shape. However, no such trend was observable at $\alpha_{TPP} = -5^{o}$, where the noise level was reduced for all of the tip shapes.

Figures 9, 10 and 11 show noise level measured at Mic 6. There is no definite difference among the four tip shapes at $\alpha_{TPP} = o$ deg and -2.5 deg. However, at $\alpha_{TPP} = -5$deg, the swept-tapered tip is about one to two dbA quieter than the swept or rectangular blades.

Forward speed has significant effects on the noise radiation. Figure 12 shows the noise level of swept-tapered tip at different forward speeds, measured at Mic 3. The rotor operated at $M_{1_0} = 0.6$ and $\alpha_{TPP} = -5$ deg. The advance ratio μ ranges from 0.15 to 0.4. Figure 13 shows the data measured at Mic 6. Similar trends were observed at both microphones. The noise level is sensitive to lift at low forward speed and relative independent of lift at high forward speed.

Figures 14 and 15 show the noise level of four tip shapes as a function of advance ratio. The trends of the four tips are similar. The swept tip appears to have the lowest noise level over the advance ratio range and swept-tapered tip second.

Figures 16 and 17 show the effects of tip path plane pitch angle on the noise level measured at Mic 3 and 6, respectively. The data were obtained at $V/\Omega R = 0.2$, $M_{1_0} = 0.6$ and $C_{LR/\sigma} = .09$. As the rotor disc was tilted forward, the separation of blade and rotor wake increased, in addition to the change in relative angle between the rotor disc and the microphone. Since the noise is not very directional at these operation conditions, directivity is not believed to be the cause of the changes in noise shown in Figure 16 and

17. As the rotor disc tilted forward, there is less interaction between the blades and the rotor wake, therefore a reduction in noise level is expected. These four tip shapes show similar trends with tip path plane tilt.

3.2 Medium Speed

The noise data presented in this section were measured at nominal 120 knots tunnel speed and 291 RPM rotor speed. These conditions correspond to $M_{1_{0}}$ = .6 and $V/\Omega R$ = .4. In this speed region, the rotor noise has a mixture of the characteristics of both low speed and high speed.

Figure 18 shows the dbA level of the four tip shapes as a function of lift (α_{TPP} = o). These curves show the typical low speed rotor noise characteristics as shown in the previous sections. The swept tip has the lowest dbA level among four tips. Figures 19 and 20 show the results at α_{TPP} = -5 deg and -10 deg. The trend shown in Figure 20 is similar to that of high the speed cases which will be described in the next section. As the tip path plane is tilted forward the relative angle between rotor disc and mic 3 decreases. In other words. the mic 3 is closer to the rotor disc plane. At high speed the impulsive noise is dominate near the rotor disc plane. This implusive noise is insensitive to lift. Figures 21, 22 and 23 are the data measured at Mic 6. They show similar trends as those measured at Mic. 3.

3.3 High Speed

Figures 24, 25 and 26 show the dbA level at Mic 3, when α_{TPP} = o deg, -5 deg and -10 deg respectively. The rotational tip Mach number was $M_{1.0}$ = 0.65, at advance ratio V/ΩR = .375. The advancing tip Mach number is 0.894. The compressibility and thickness effects are probably the dominant factors in the noise radiation. In contrast to the low speed case, the dbA level is basically independent of lift. Figures 27, 28 and 29 show the noise levels measured at Mic 6. Similar trends to those noted above are observed. The dbA level of the swept tip blade is lowest among four tip shapes. In the case of low tip path plane pitch (α_{TPP} = o deg and -5 deg), the swept-tapered tip radiates about 0.5 to 1 dbA less than rectangular tip and trapezoidal tip.

3.4 Mach Number Effects

(i) dbA Level

The tip Mach number is one of the most important parameters on determining the noise radiation. Figures 30 and 31 shown the dbA level as a function of advancing tip Mach number, as measured at MIC 3 and MIC 6, respectively. The data shown in these two figures were measured at $\alpha_{TPP} = -5^{o}$, a nominal lift of $C_{LR/\sigma} = .07$ and the other nominal conditions:

At lower advancing tip Mach number the swept tip seems to indicate the lowest dbA level. The other three tips show little difference among them. At advancing tip Mach number above 0.9, the dbA level of swept-tapered tips appears to be the lowest.

(ii) Waveform

The noise waveforms may be more useful in the study of the high speed impulsive noise than the integrated dbA readings. Figures 32 through 39 show the Mic 3 acoustical waveforms measured at $V/\Omega R = 0.375$, $\alpha_{TPP} = -5^{o}$, and $C_{LR/\sigma} = 0.07$ (nominal). The detailed rotor operational conditions are listed in Table 4. At moderate and high advancing tip Mach number a distinctive negative pulse can be observed in the waveform, occuring once every blade passage. This waveform is relatively symmetric. As the advancing tip Mach number increases, the waveform becomes unsymmetric. Sawtooth pulse shapes were observed at high Mach number. Similar waveforms were observed in the in-flight[17].

Figure 32(a) is the raw data from the trapezoidal tip blade neither averaged nor filtered. Figure 32(b) is the unaveraged data after removing all energy below 25 Hz. The main effect of 25 Hz high pass filtering is to eliminate the first blade passage harmonic which is below 25 Hz. As can be seen, the negative pulse shape and amplitude does not have any observable changes. This is because the harmonic content below 25 Hz in this negative pulse is not significant. Figure 32(c) shows the effects of averaging. After averaging 50 time the noise unrelated to the blade passage frequency is essentially averaged out. The tunnel background noise and rotor broadband noise are not harmonics of the rotor rotational frequency, and are therefore reduced or eliminated. However, the reflected noise from the tunnel surfaces cannot be averaged out, because they are also periodic. The nearest surface is the floor. The difference of sound traveling time between incidence and reflection is about 4 msec. The reflections from other surfaces will occur even later. The negative pulse width is about 4 msec. Therefore, the reflections should not mask the main negative pulse.

Helicopter impulsive noise is rather directional, and the sound to be reflected travels along different paths from that of incident sound. In the case of thickness noise, the reflection started with a weaker amplitude in the first place because of its directivity, and is further reduced due to reflection. These combined facts should help our ability in the analysis of helicpter impulsive noise measured in a large hard-wall wind tunnel. As a matter of fact, very little reflection off the tunnel floor can be observed on the acoustical waveform traces. Figure 33(d) shows the combined results of 50 revolution averaging and 25 Hz high pass filtering. The amplitude of the negative pulse can be readily distinguished. Figure 33 and 34 are the data from the trapezoidal tip blades at $M_{1,90}$ = .939 and .966, respectively. Figure 35, 36 and 37 show the acoustical waveform from the swept-tapered tip blades, and Figure 38 and 39 show the data of swept tip and rectangular tip blades, respectively.

The acoustic waveforms shown in these figures for different tip shapes can be used as data bases in the evaluation of various theoretical prediction schemes for the strong impulsive noise at high speed.

Figure 40 shows the amplitude of the negative acoustical pulses of four tips at different advancing tip Mach numbers. The swept-tapered tip blade produces the lowest impulsive noise. At $M_{1,90}$ = .9 (nominal) the impulsive noise of swept-tapered tip blade is the lowest among the four tips. However, the dbA results of figures 30 and 31 shows the noise level of swept tip blades is the lowest among four tip shapes. It is felt dbA probably is not always adequate for judging the impulsive noise of helicopter rotors.

Conclusions

The acoustic data of a 44-foot rotor with four blade tip shapes were measured in the NASA, Ames Research Center 40- by 80-Foot Wind Tunnel. Due to background noise and reverberation no absolute dbA level could be obtained without extensive corrections. However, the relative changes of dbA levels due to the differences in tip shapes are generally usefule in assessing the tested four blades, but may not always be adequate when strong impulsive noise occurs.

Below the advancing tip Mach number of about 0.89, the dbA data appear to indicate that the swept tip is the quietest, swept-tapered tip second, trapezoidal tip third, and rectangular tip the most noisy.

At high tip Mach number a distinct negative acoustical pulse which occurs once per blade passage was observed in the time waveforms. The amplitudes of these pulses are strongly dependent on the advancing tip Mach number.

The pulse shape is symmetric at moderate tip Mach number, but changes to sawtooth shapes at very high Mach number. Above the advancing tip Mach number of about 0.89 and based on the amplitudes of impulsive noises the data indicate swept-tapered tip is the quietest, trapezoidal tip second, swept tip third, and rectangular tip loudest.

Table 1 - Microphone Locations

MIC #	X (ft)	X (m)	Y (ft)	Y (m)	Z (ft)	Z (m)	Above floor (ft)	Above floor (m)	Angle below horizontal plane (deg)
1	-65	-19.8	2	0.61	-17.4	5.30	4	1.22	15
2	-8.7	-2.65	6.2	1.89	-10.1	3.08	9.9	3.02	43.6
3	-63	-19.2	0	0	-13.8	4.21	7.5	2.29	12.4
4	-61	-18.6	-2	0.61	-8.6	2.62	12.8	3.90	8
5	-62.3	-19.0	18.2	5.55	-13.7	4.18	7.7	2.35	11.9
6	-11.4	-3.47	11.8	3.60	-12.8	3.90	7.2	2.19	38
7	-62.3	-19.0	-18.2	5.55	-13.7	4.18	7.7	2.35	11.9

Table 2 - Background Noise Correction

Measured data (dbA)	Background Noise (dbA)	Difference (dbA)	Corrected rotor noise (dbA)
110	100	10	109.5
109	100	9	108.4
108	100	8	107.3
107	100	7	106.0
106	100	6	104.7
105	100	5	103.3
104	100	4	101.8
103	100	3	100.0
102	100	2	97.7
101	100	1	94.1

Table 3 - Rotor Nominal Conditions in Figures 30 and 31

$V/\Omega R$	$M_{1,0}$	$M_{1,90}$
.2	.55	.66
.15	.6	.69
.2	.6	.72
.25	.6	.75
.3	.6	.78
.375	.6	.825
.4	.6	.84
.375	.65	.89
.375	.68	.935
.375	.7	.963

Table 4 - Rotor Conditions in Figures 30 through 40

Tip	Run. Point	$V_{1,\ 90}$ (m/sec)	V_∞ (m/sec)	ρ_o (kg/m^3)	C_s (m/sec)	$C_{LR/\sigma}$
Trapezoidal	38.6	223.1	83.69	1.153	342.2	.0687
Trapezoidal	58.5	234.1	87.45	1.148	342.6	.0696
Trapezoidal	58.20	242.0	90.79	1.130	344.7	.0658
Swept-tapered	21.26	225.6	84.62	1.120	345.9	.0766
Swept-tapered	55.31	233.5	87.96	1.139	342.8	.0731
Swept-tapered	56.4	239.6	90.33	1.147	341.3	.0707
Swept	49.45	225.2	84.57	1.130	345.5	.0704
Rectangular	46.5	223.1	83.69	1.151	341.7	.0703

References

1. Cox, C. R.: "Aerodynamic Sources of Rotor Noise". Journal of the American Helicopter Society, January 1973.

2. Homicz, G. F. and George, A. R.: "Broadband and Discrete Frequency Radiation from Subsonic Rotors". J. Sound Vibration. 36(2), 1974.

3. Amiet, R. K.: "Noise Produced by Turbulent Flow into a Propeller or Helicopter Rotor". AIAA Paper 76-560, AIAA 3rd Aeroacoustics Conference., 1976.

4. George, A. R. and Kim, Y. N.: "High Frequency Broadband Rotor Noise". AIAA Paper 76-561, AIAA 3rd Aeroacoustics Conference, 1976.

5. Soderman, P. T.: "Leading Edge Serration Which Reduces the Noise of Low-Speed Rotors". NASA TND-7371, 1973.

6. Lee, A., Aravamudan, K., Bauer, P. and Harris, W. R.: "An Experimental Investigation of Helicopter Rotor High Frequency Broadband Noise. AIAA Paper 77-1339, AIAA 4th Aeroacoustics Conference, 1977.

7. Deming, A. F.: "Noise from Propellers with Symmetrical Sections at Zero Blade Angle". NACA TN 605, 1973.

8. Lyon, R. H.: "Radiation of Sound by Airfoils that Accerlerate Near the Speed of Sound"., J. Acoustics Society American 49, 894-905, 1971.

9. Lowson, M. V., Hawkings, D. L.: "Noise of High Speed Rotors, AIAA Paper 75-450, AIAA 2nd Aeroacoustics Conference, 1975.

10. Lyon, R. H., Mark, W. D. and Pyle, R. W., Jr.: "Synthesis of Helicopter Rotor Tips for Less Noise, Helicopter Noise Symposium, ARO-Durham, September 1971.

11. Lowson, M. V., Whatmore, A., and Whitfield, C. E.: "Source Mechanisms for Rotor Noise Radiation". TT7202, Department of Transportation Technology, Loughborough University of Technology, March 1972.

12. Farassat, F.: "Theory of Noise Generation from Moving Bodies with an Application to Helicopter Rotors". NASA TR R-451, 1973.

13. Farassat, F. and Brown, T. J.: "A New Capability for Predicting Helicopter Rotor and Propeller Noise Including the Effect of Forward Motion". NASA TMX-74037, 1977.

14. Mantay, W. R., Shidler, P. A., and Campbell, R. L.: Some Results of the Testing of a Full-Scale Ogee Tip Helicopter Rotor; Acoustics, Loads, and Performance". AIAA Paper 77-1340, AIAA 4th Aeroacoustics Conference, 1977.

15. Stroub, R. H.: "Full Scale Investigation of Four Rotor Tip Shapes". NASA TM , 1978.

16. Cambra, J. M. and Tolari, G. P.: "Real-Time Computer Data System for the 40- by 80-Foot Wind Tunnel Facility at Ames Research Center". NASA TND-7970, 1975.

17. Schmitz, F. A. and Boxwell, D. A.: "In-Flight Far-Field Measurement of Helicopter Noise". Journal of the American Helicopter Society, October 1976.

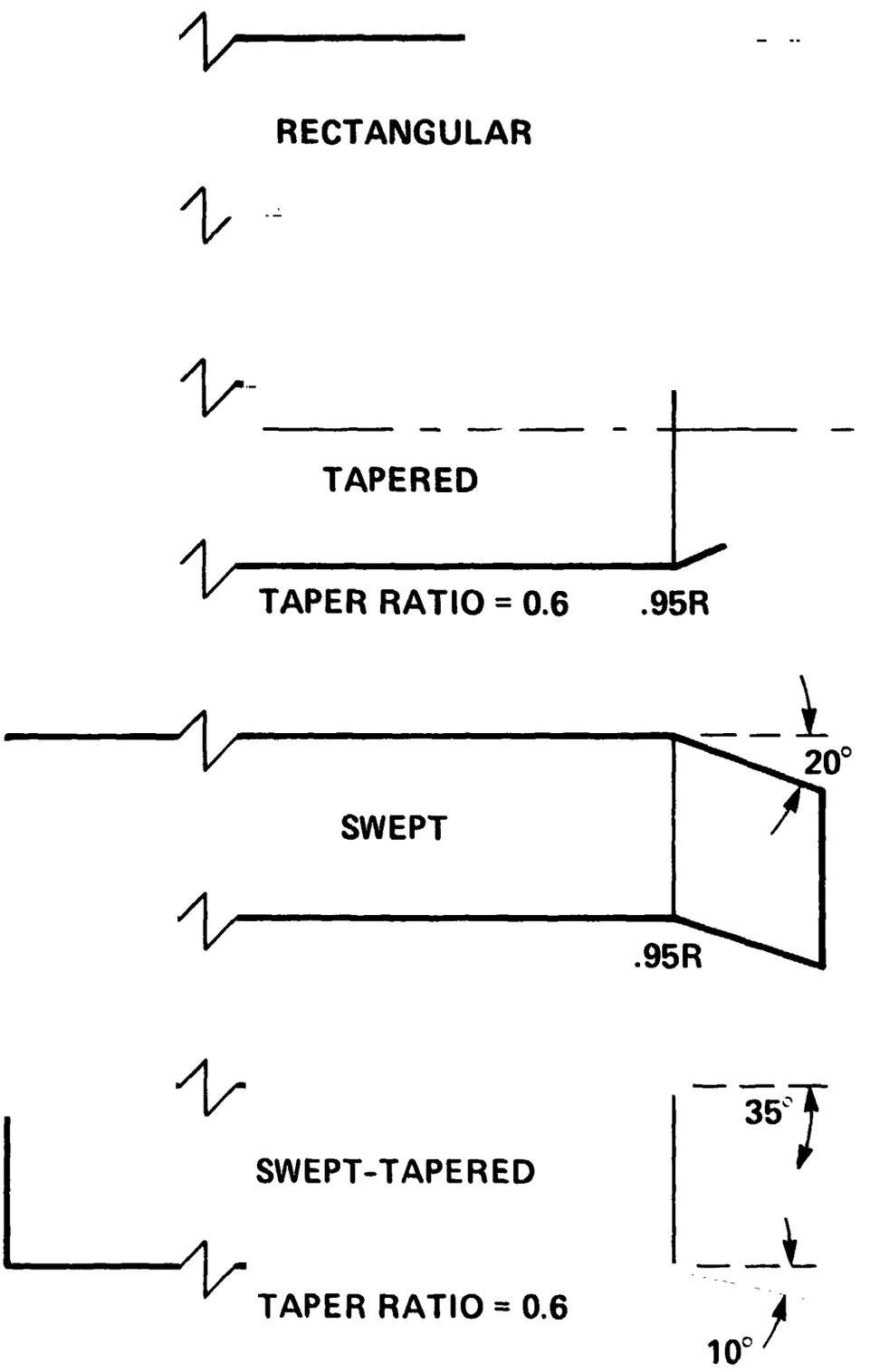

Figure 1 - Four tip shapes tested

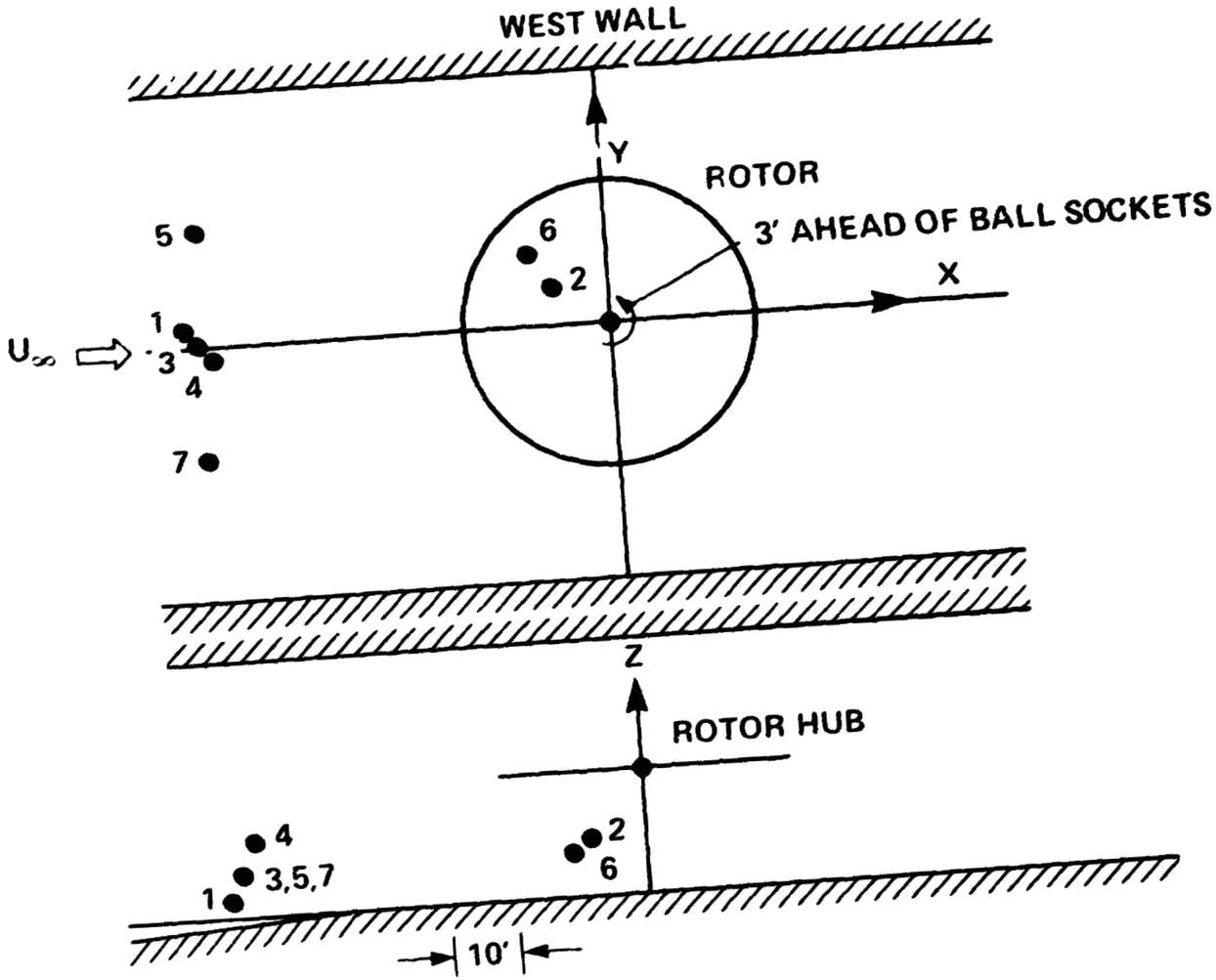

Figure 2 - Microphone locations

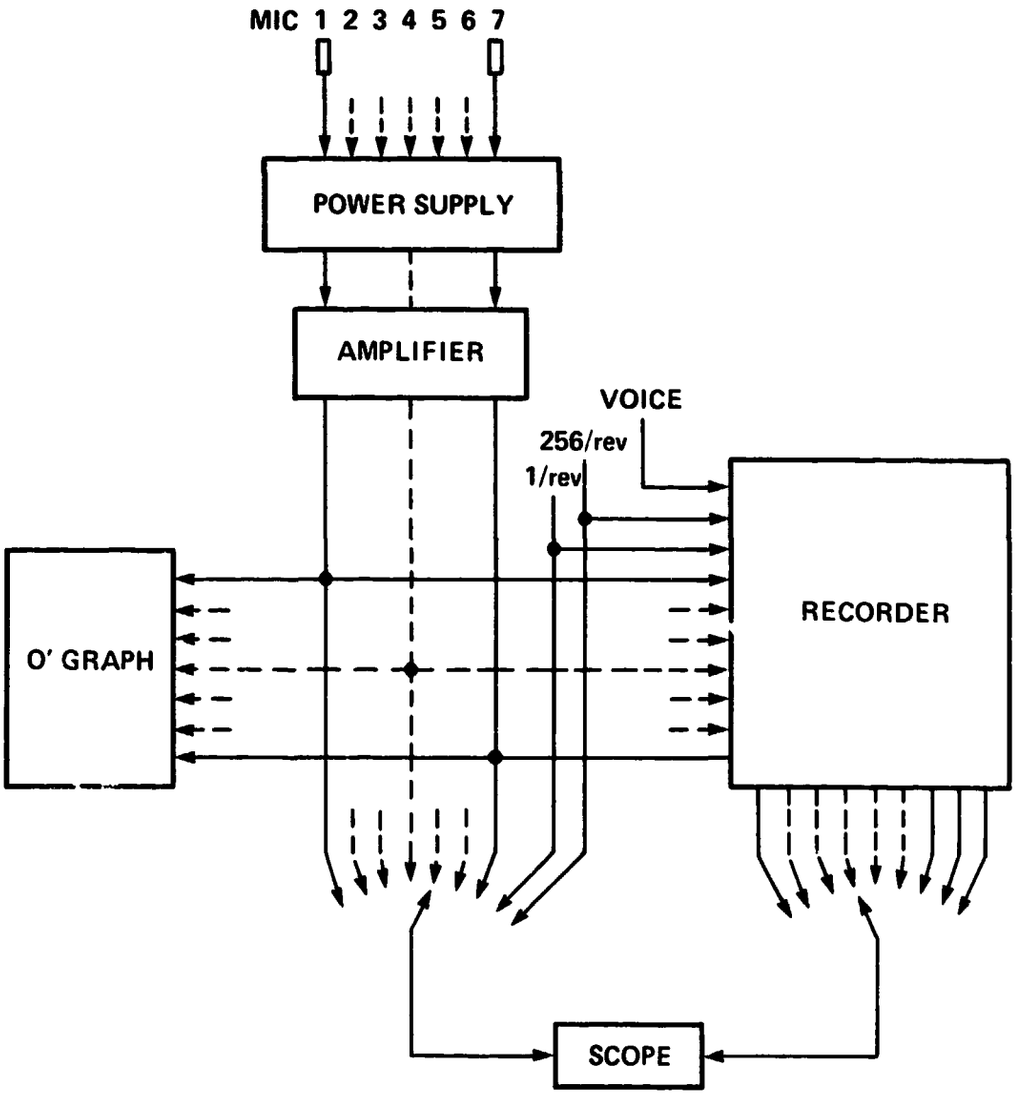

Figure 3 - Acoustic instrumentation set-up

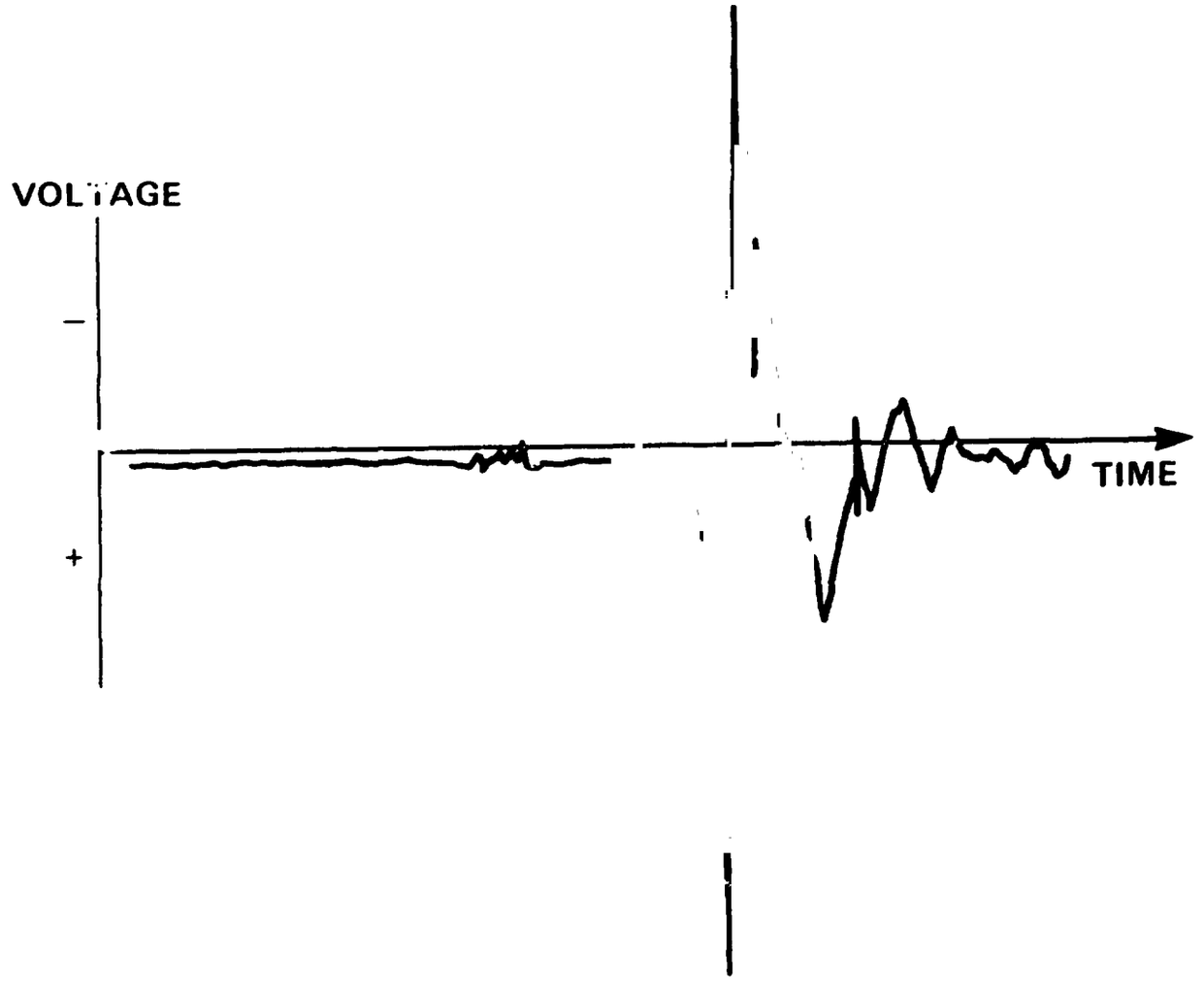

Figure 4 - Typical trace of polaritometer

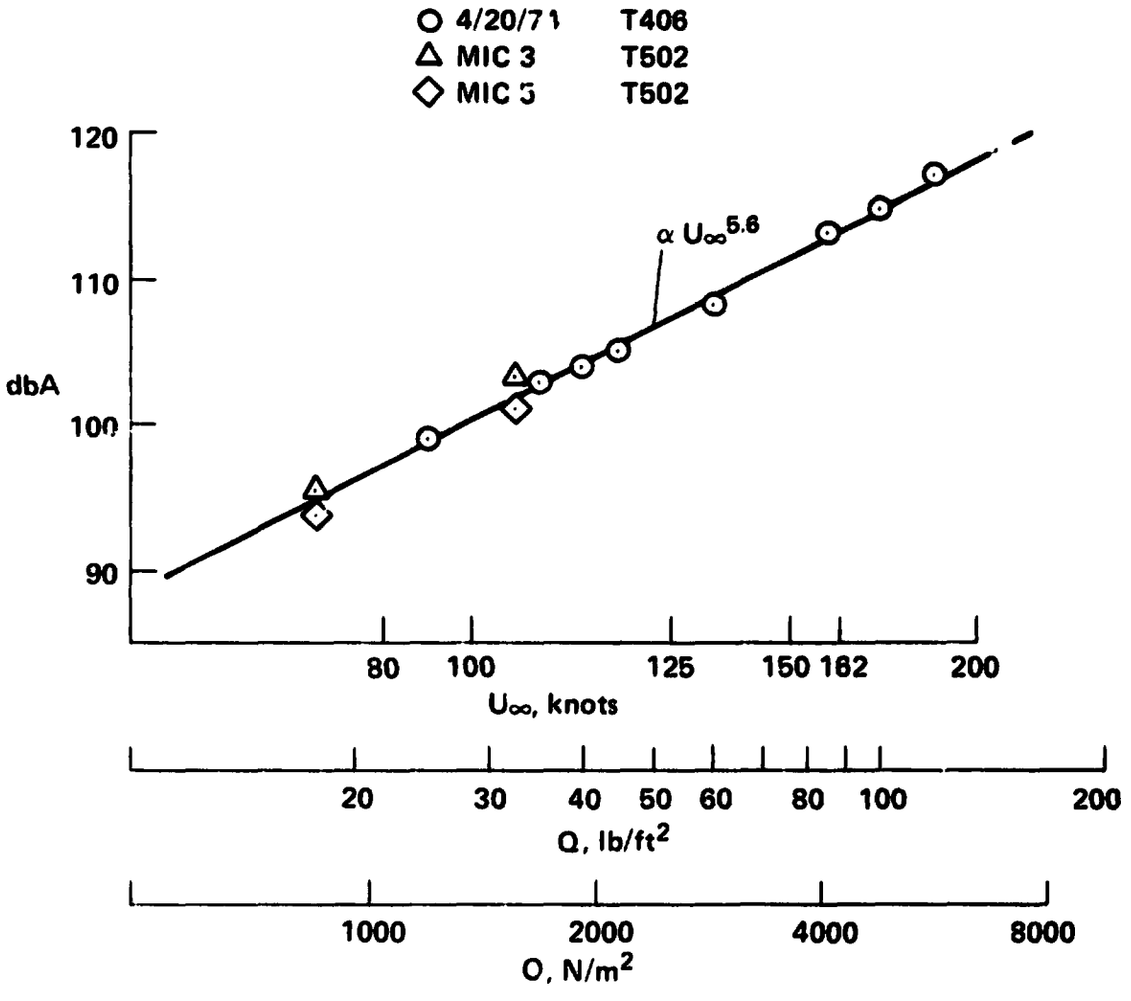

Figure 5 - Wind tunnel background noise

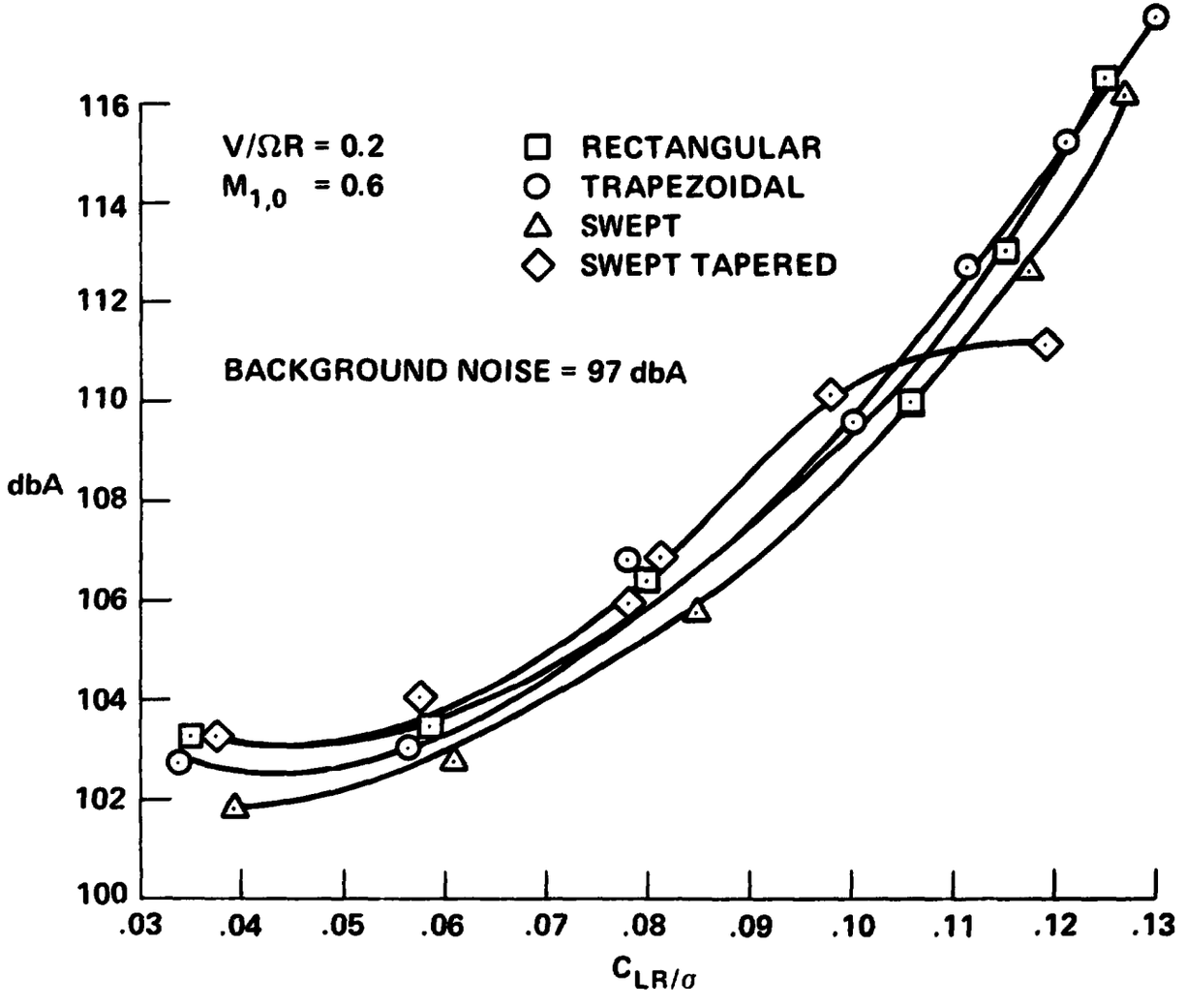

Figure 6 - dbA noise levels as a function of $C_{LR/\sigma}$, Mic 3, α_s = o deg

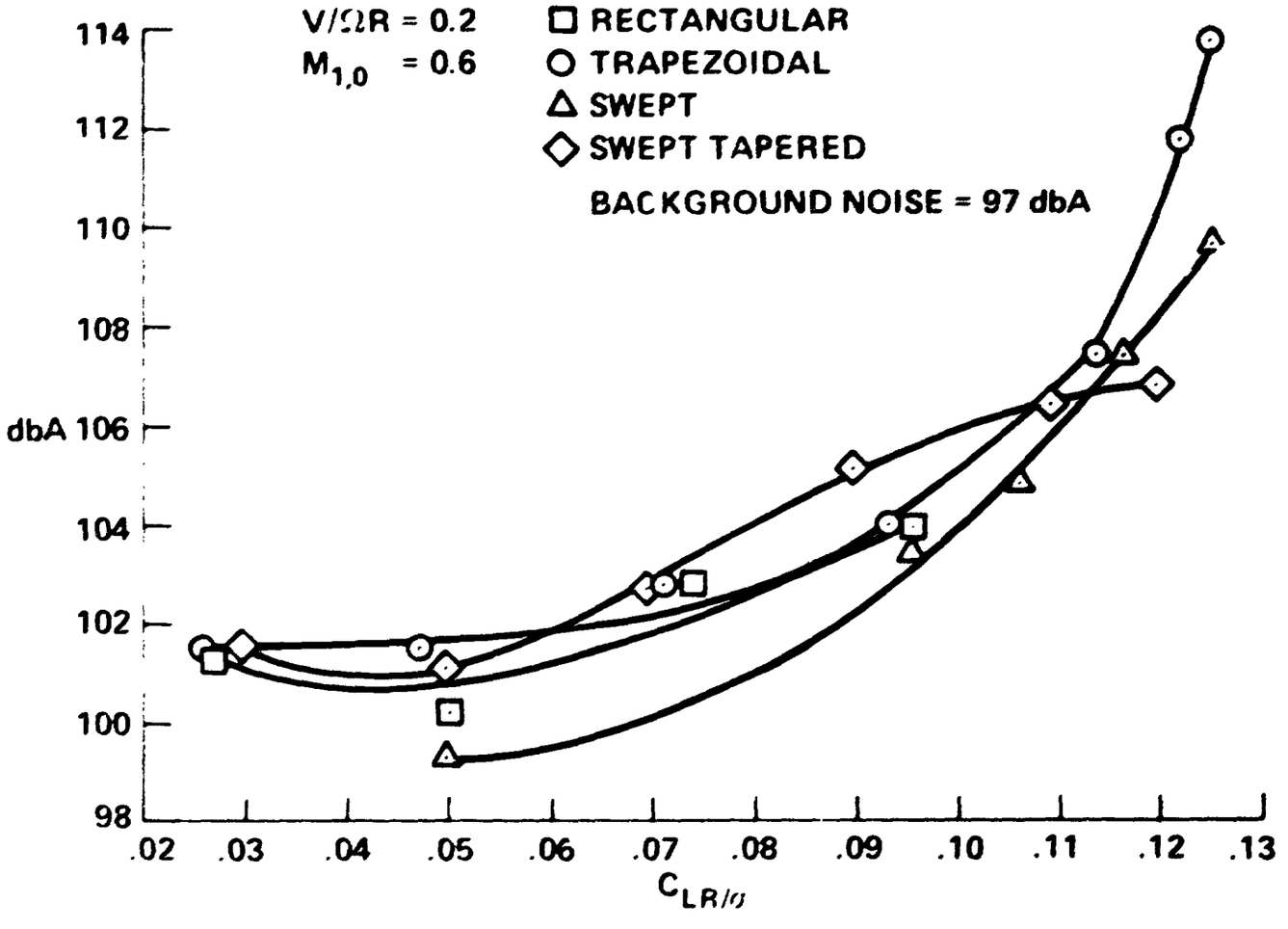

Figure 7 - dbA noise levels as a function of $C_{LR/\sigma}$
$M_{1,0}$ = 0.6, α_s = -2.5 deg

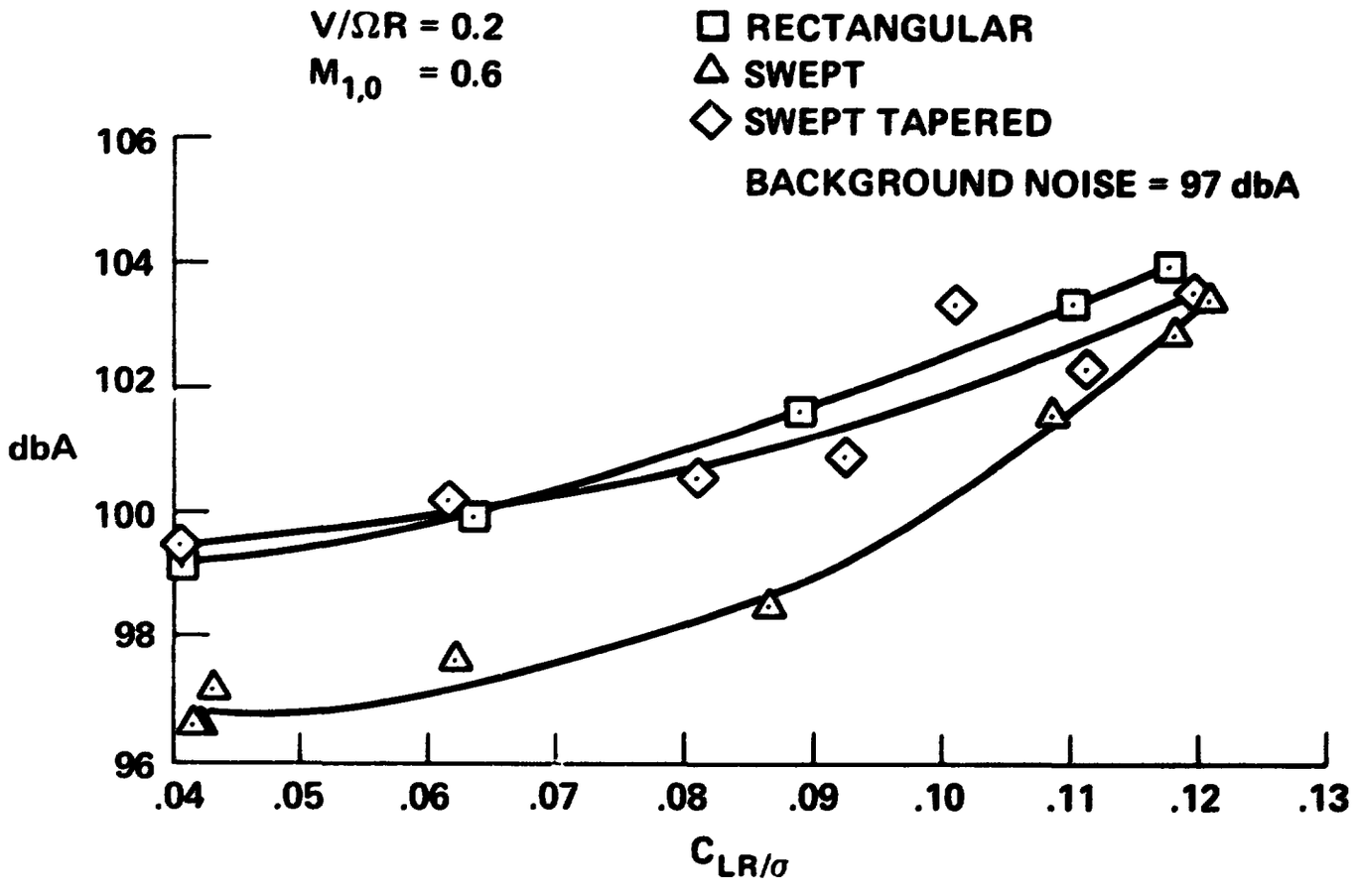

Figure 8 - dbA noise levels as a function of $C_{LR/\sigma}$, Mic 3, α_s = -5 deg

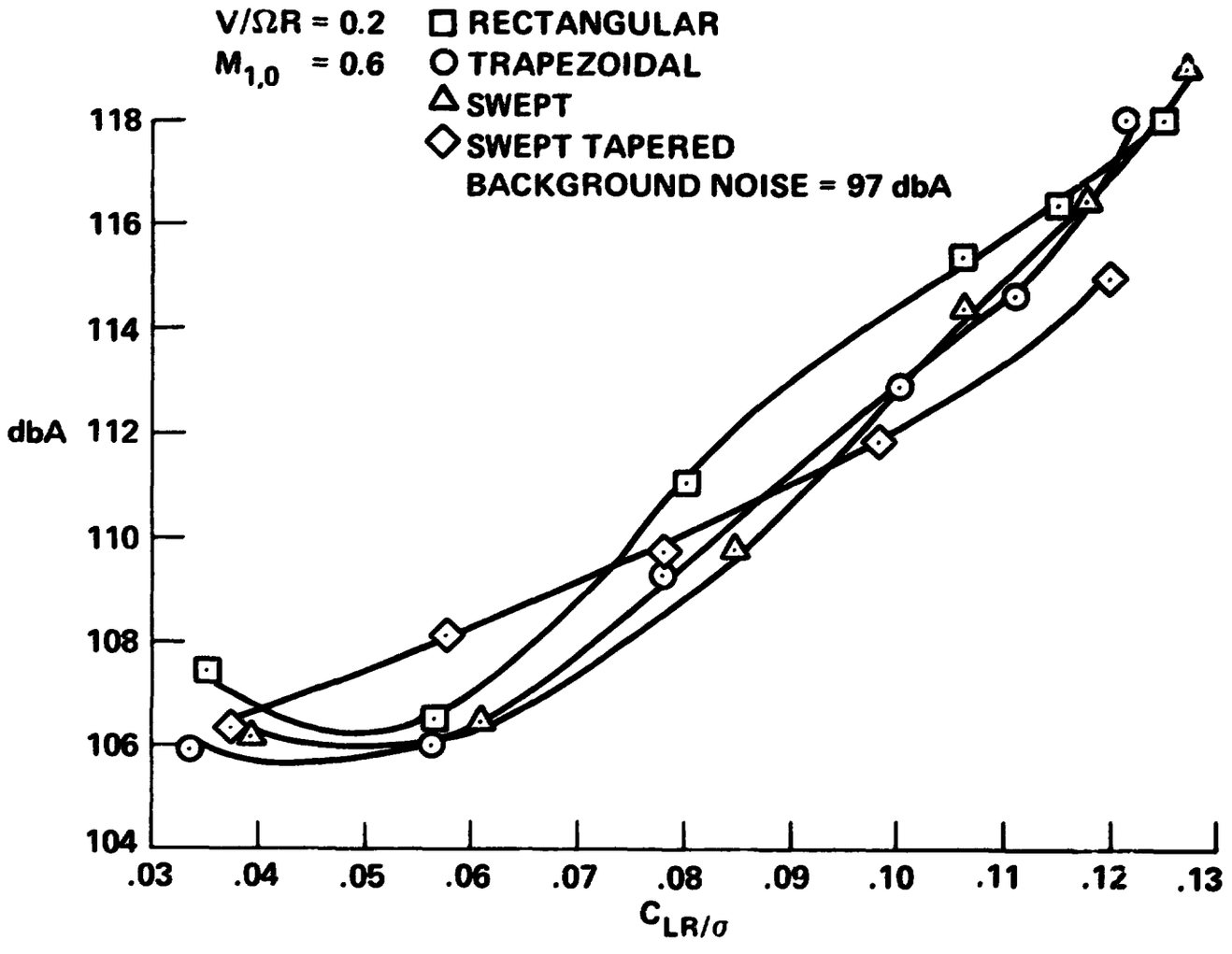

Figure 9 - dbA noise levels as a function of $C_{LR/\sigma}$, Mic 6, α_s = o deg

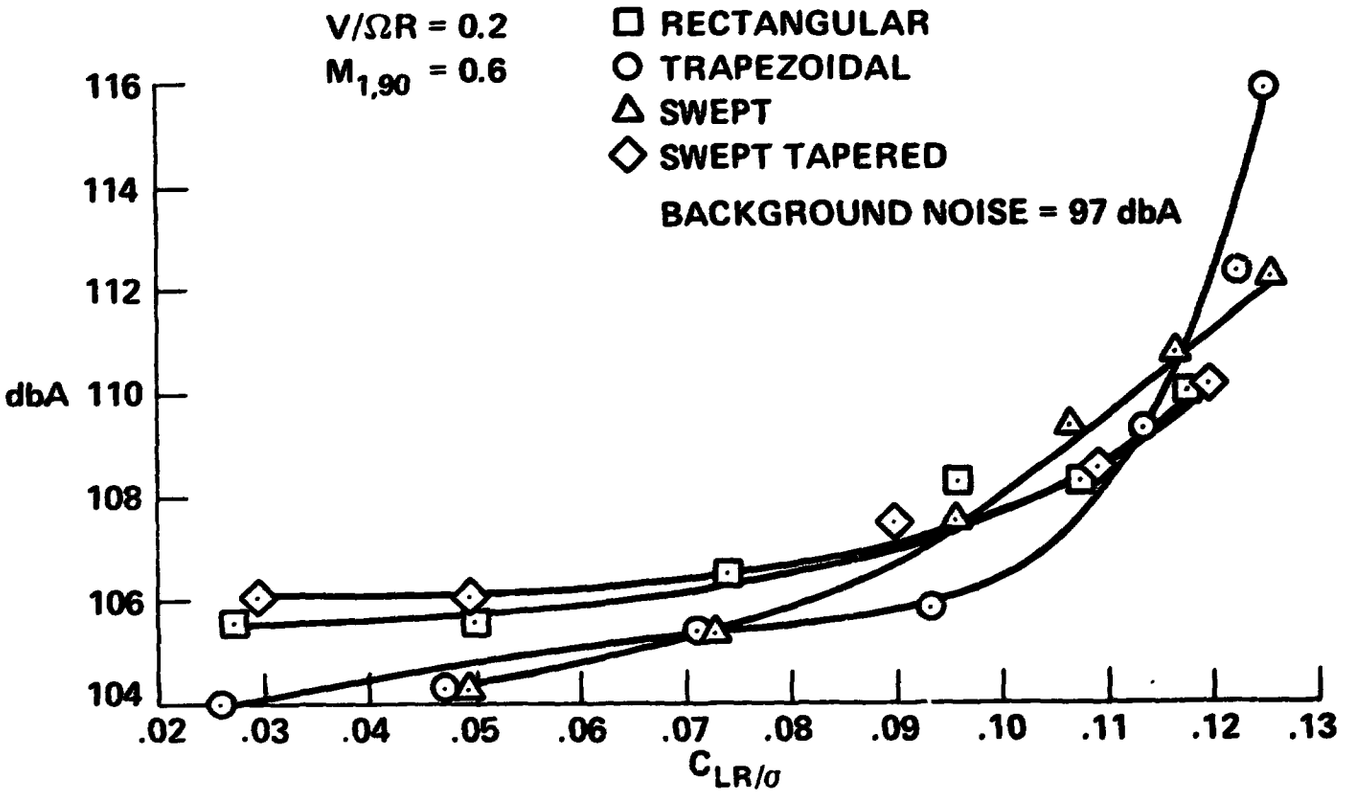

Figure 10 - dbA noise levels as a function of $C_{LR/\sigma}$, Mic 6, α_s = -2.5 deg

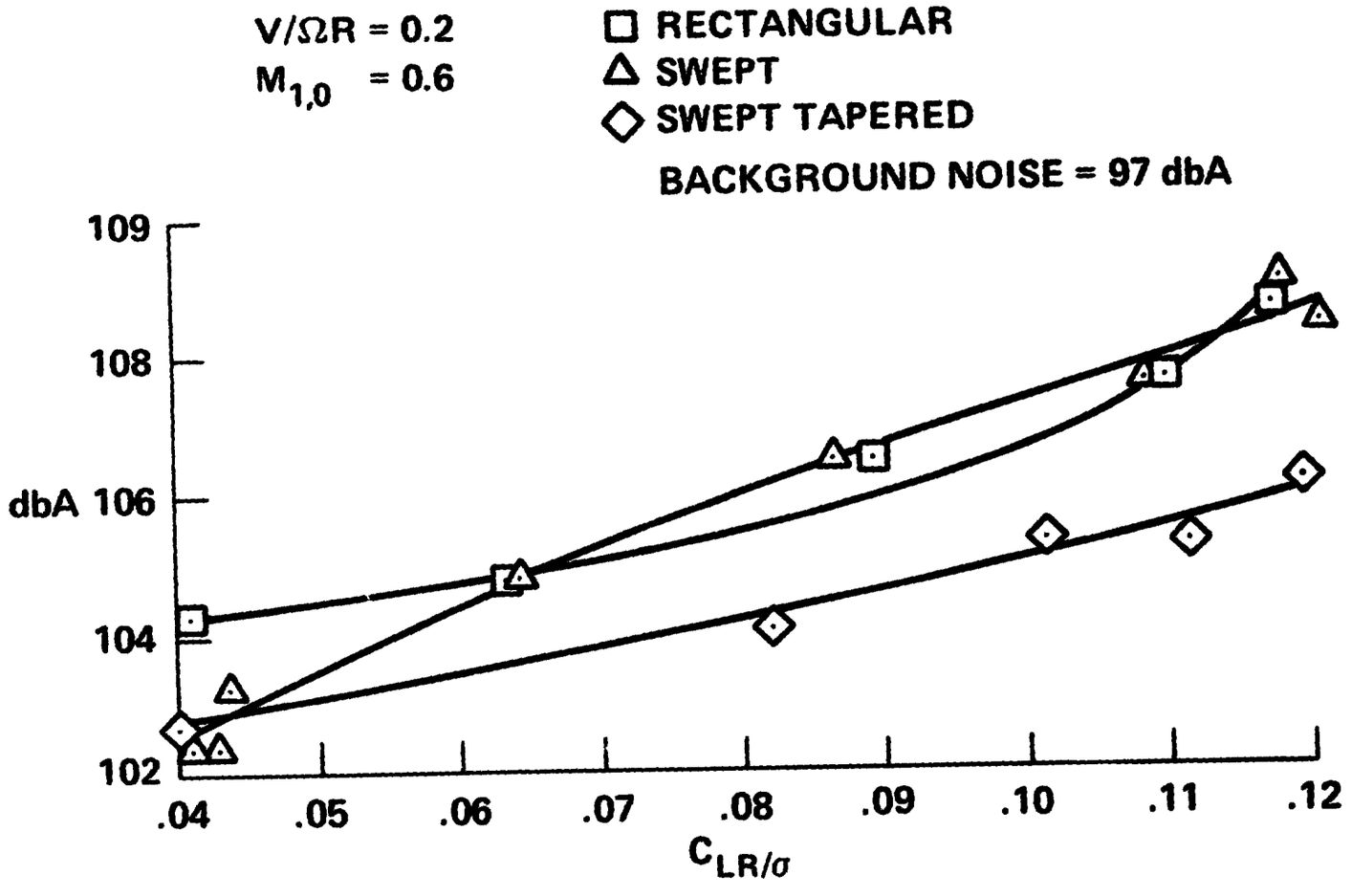

Figure 11 - dbA noise levels as a function of $C_{LR/\sigma}$, Mic 6, α_s = -5 deg

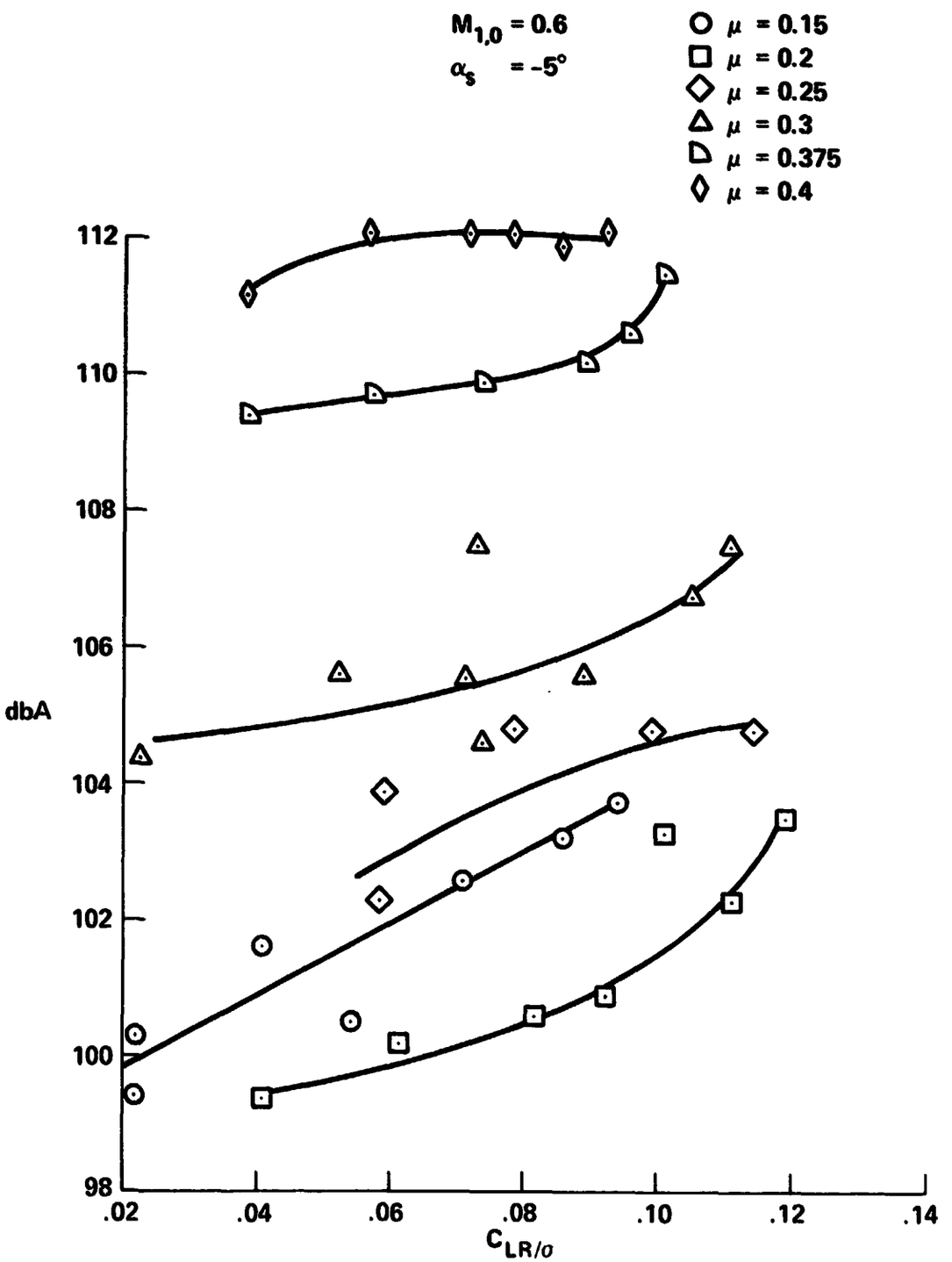

Figure 12 - The dbA noise levels of swept tapered tip blades at different forward speeds, Mic 3

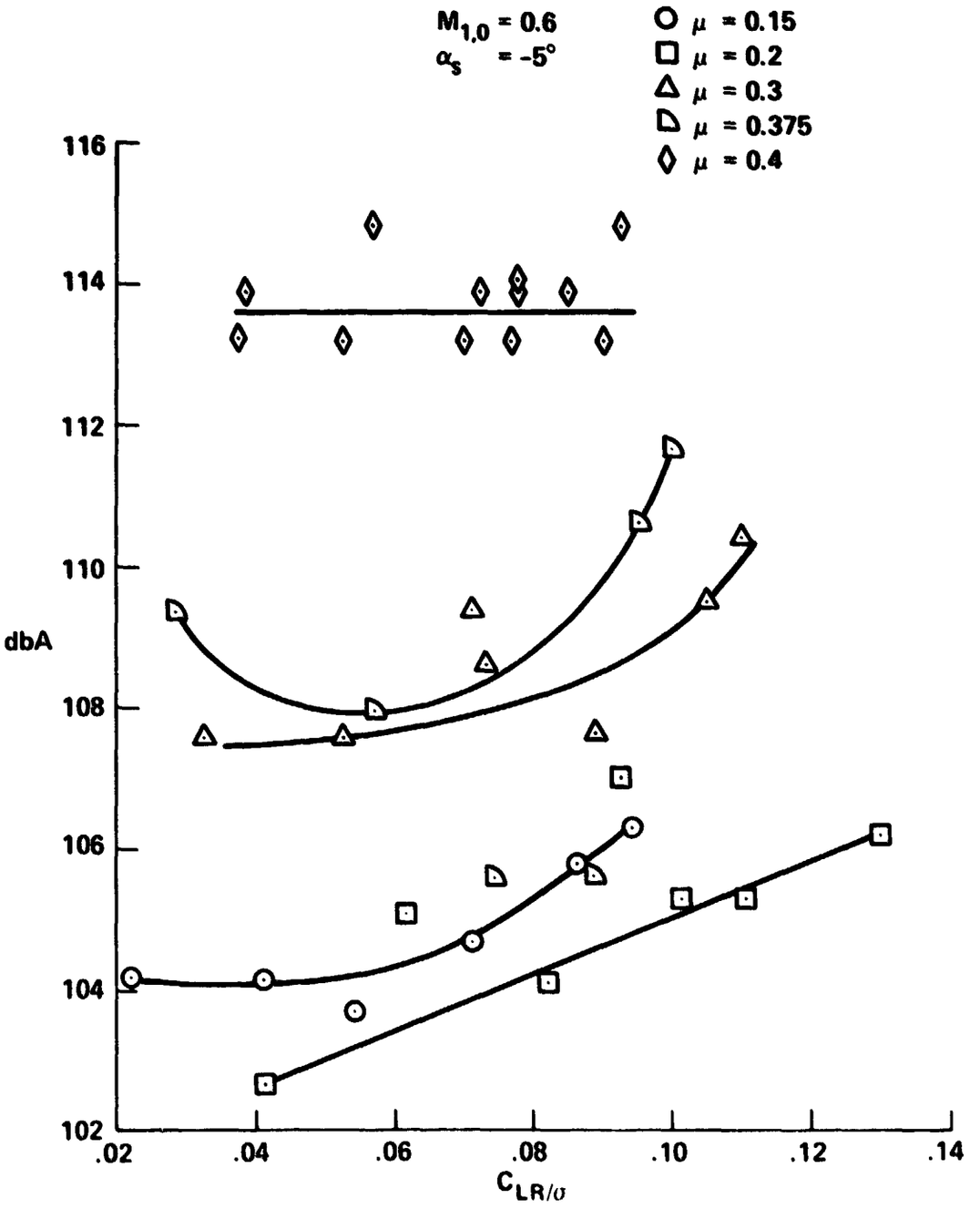

Figure 13 - The dbA noise levels of swept tapered tip blades at different forward speeds, Mic 6

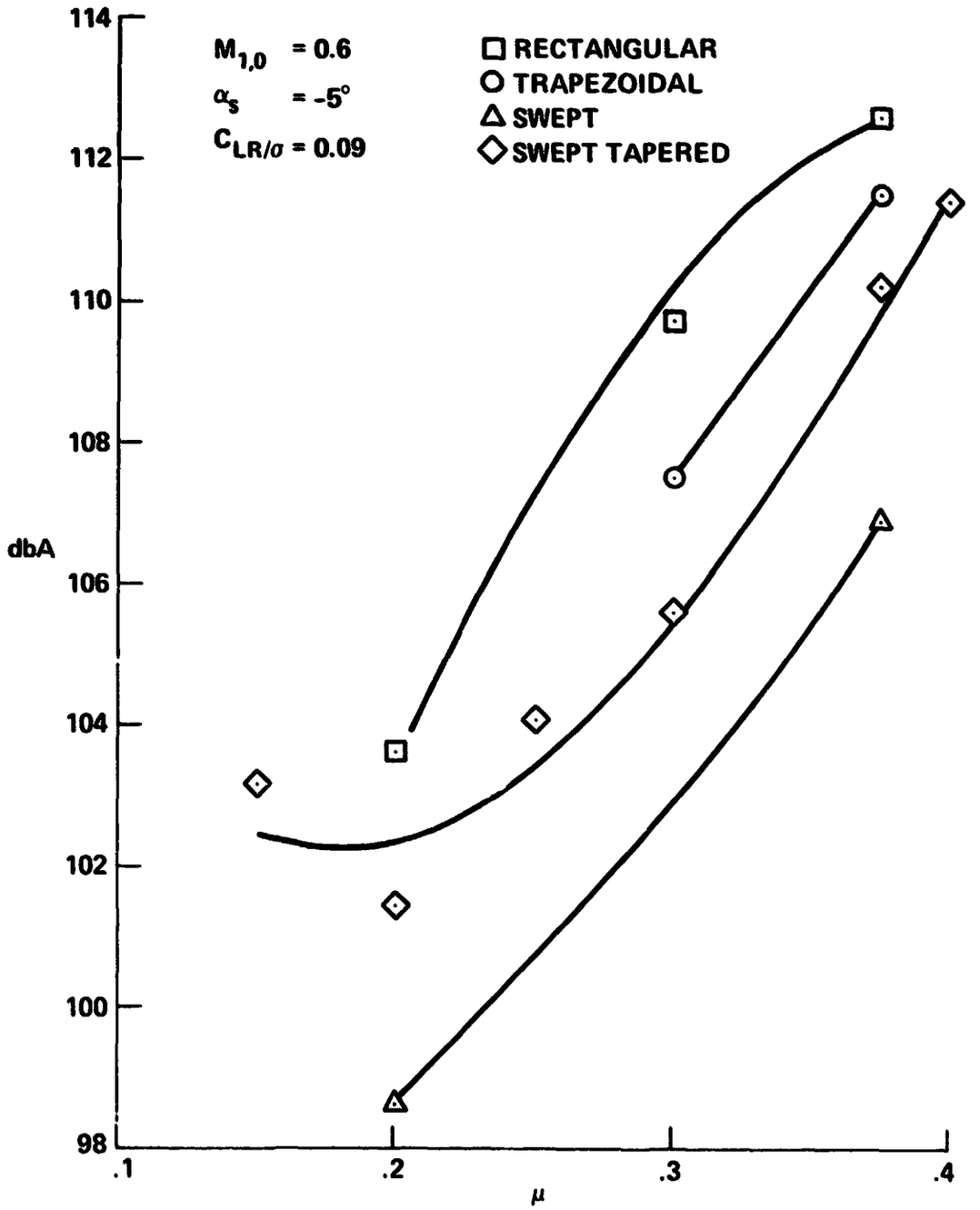

Figure 14 - dbA noise level vs advance ratio, Mic 3

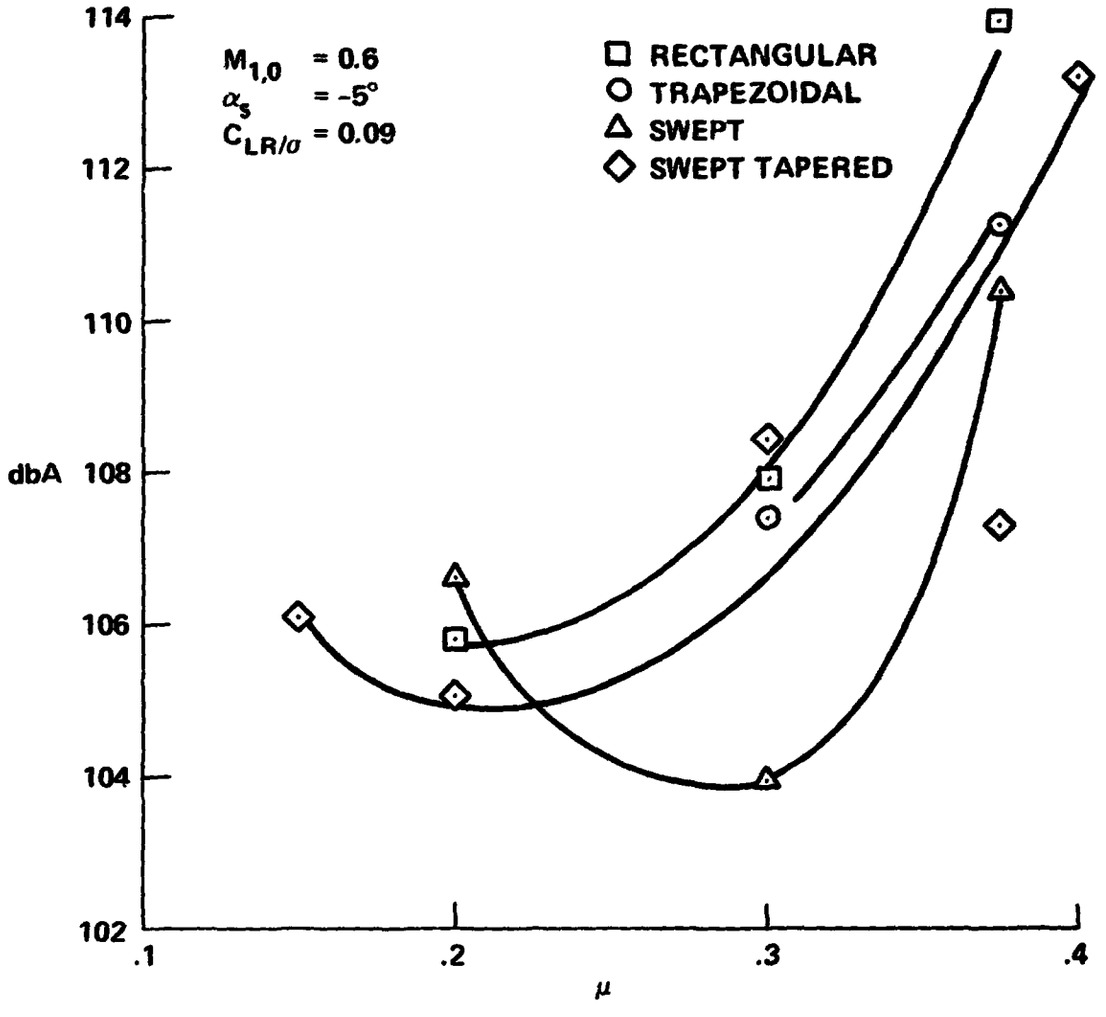

Figure 15 - dbA noise level vs advance ratio, Mic 6

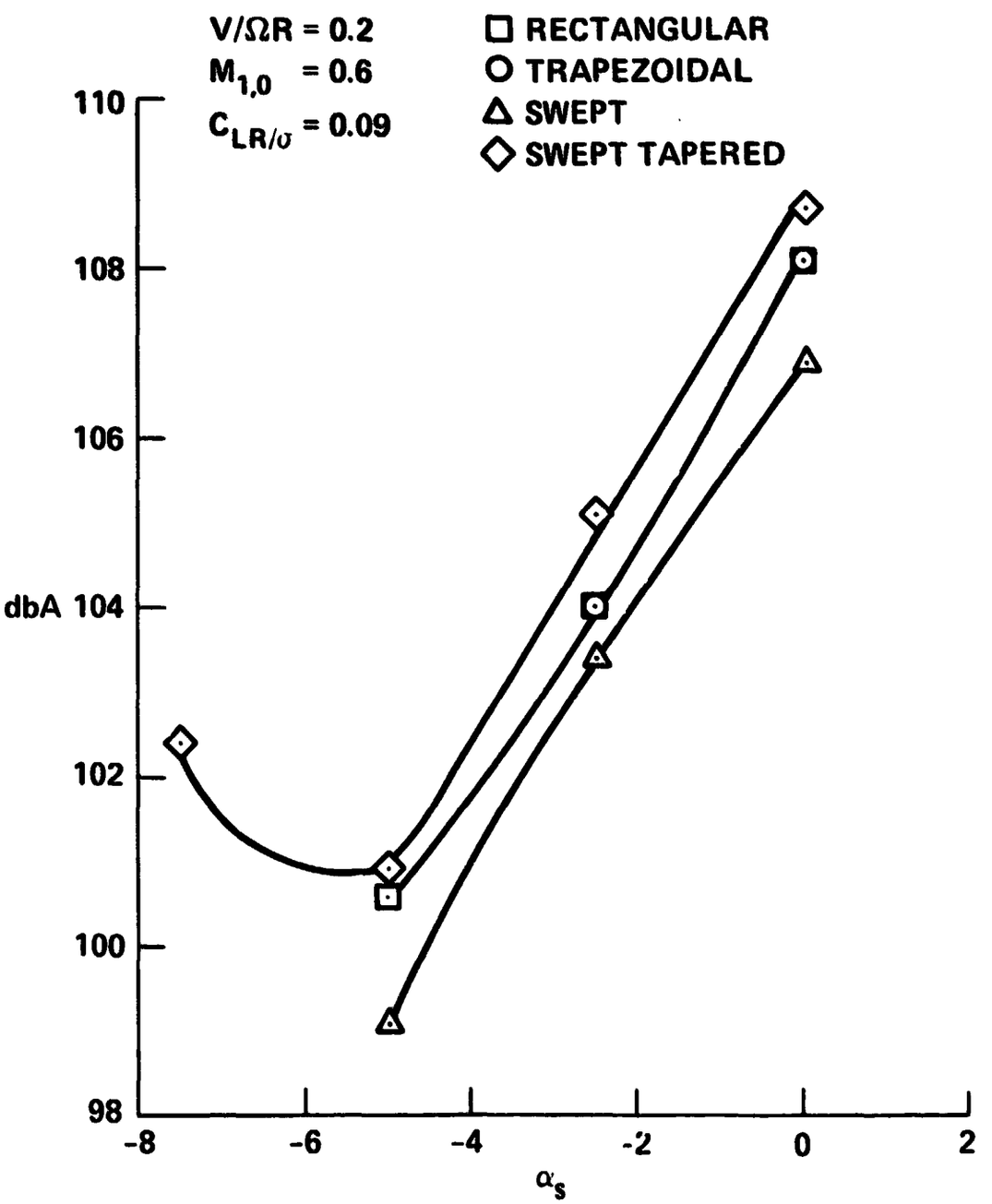

Figure 16 - The effect of tip path plane angle-of-attack on dbA level, Mic 3

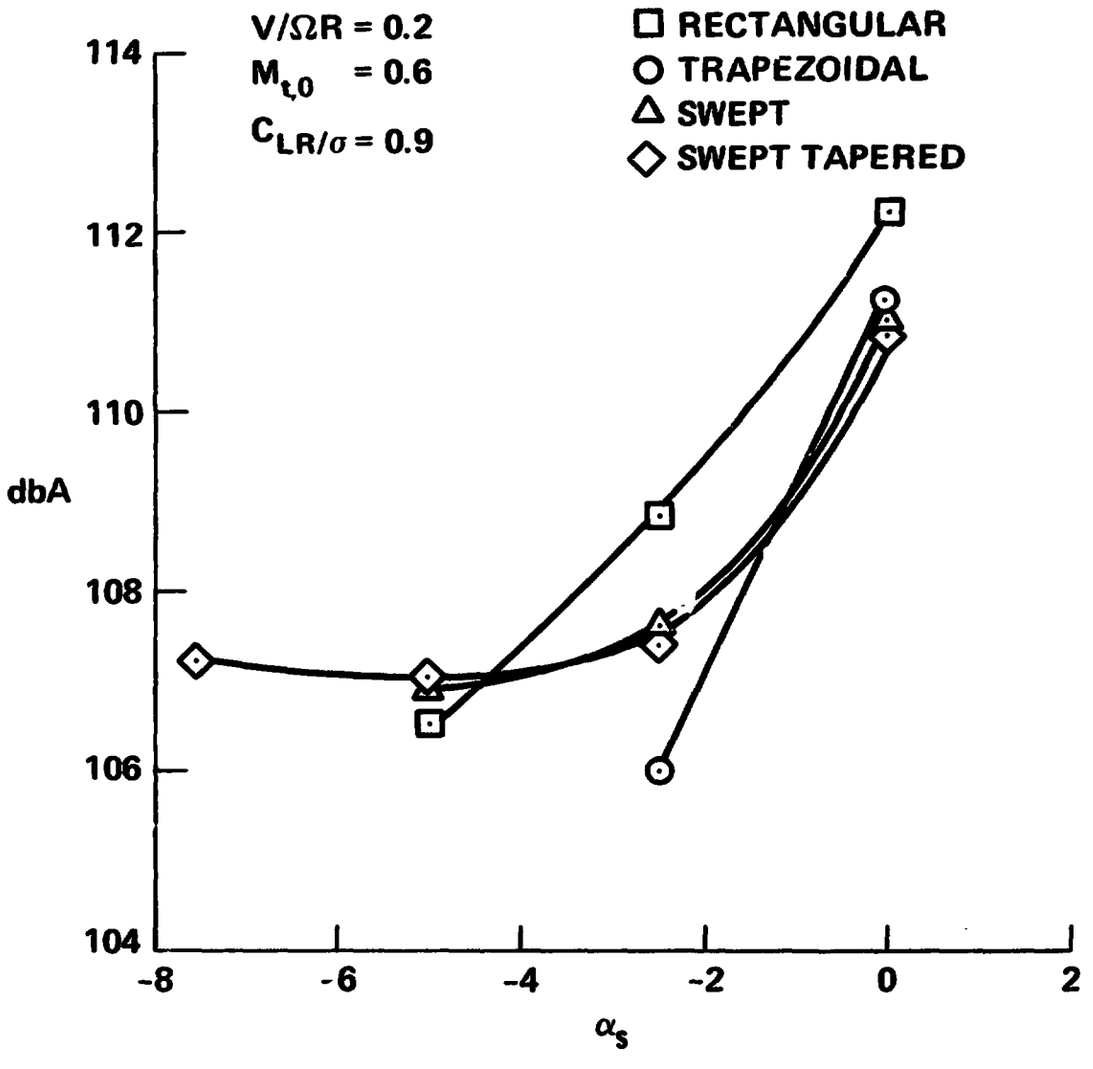

Figure 17 - The effect of tip path plane angle-of-attack on dbA level. Mic 6

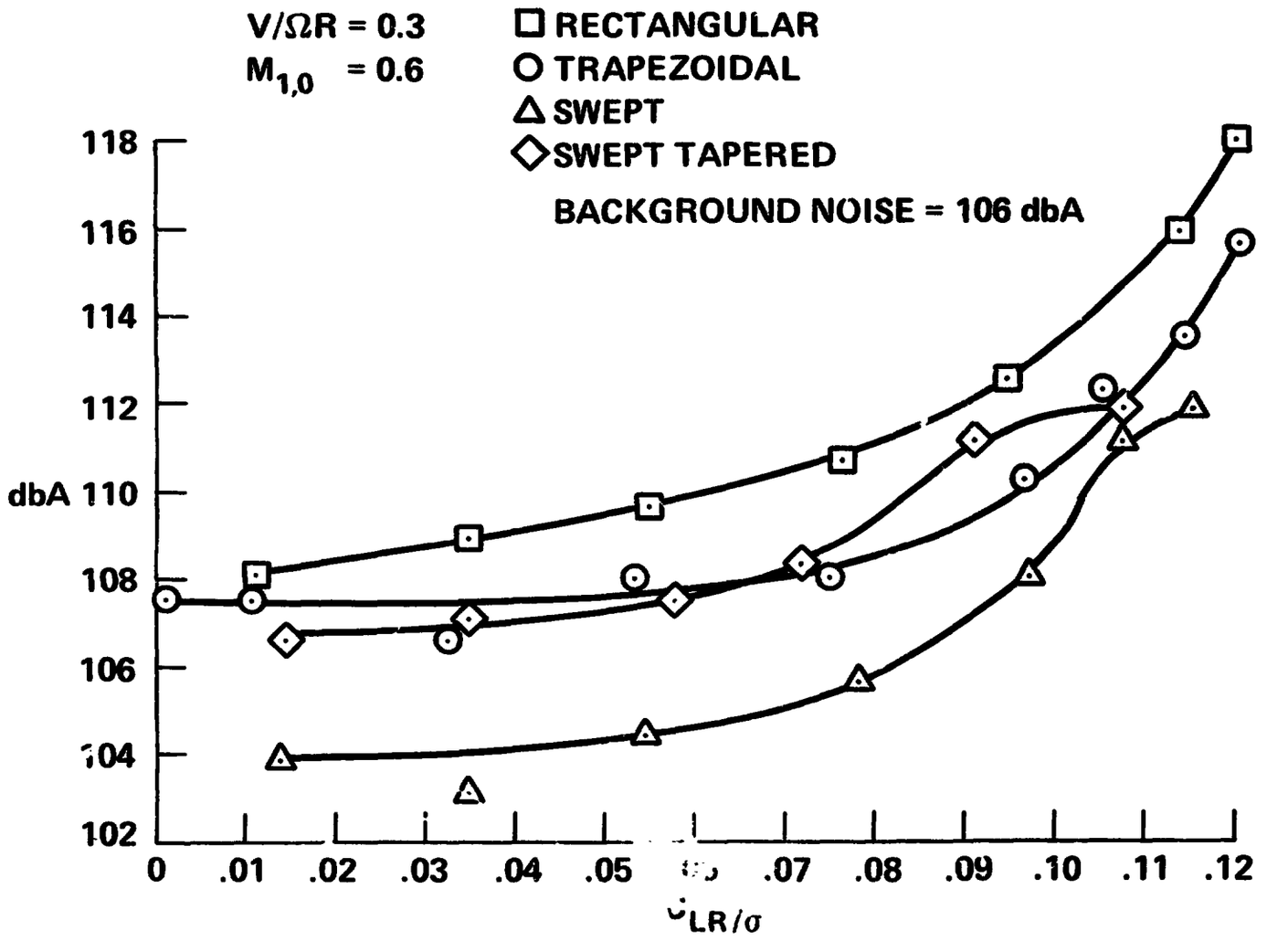

Figure 18 - The acoustic effect of tip shape as a function of $C_{LR/\sigma}$, Mic 3, α_s = o deg

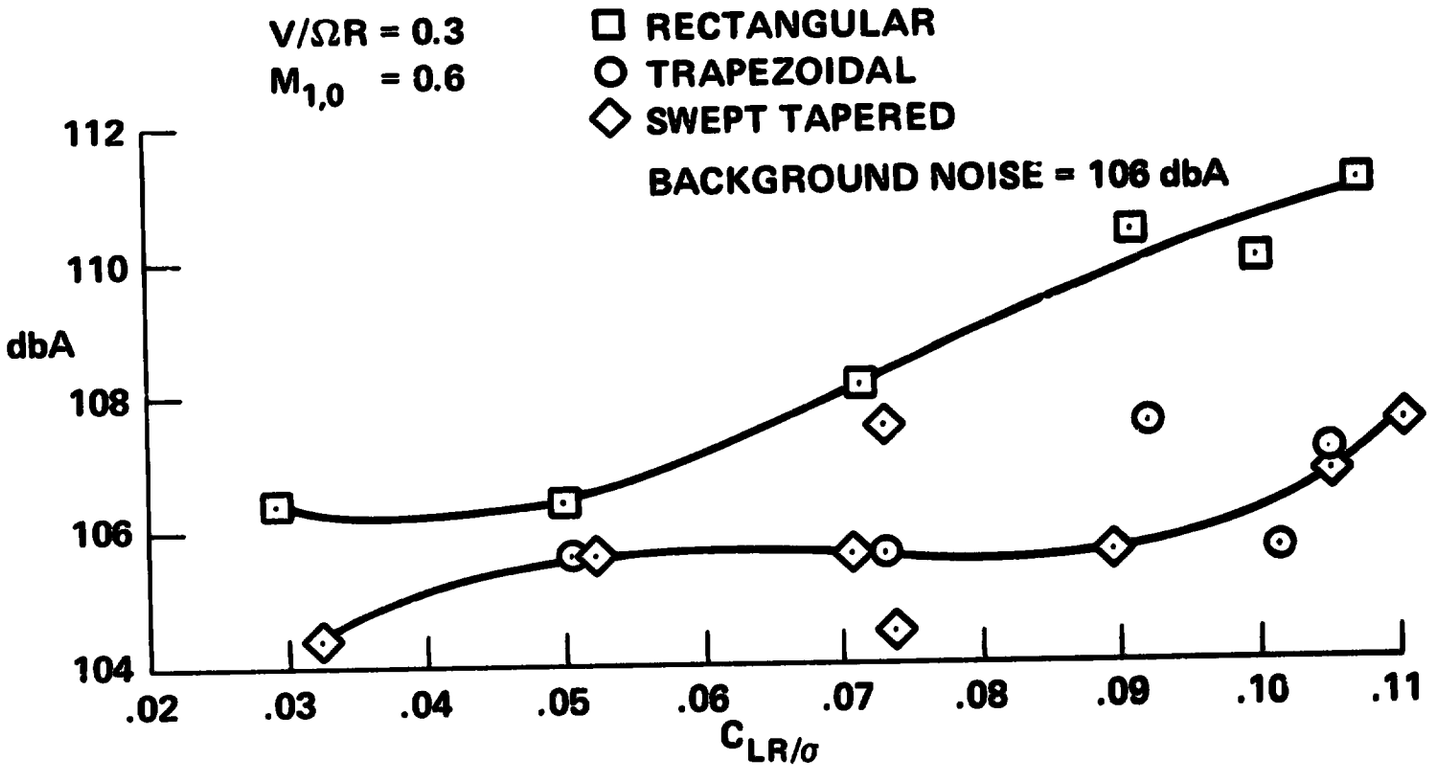

Figure 19 - The acoustic effect of tip shape as a function of $C_{LR/\sigma}$, Mic 3, α_s = -5 deg

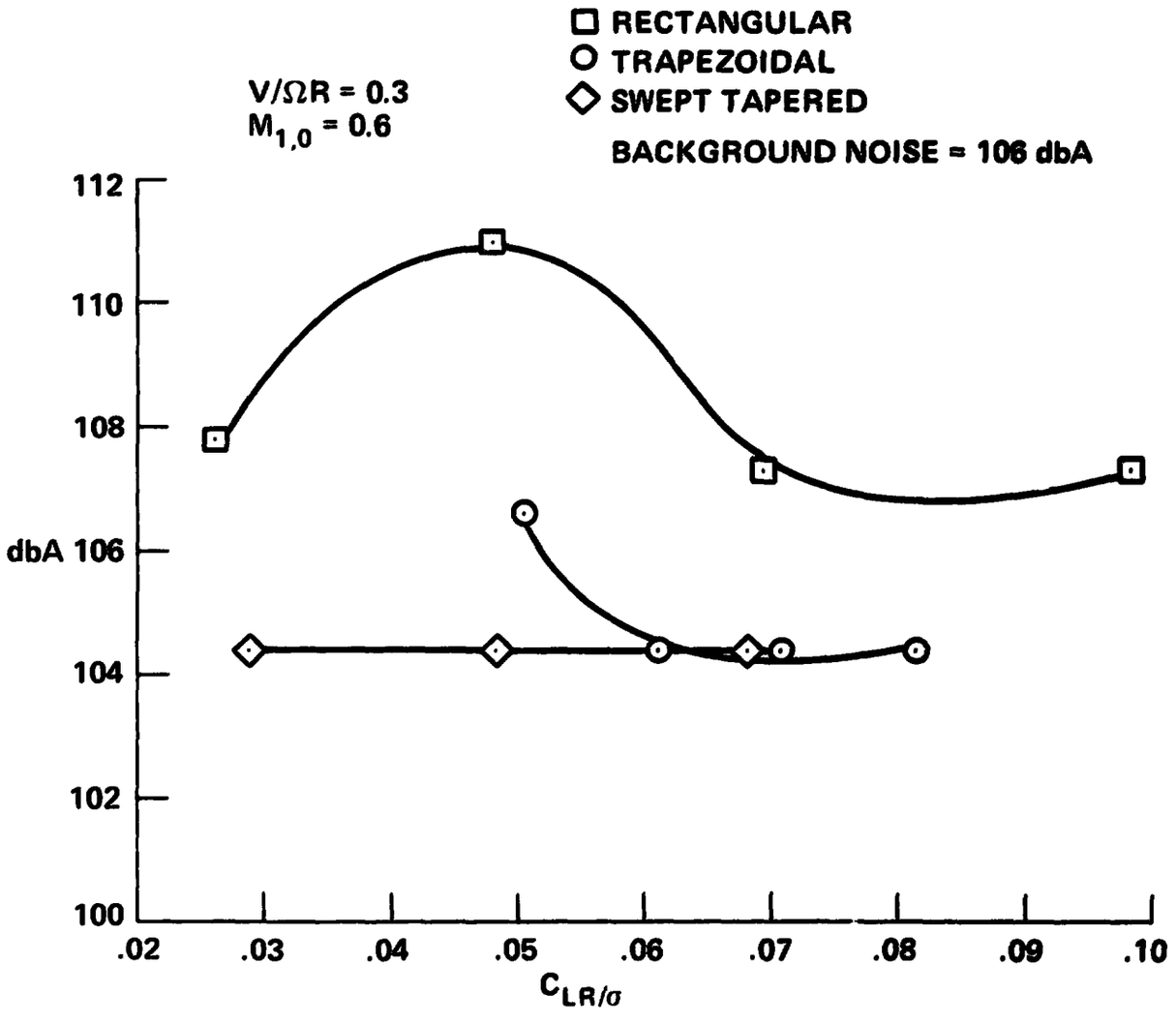

Figure 20 - The acoustic effect of tip shape as a function of $C_{LR/\sigma}$, Mic 3, α_s = -10 deg

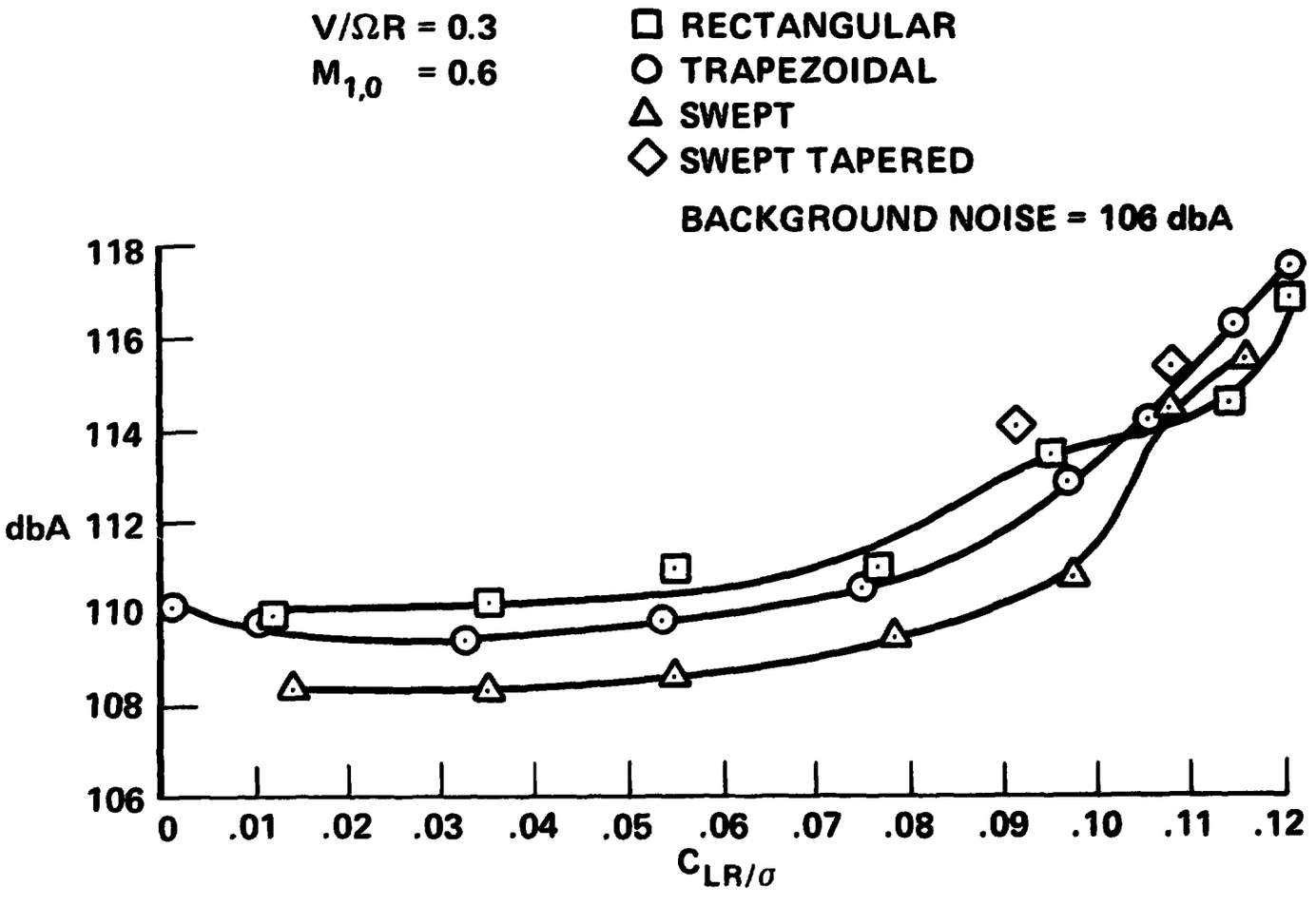

Figure 21 - The acoustic effect of tip shape as a function of $C_{LR/\sigma}$, Mic 6, α_s = o deg

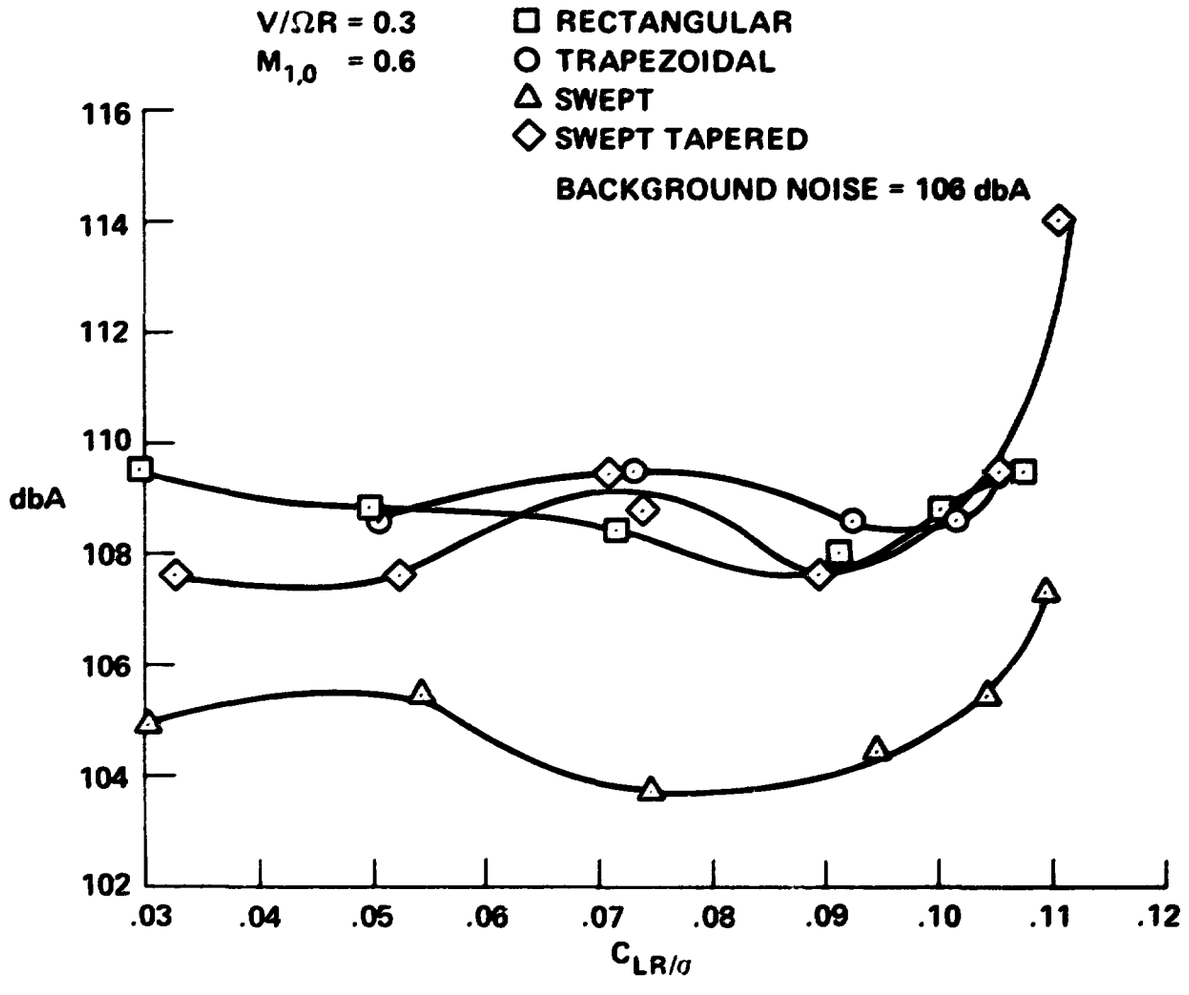

Figure 22 - The acoustic effect of tip shape as a function of $C_{LR/\sigma}$, Mic 6, α_s = -5 deg

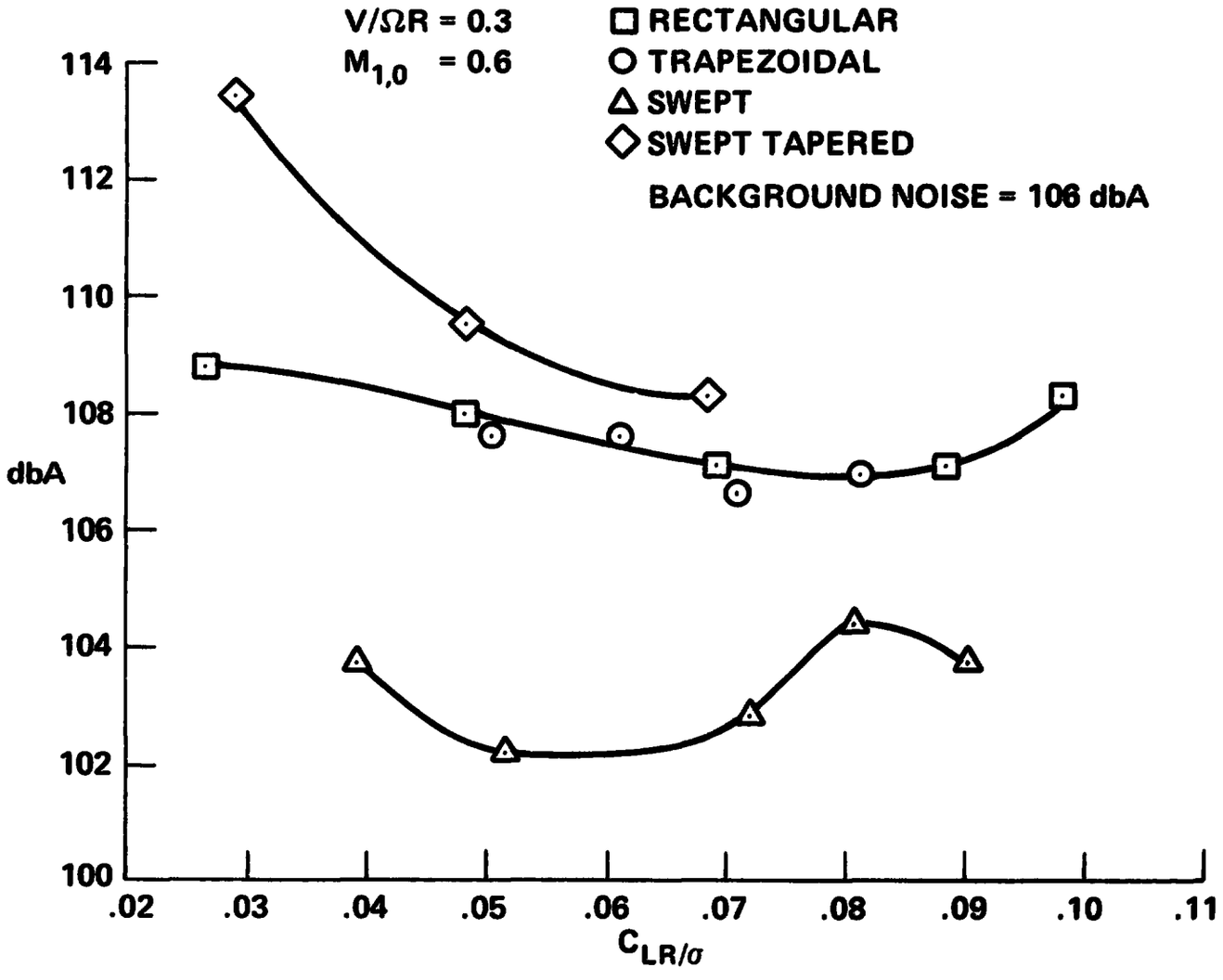

Figure 23 - The acoustic effect of tip shape as a function of $C_{LR/\sigma}$, Mic 6, α_s = -10 deg

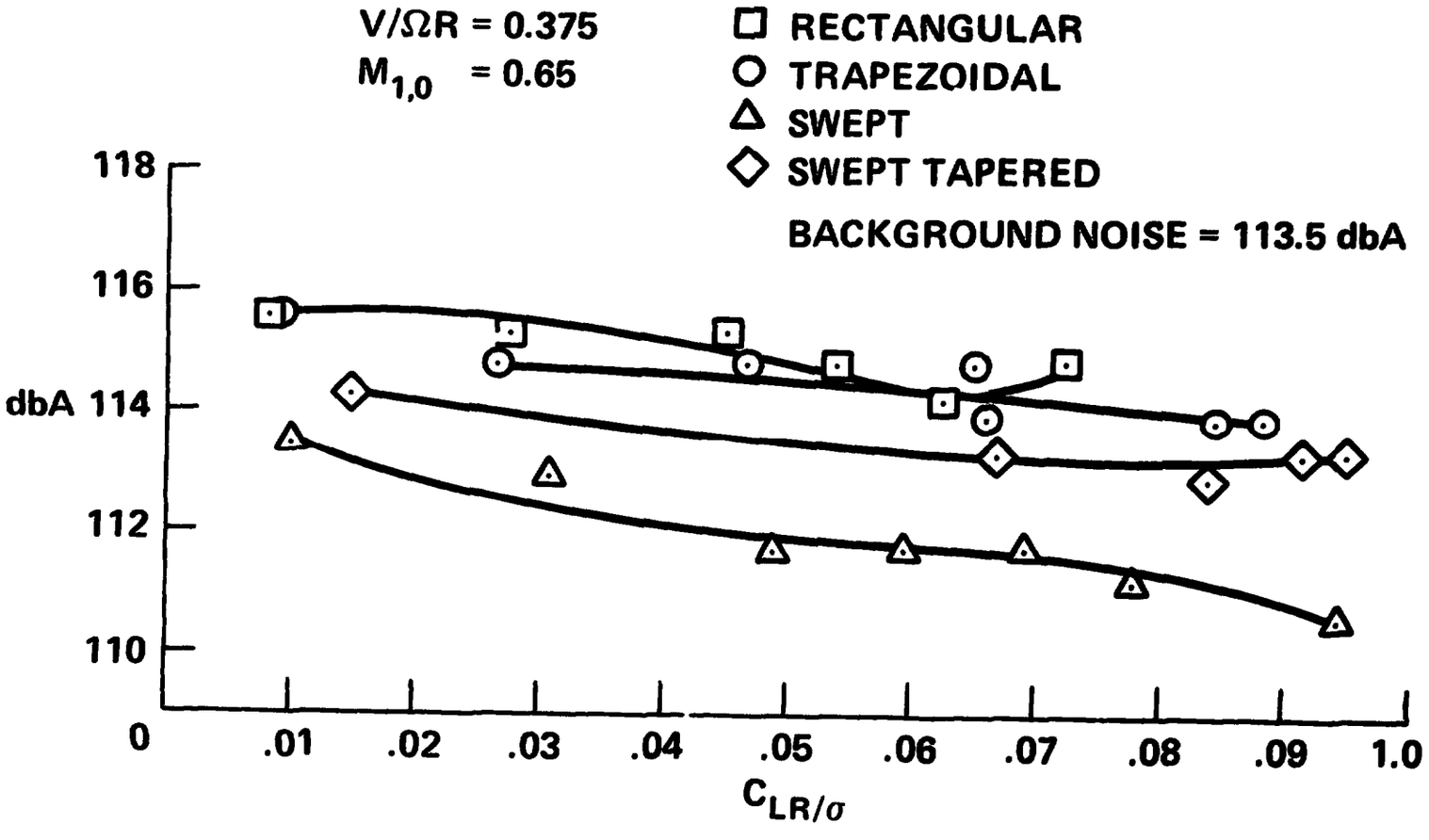

Figure 24 - The dbA levels of different tip shapes at high speed, Mic 3, α_s = o deg

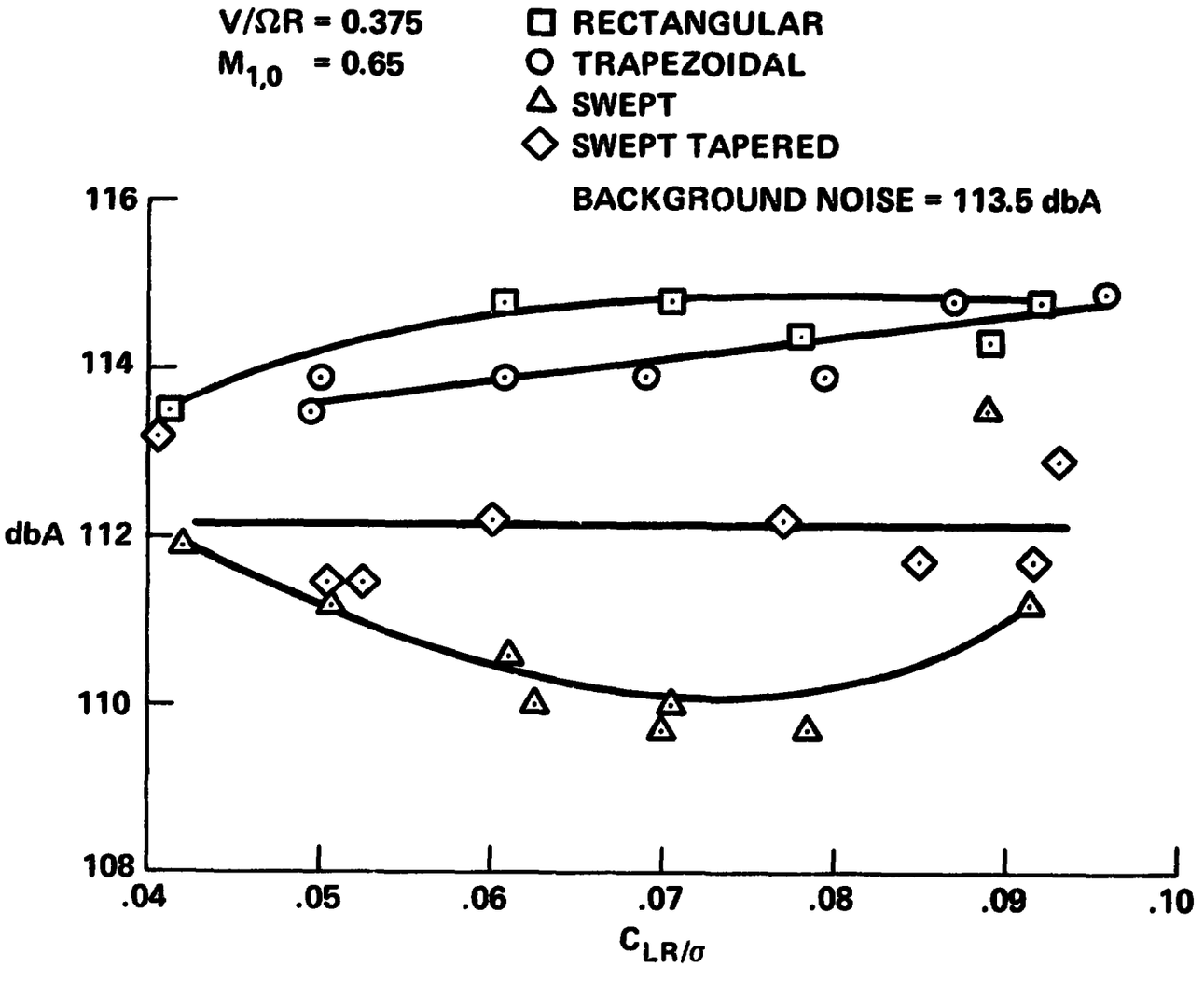

Figure 25 - The dbA levels of different tip shapes at high speed, Mic 3, α_s = -5 deg

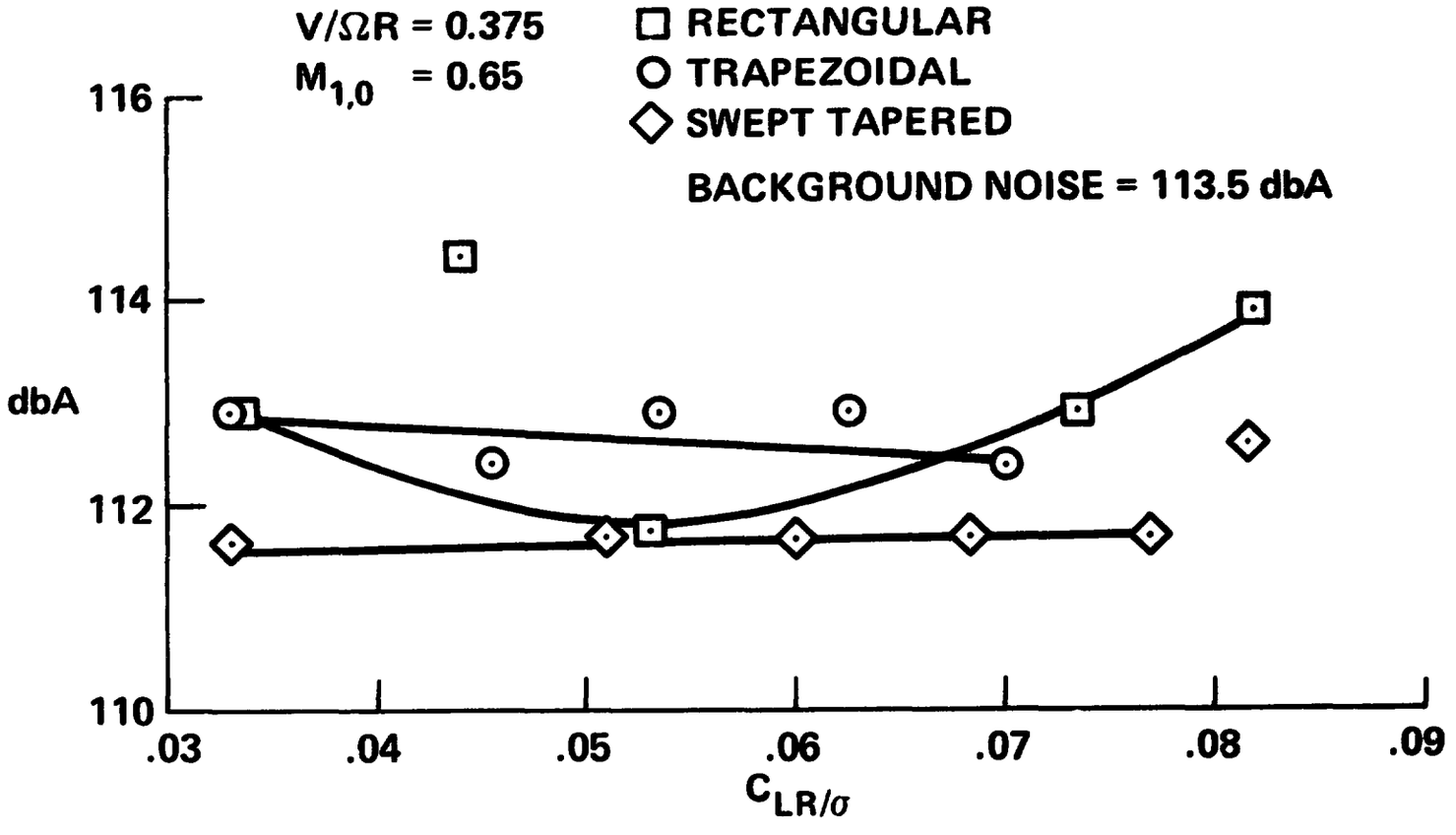

Figure 26 - The dbA levels of different tip shapes at high speed, Mic 3, α_s = - 10 deg

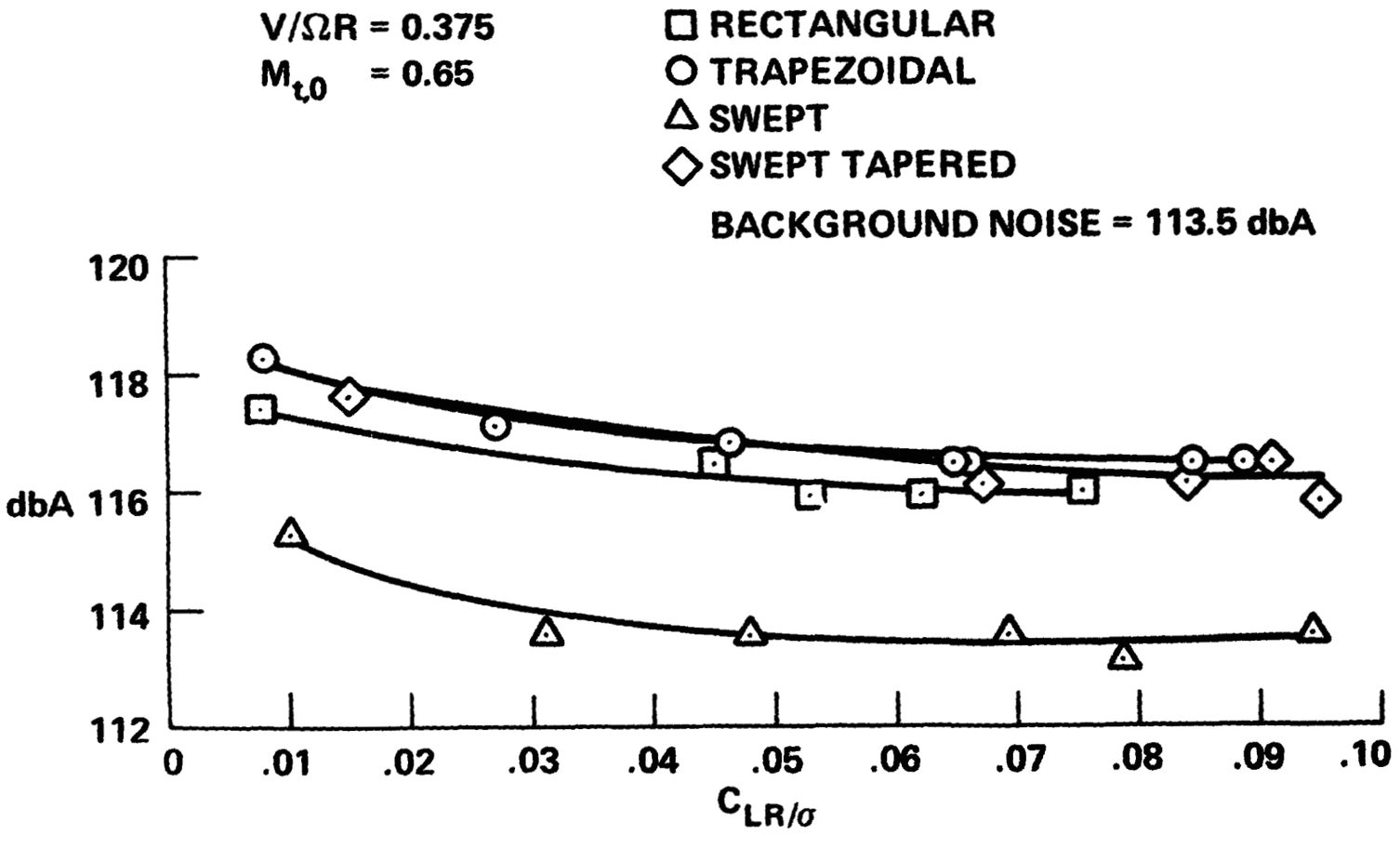

Figure 27 - The dbA levels of different tip shapes at high speed, Mic 6, α_s = o deg

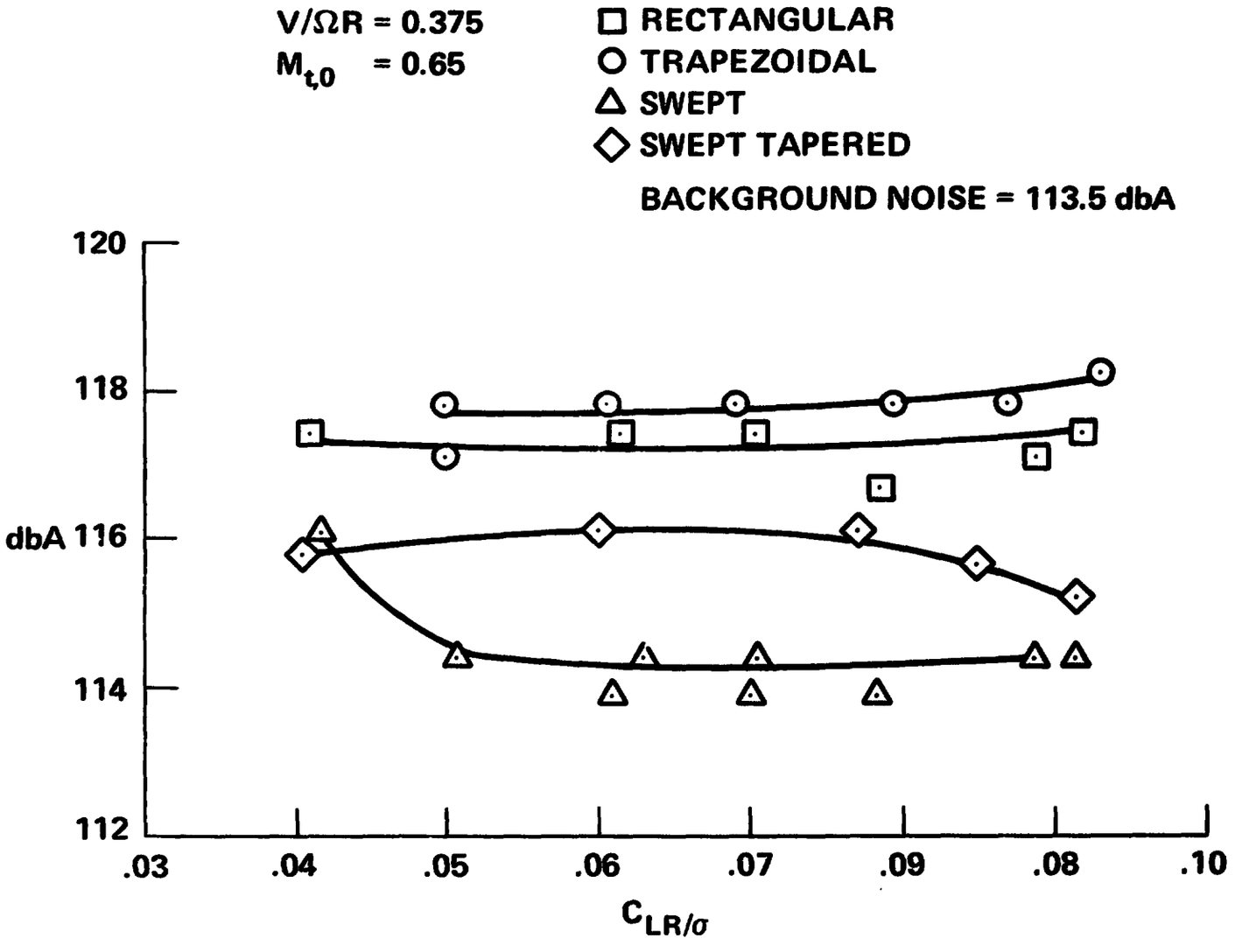

Figure 28 - The dbA levels of different tip shapes at high speed, Mic 6, α_s = -5 deg

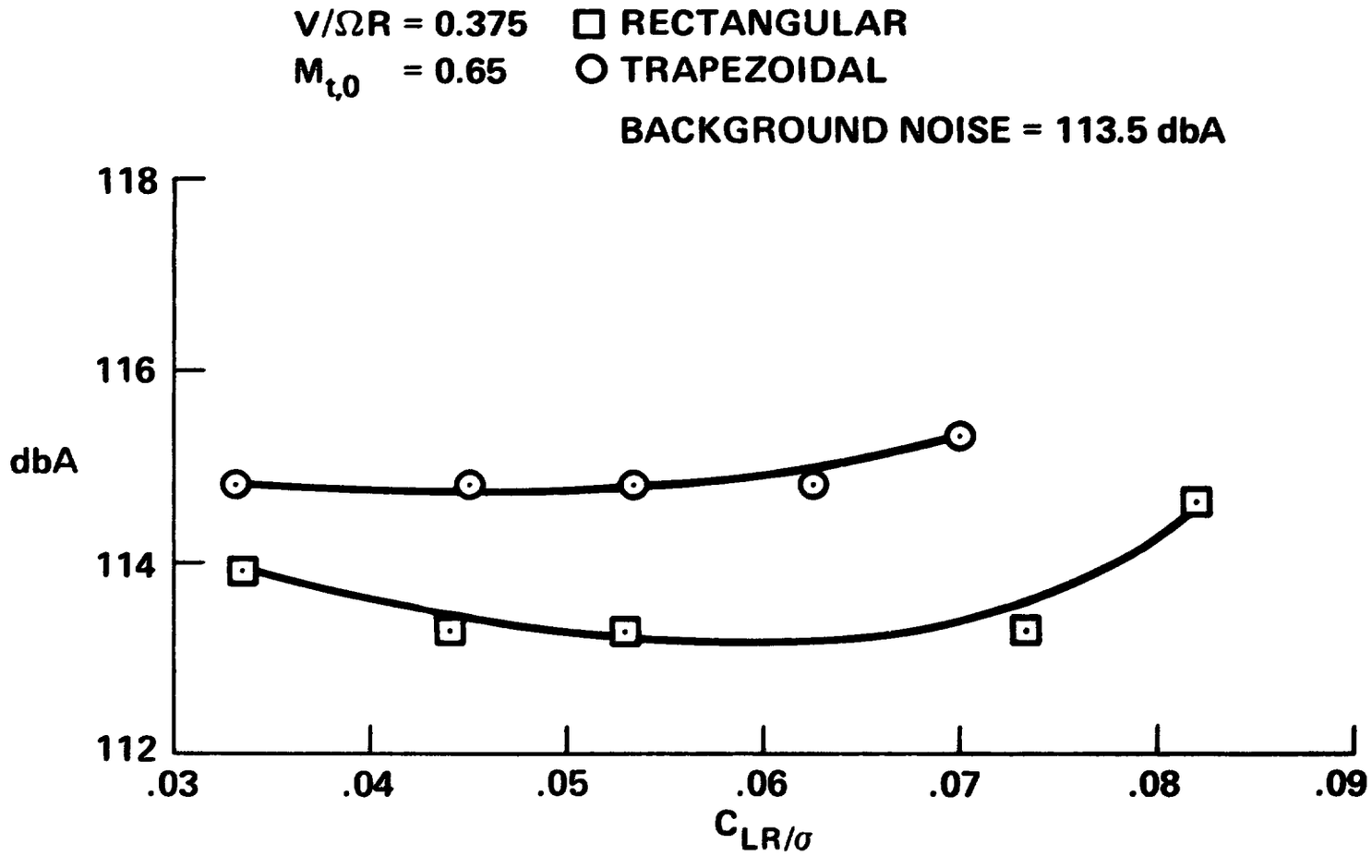

Figure 29 - The dbA levels of different tip shapes at high speed, Mic 6, α_s = -10 deg

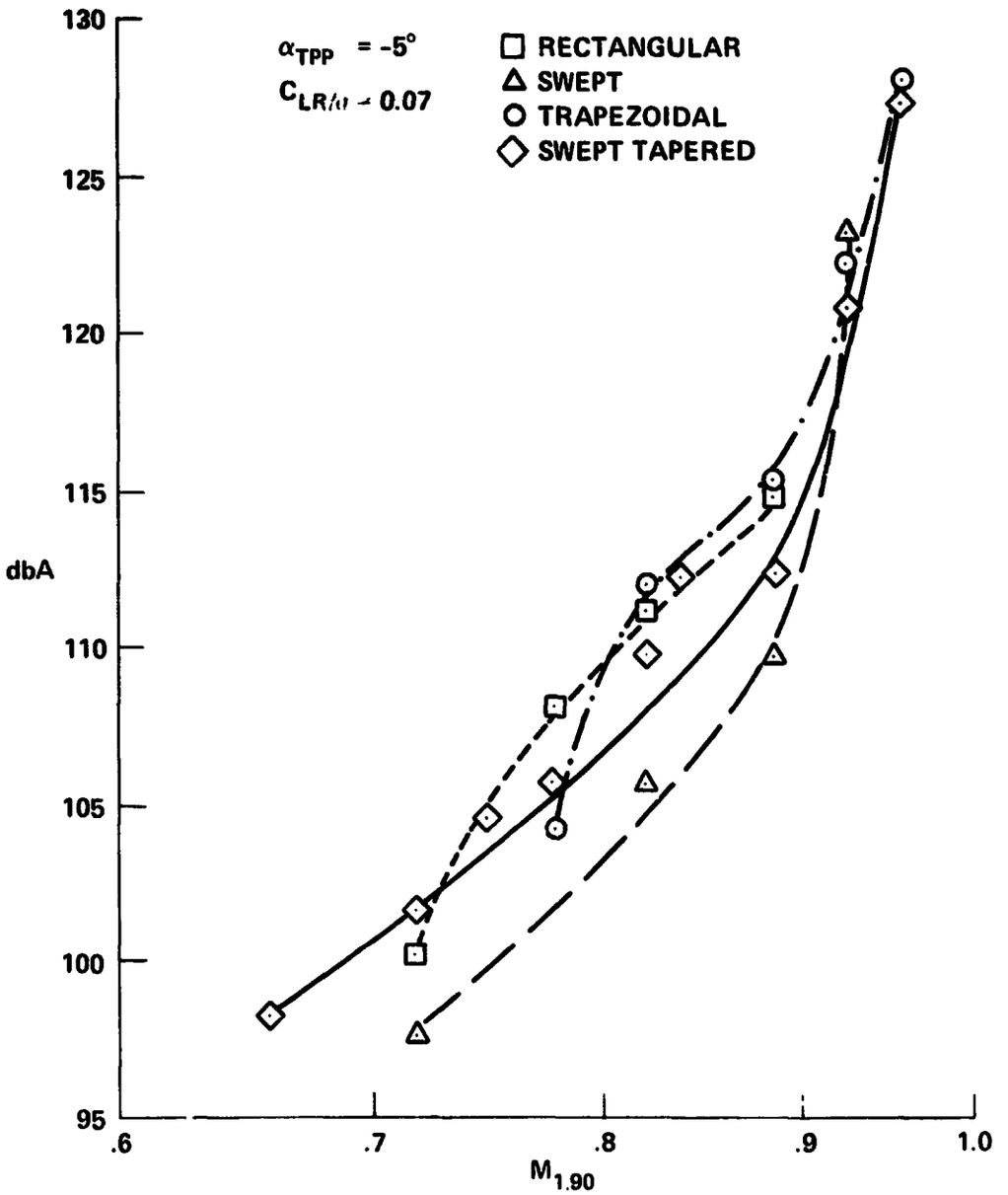

Figure 30 - The effect of Mach r mber on dbA level, Mic 3

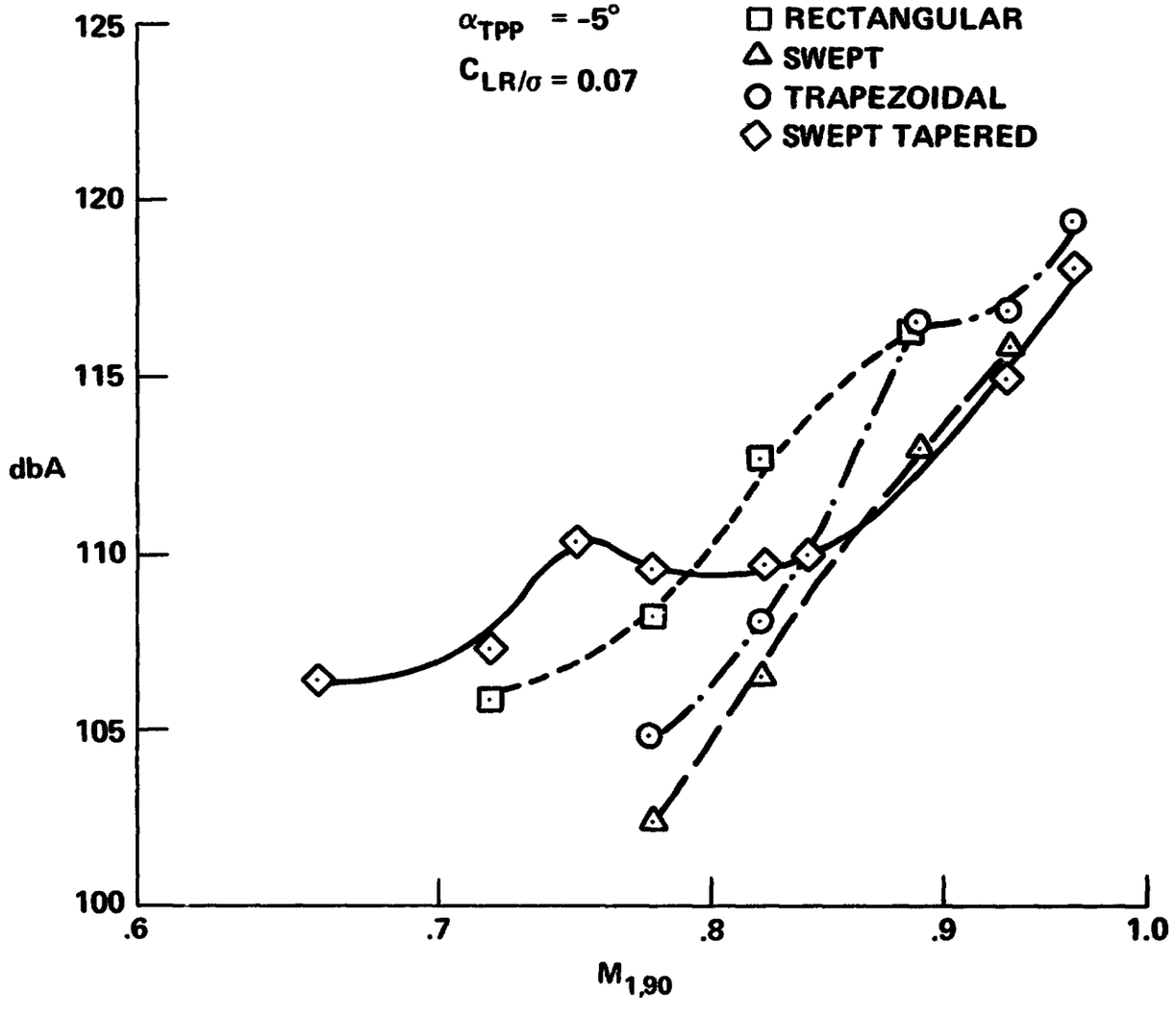

Figure 31 - The effect of Mach number on dbA level, Mic 6

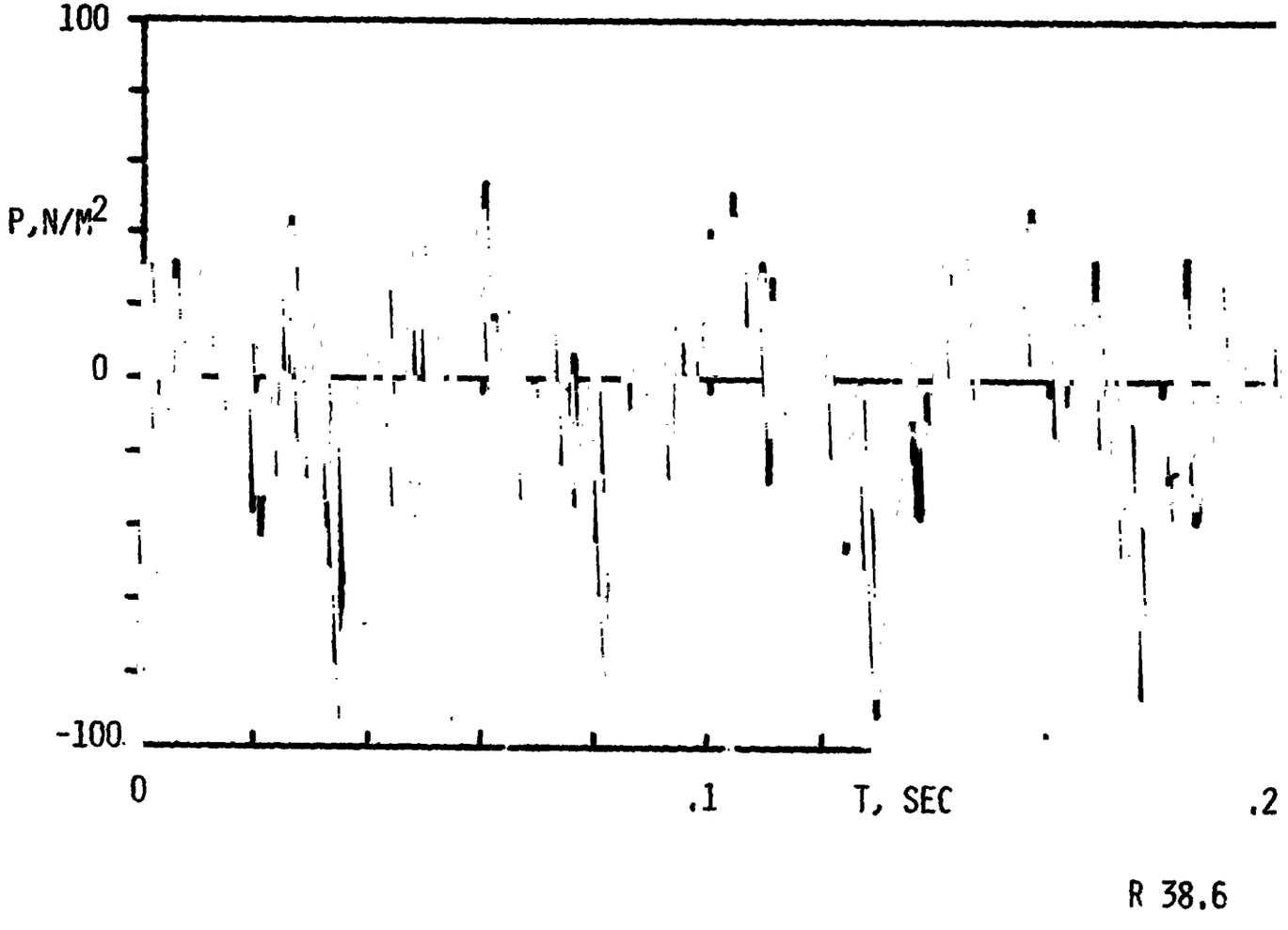

(a) Raw Data

Figure 32 - Acoustical Waveform from Trapezoidal Tip Blades, Mic 3, $M_{1,\ 90} = 0.897$

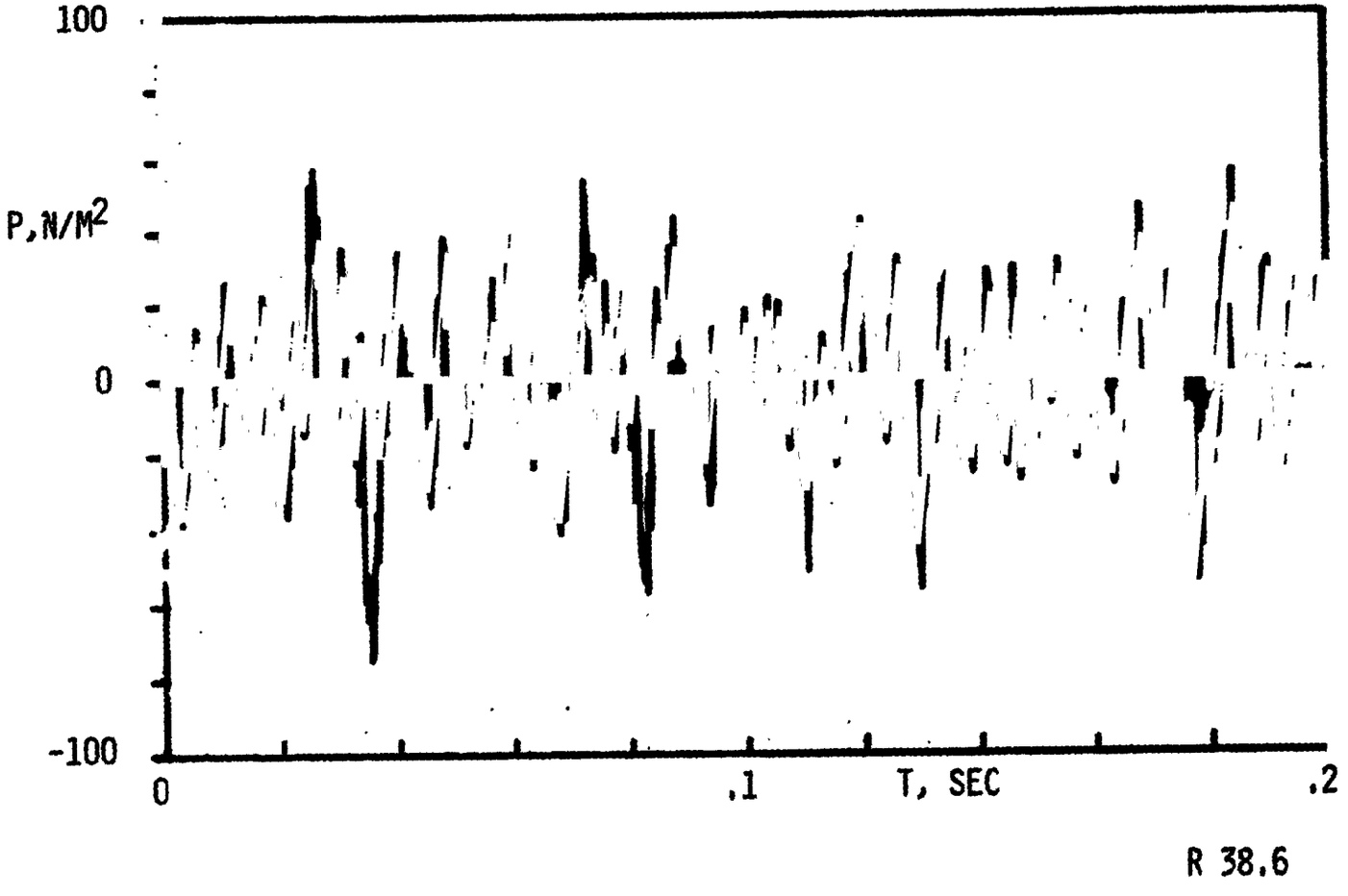

Figure 32 (b) - 25 Hz high pass digitally filtered.

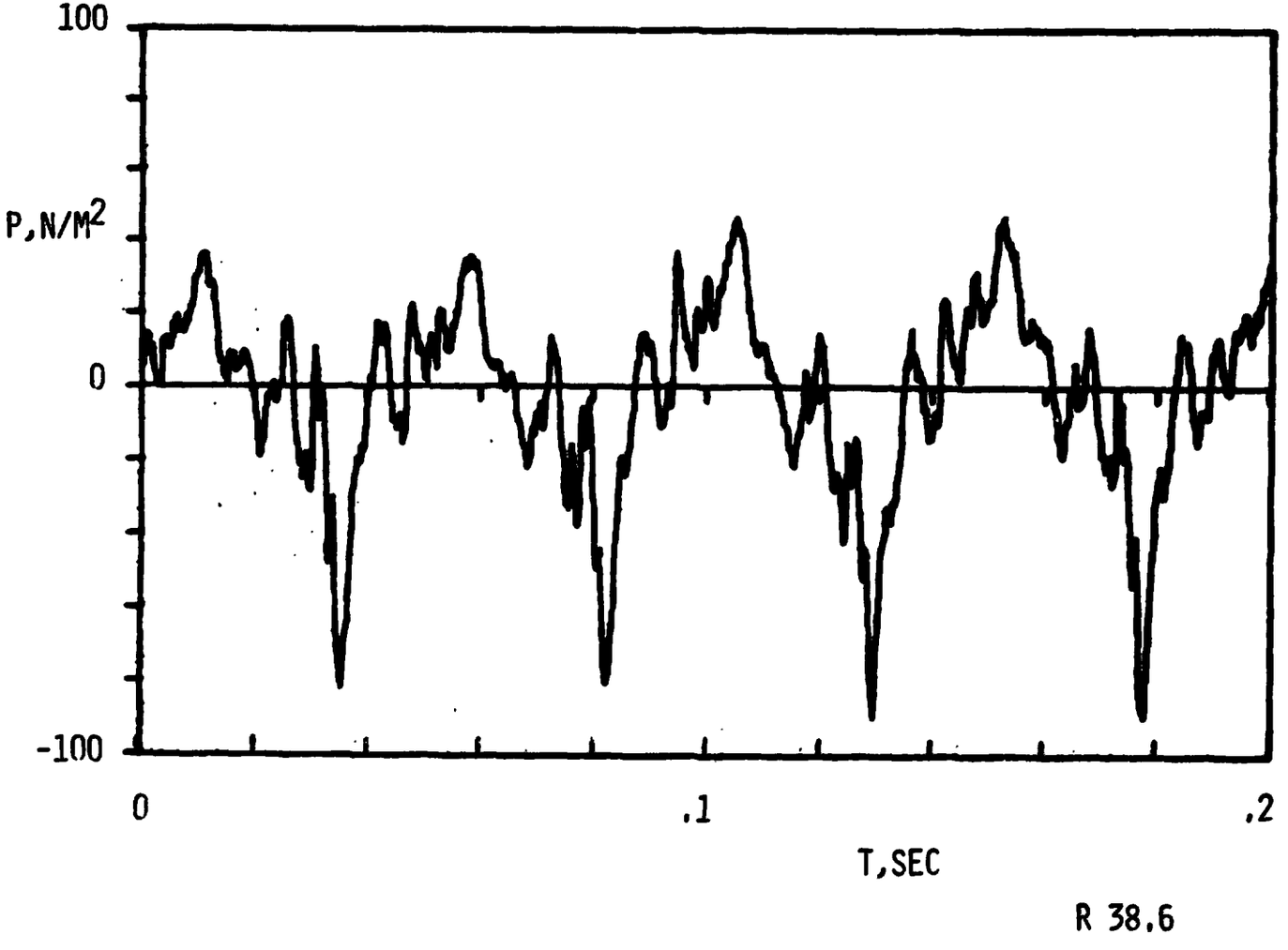

Figure 32 (c) - 50-ensemble averaged, no filtering

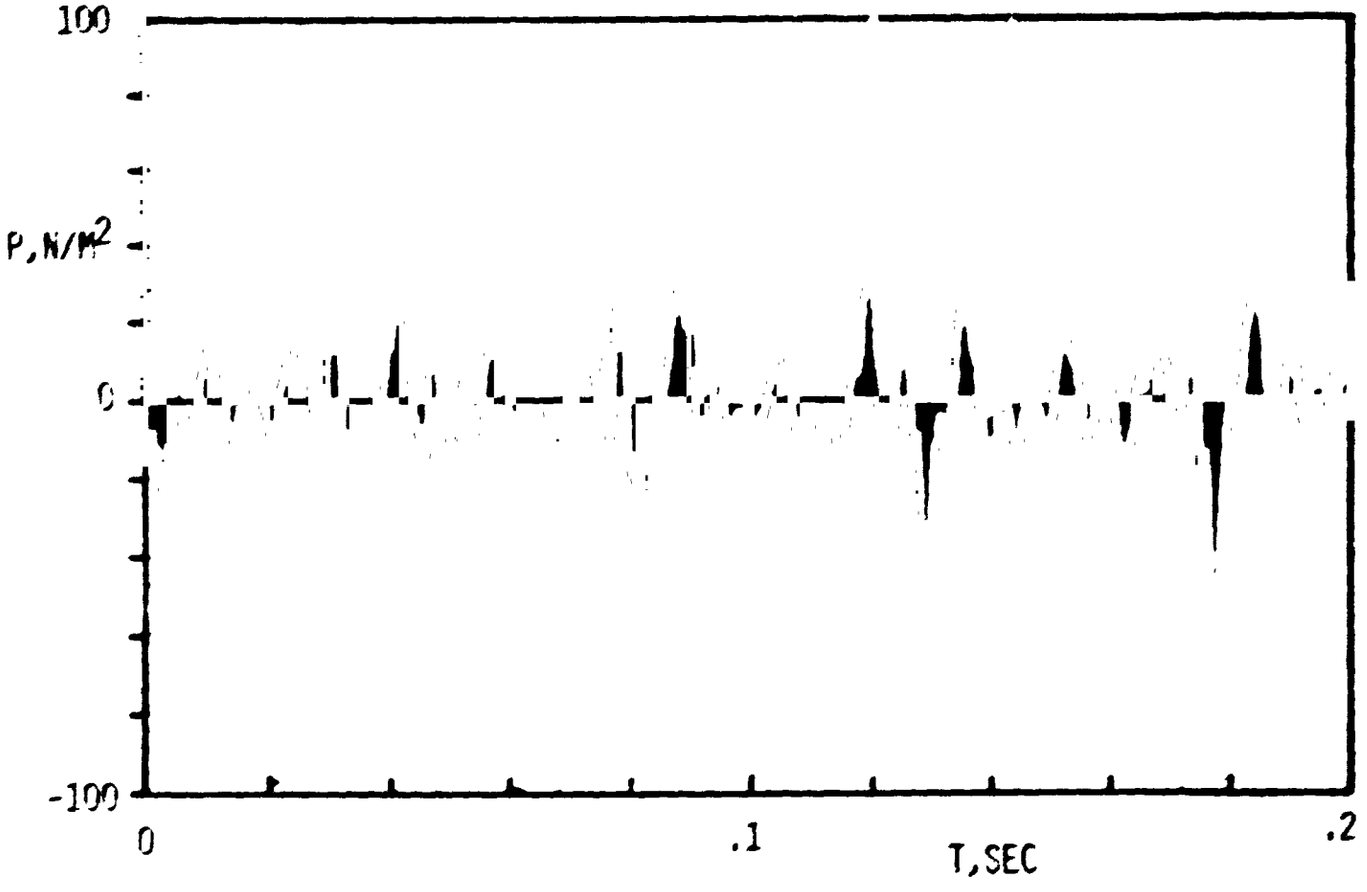

Figure 32 (d) - 50-ensemble averaged, 25 Hz high pass digitally filtered

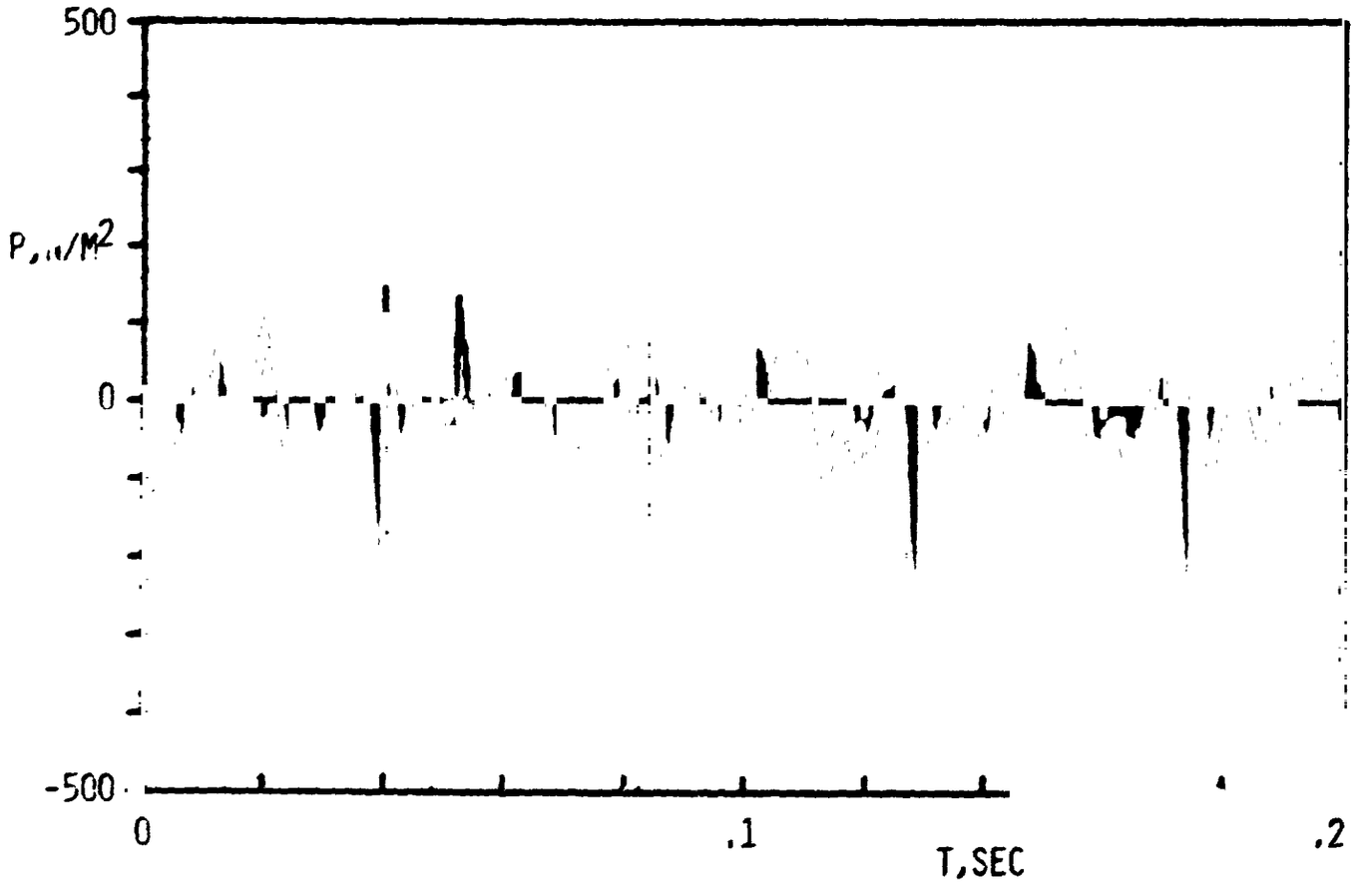

(a) Raw Data

Figure 33 - Acoustical Waveform from trapezoidal Tip Blades, Mic 3, $M_{1,\ 90} = 0.939$

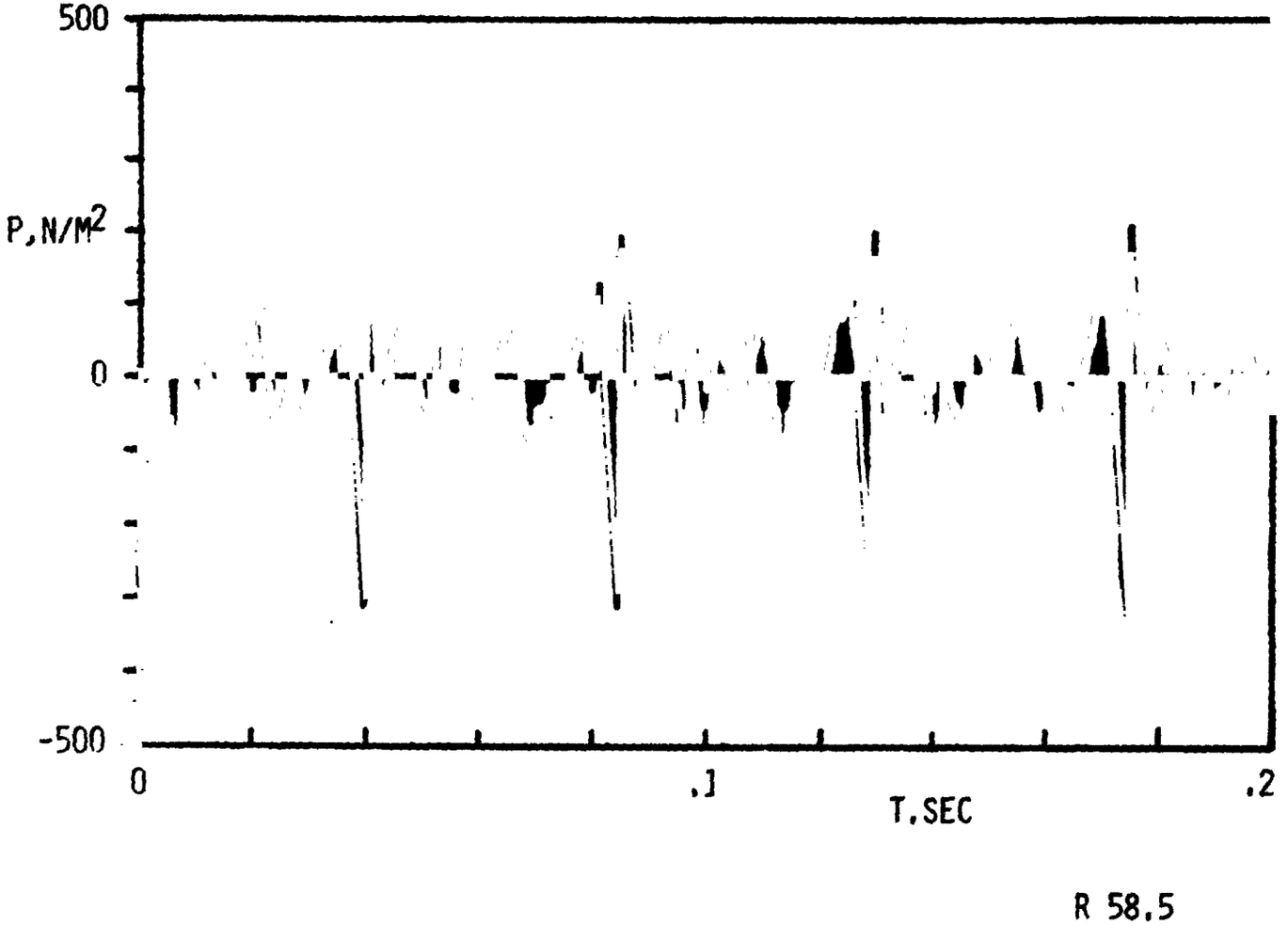

Figure 33 (b) - 25 Hz high pass digitally filtered

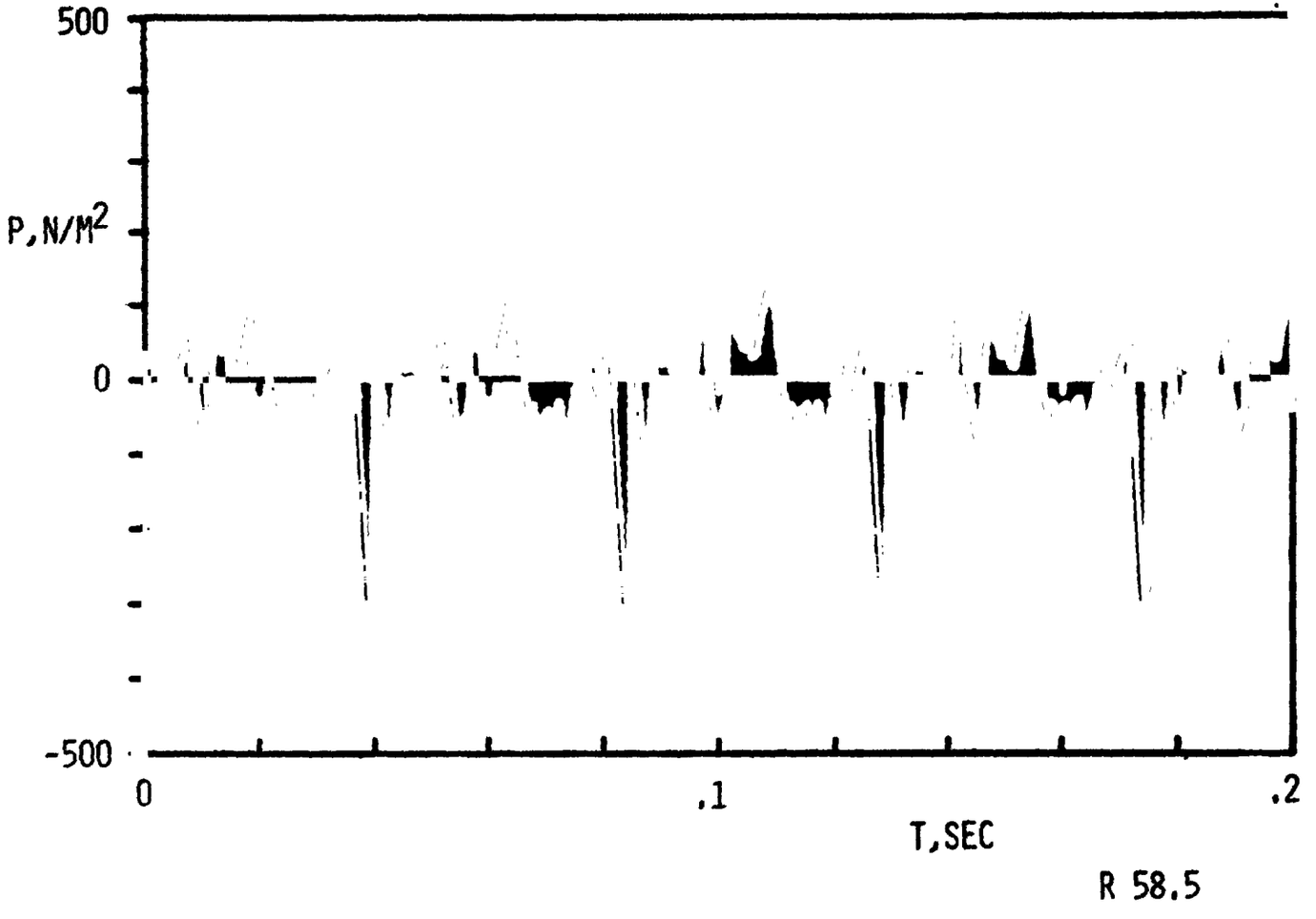

Figure 33 (c) - 50-ensemble averaged, no filtering

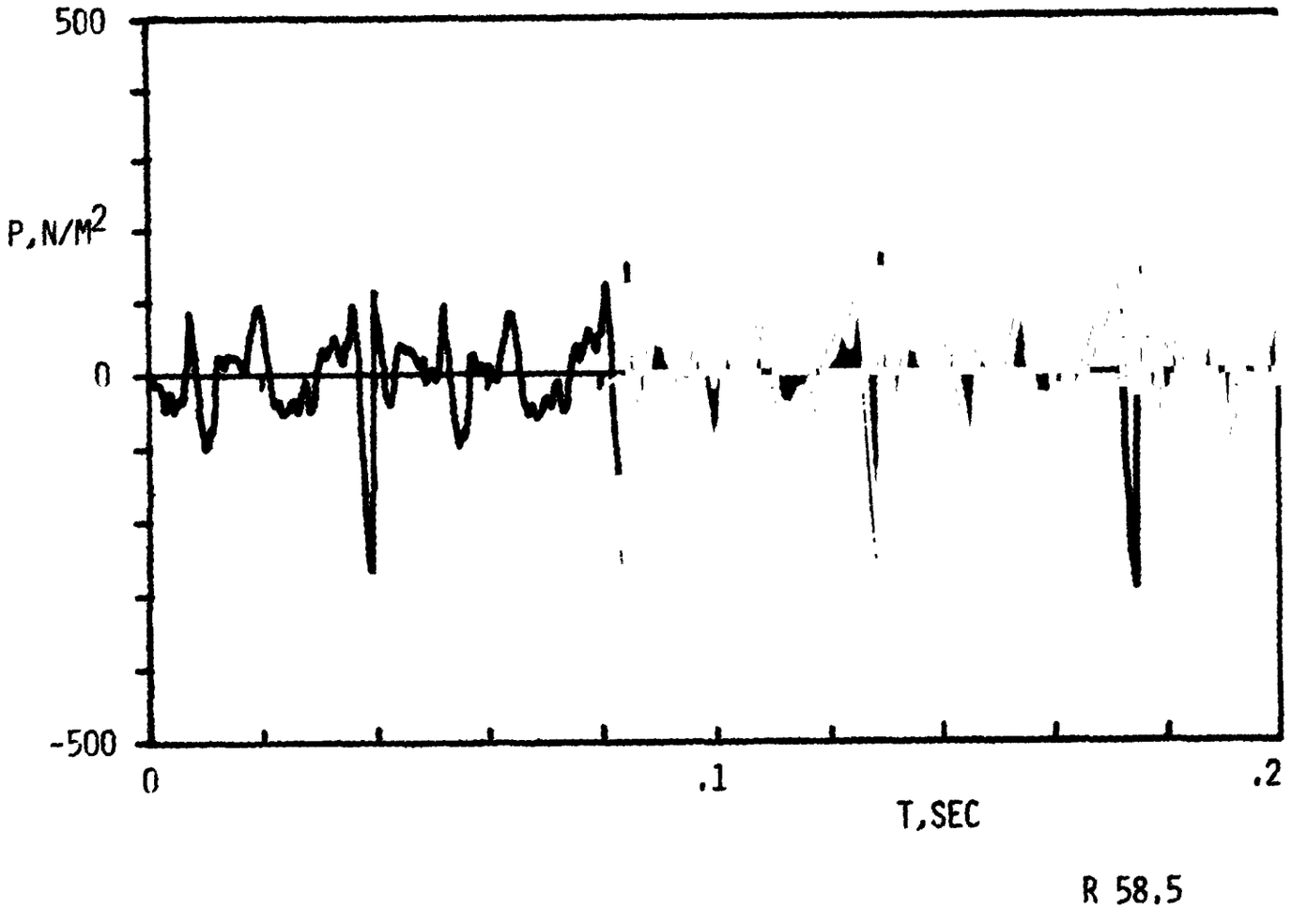

Figure 33 (d) - 50-ensemble averaged, 25 Hz high pass digitally filtered

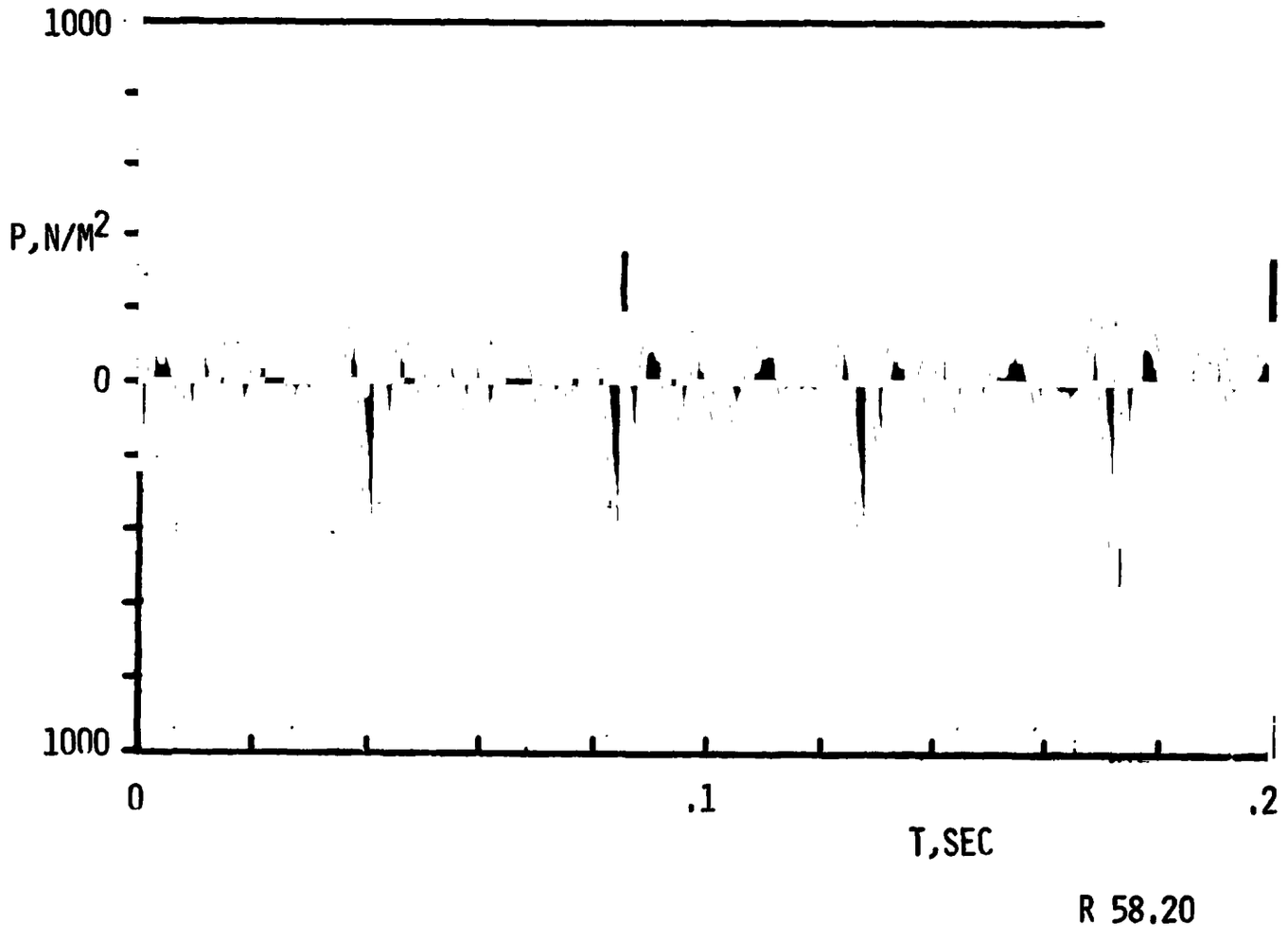

(a) Raw Data

Figure 34 - Acoustical Waveform from trapezoidal Tip Blades, Mic 3, $M_{1,\ 90} = 0.966$

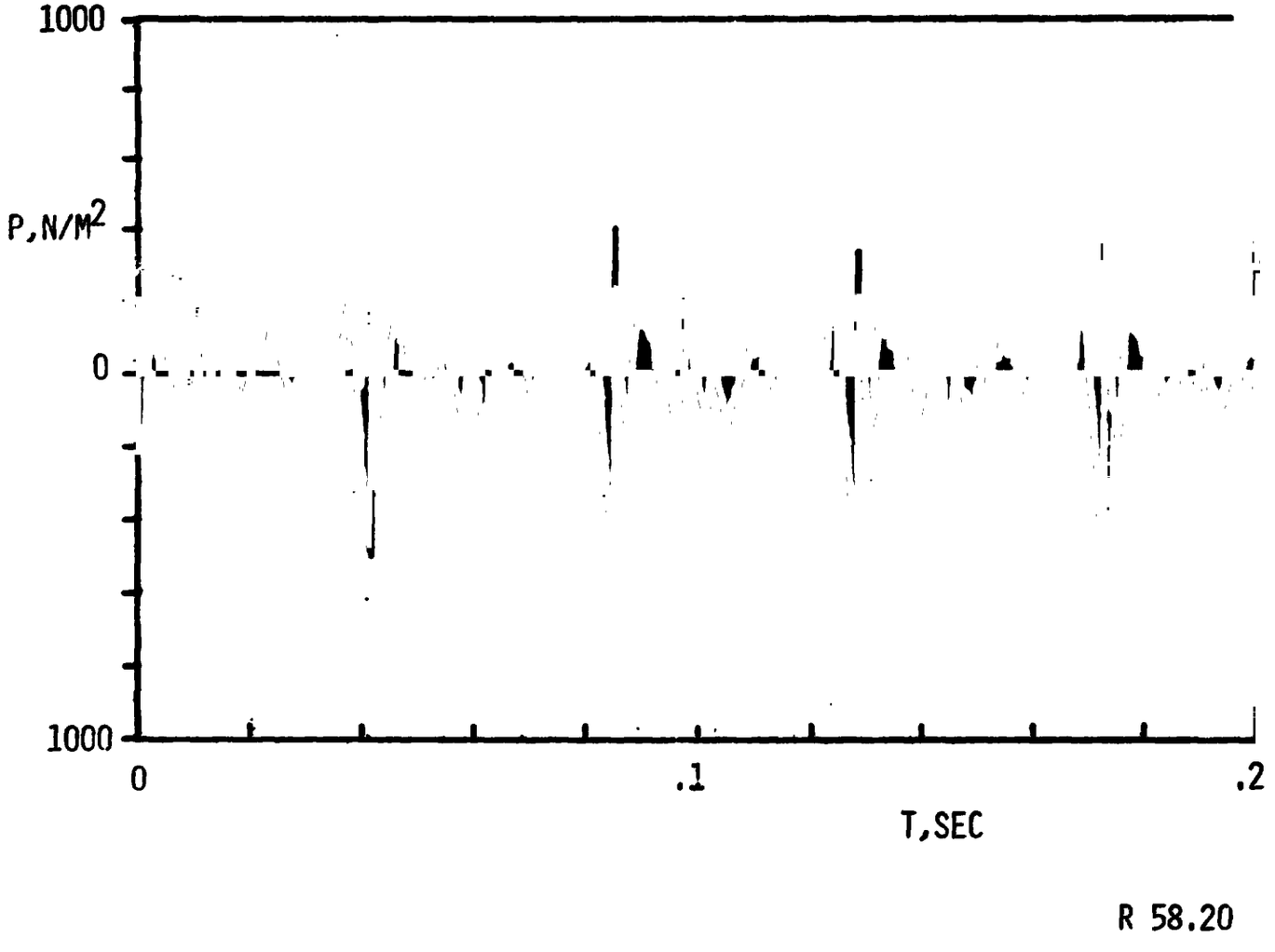

Figure 34 (b) - 25 Hz high pass digitally filtered

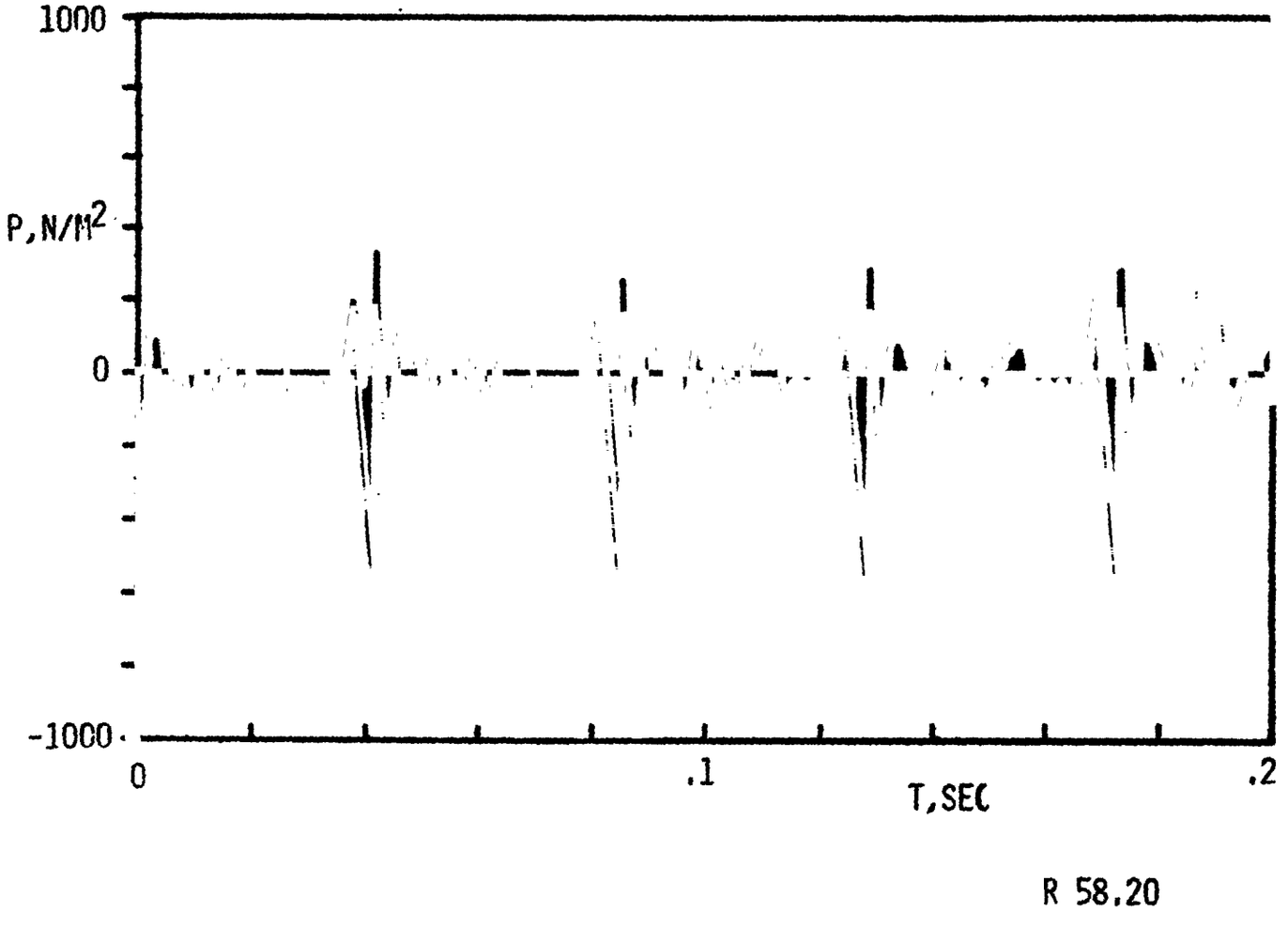

Figure 34 (c) - 50-ensemble averaged, no filtering

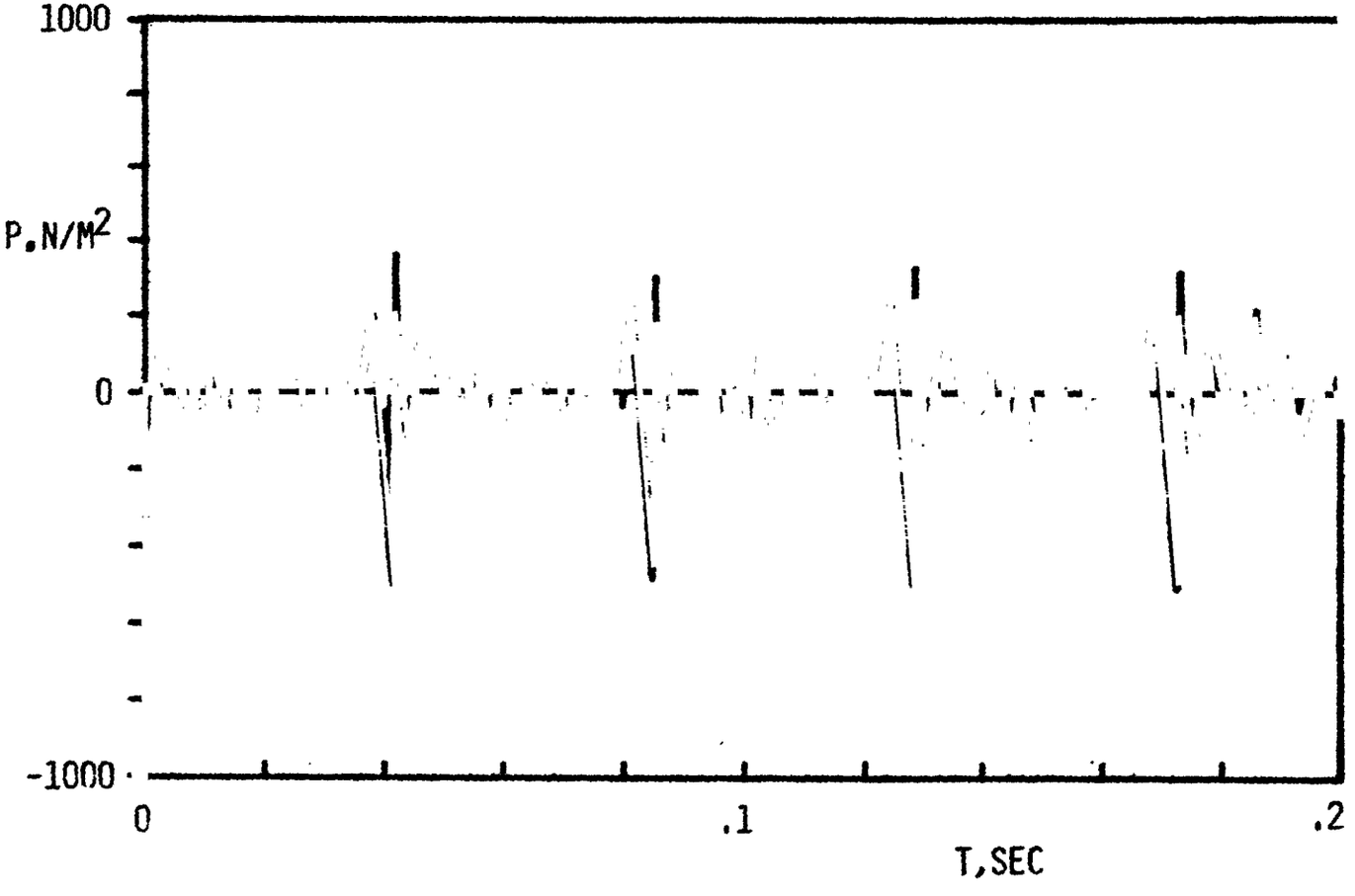

Figure 34 (d) - 50-ensemble averaged, 25 Hz high pass digitally filtered

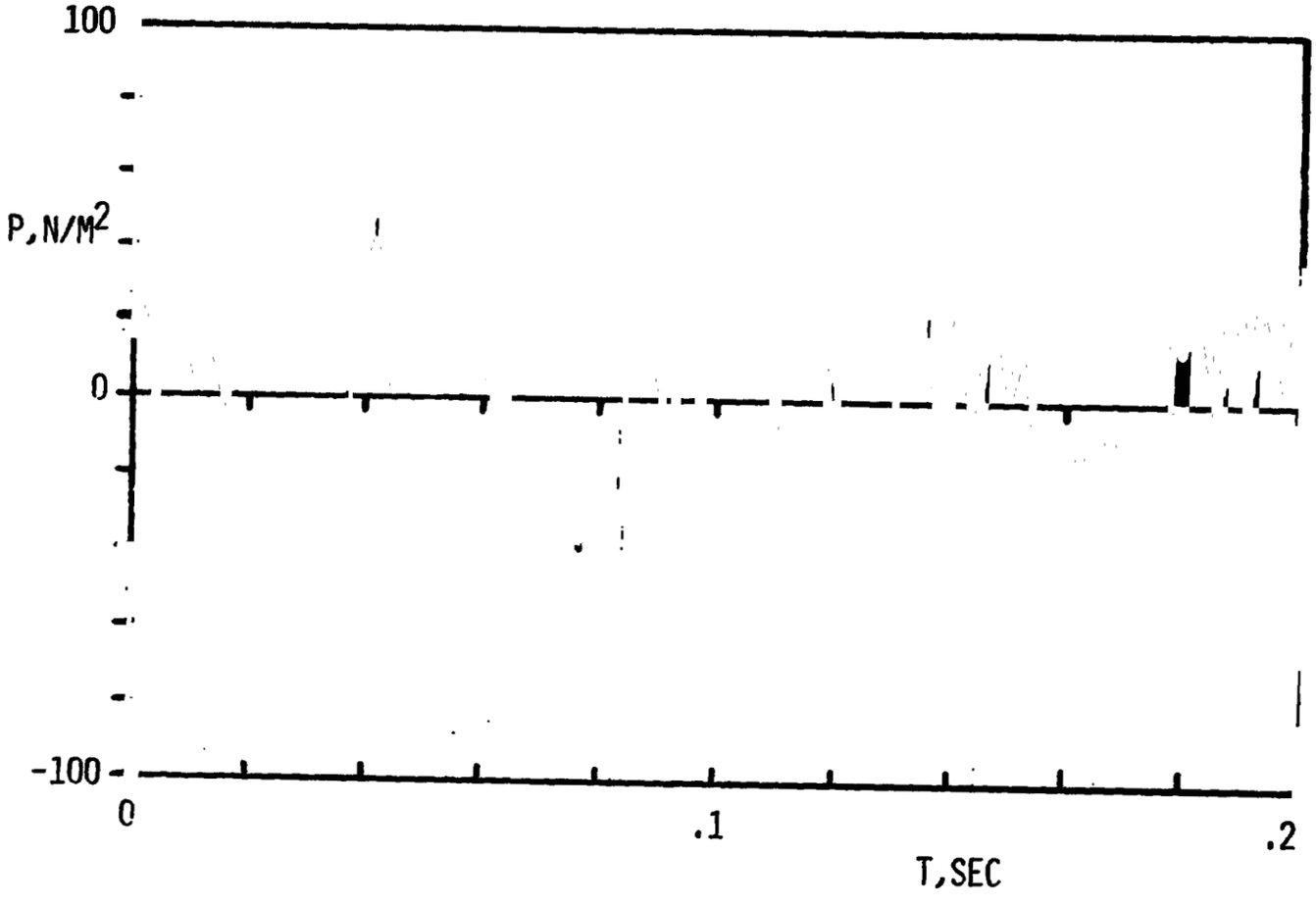

(a) 50- ensemble averaged

Figure 35 - Acoustical Waveform from swept-tapered tip blades, Mic 3, $M_{1,\ 90} = 0.966$

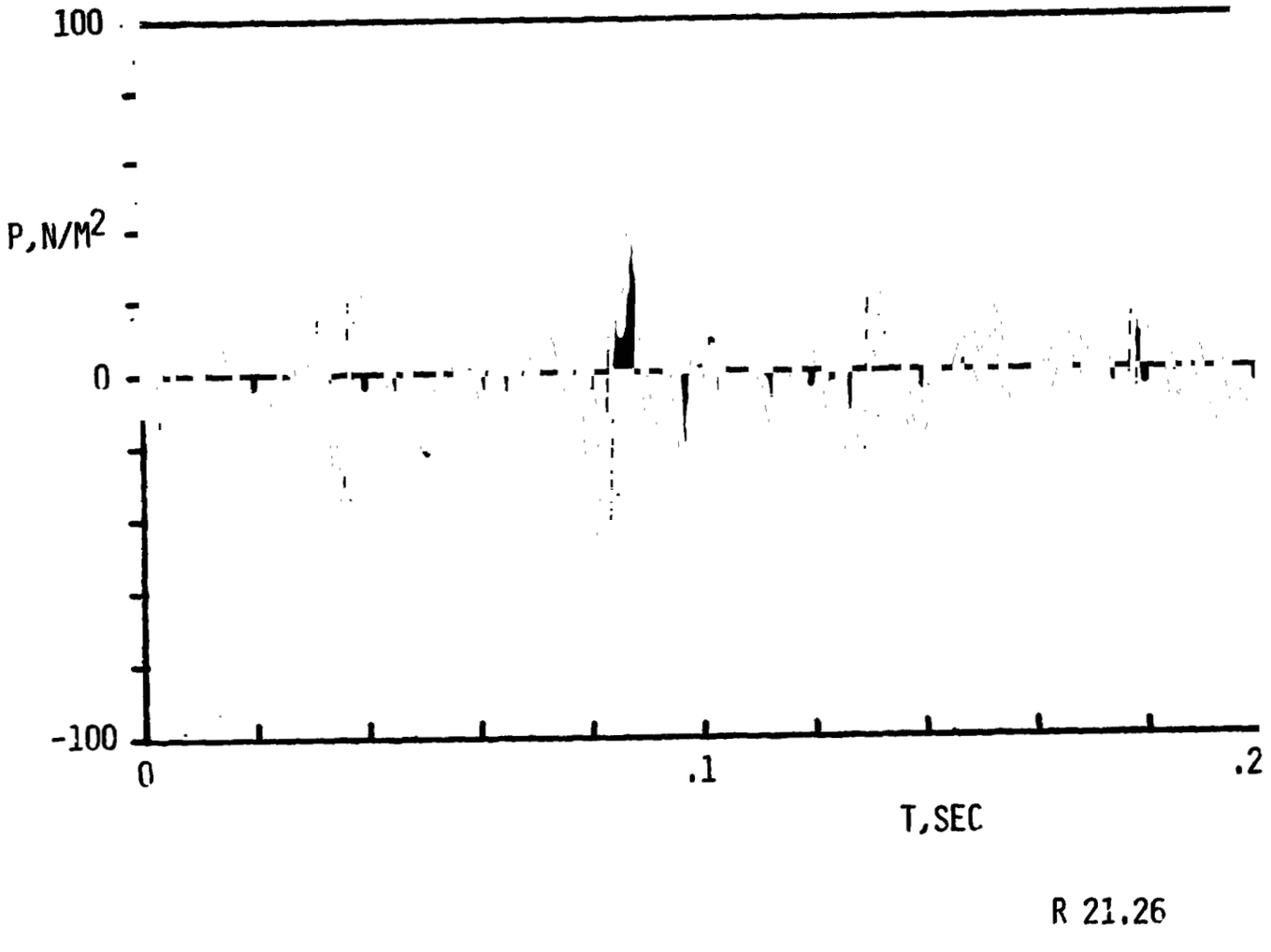

Figure 35 (b) - 50-ensemble averaged, 25 Hz high pass digitally filtered

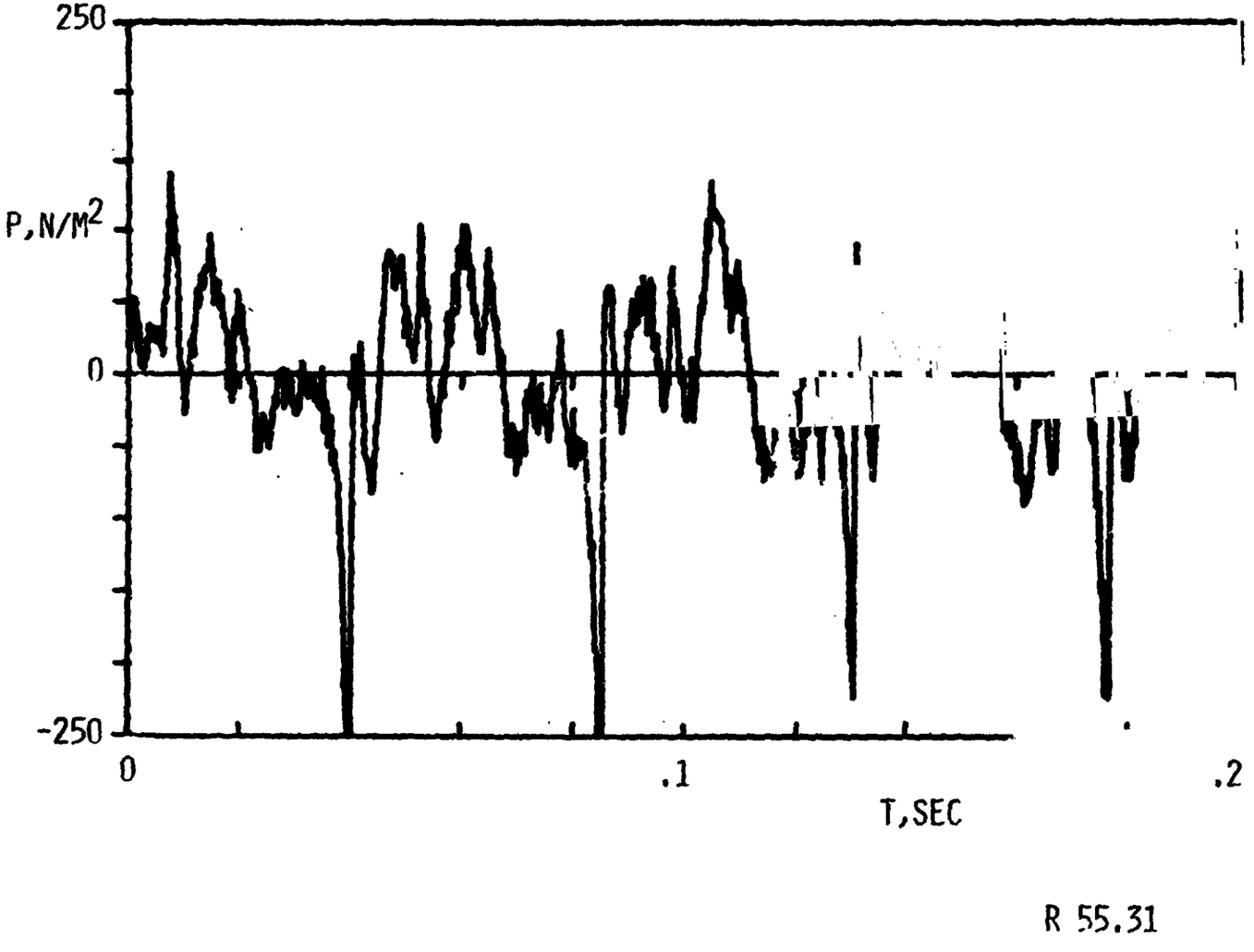

(a) Raw Data

Figure 36 - Acoustical Waveform from swept-tapered tip blades, Mic 3, $M_{t,\ 90} = 0.937$

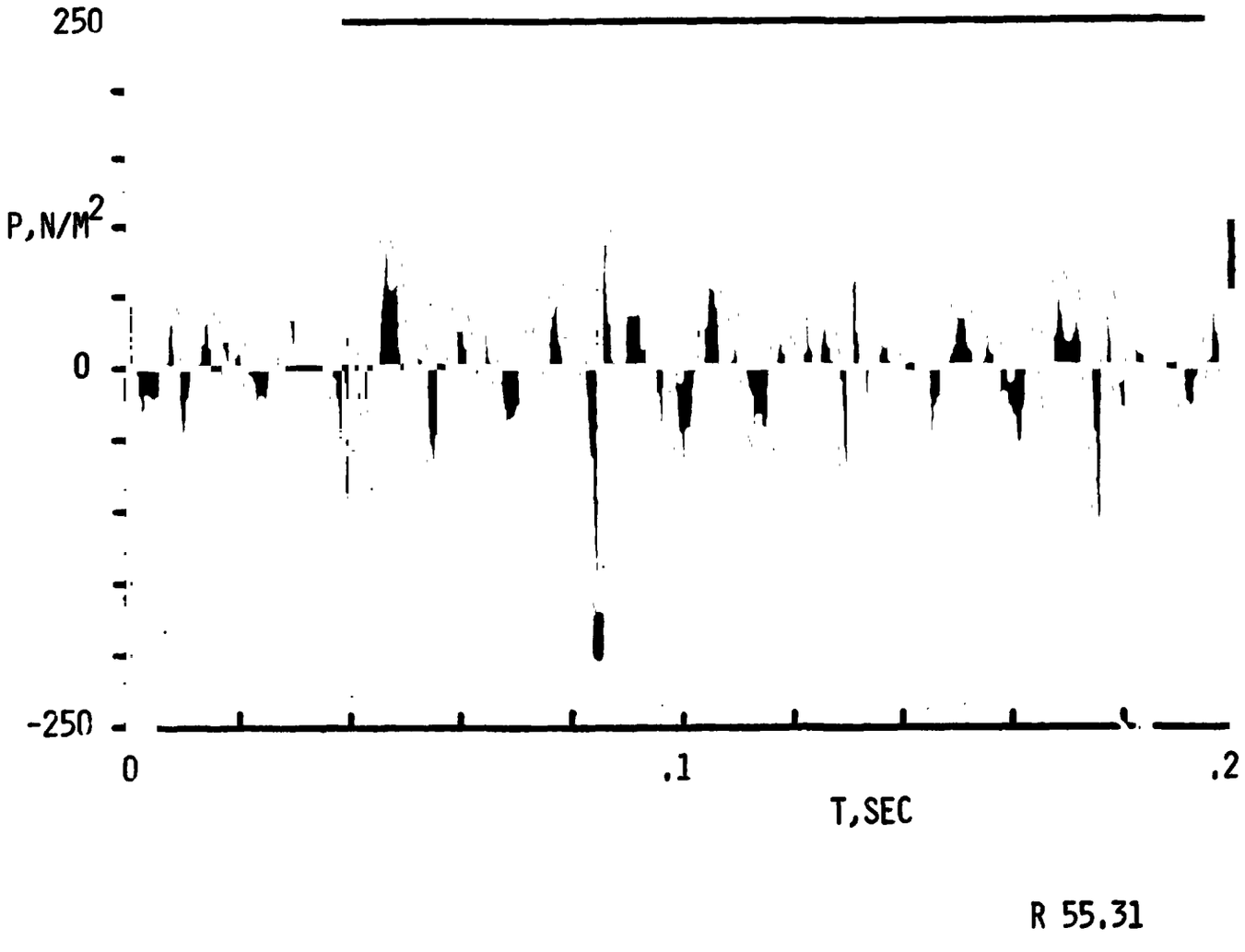

Figure 36 (b) - 25 Hz high pass digitally filtered

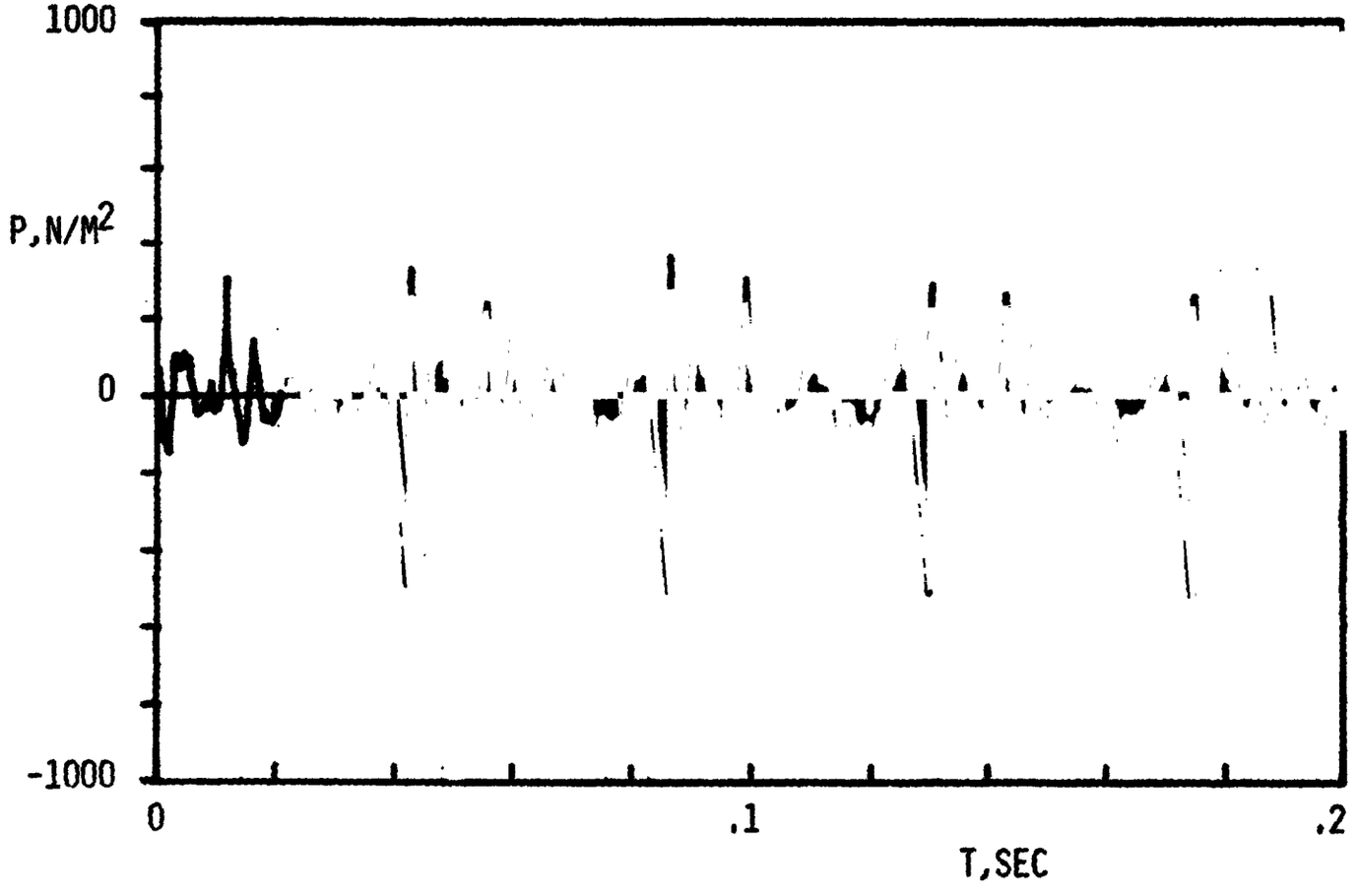

(a) Raw Data

Figure 37 - Acoustical Waveform from swept-tapered tip blades, Mic 3, $M_{1,\ 90} = 0.966$

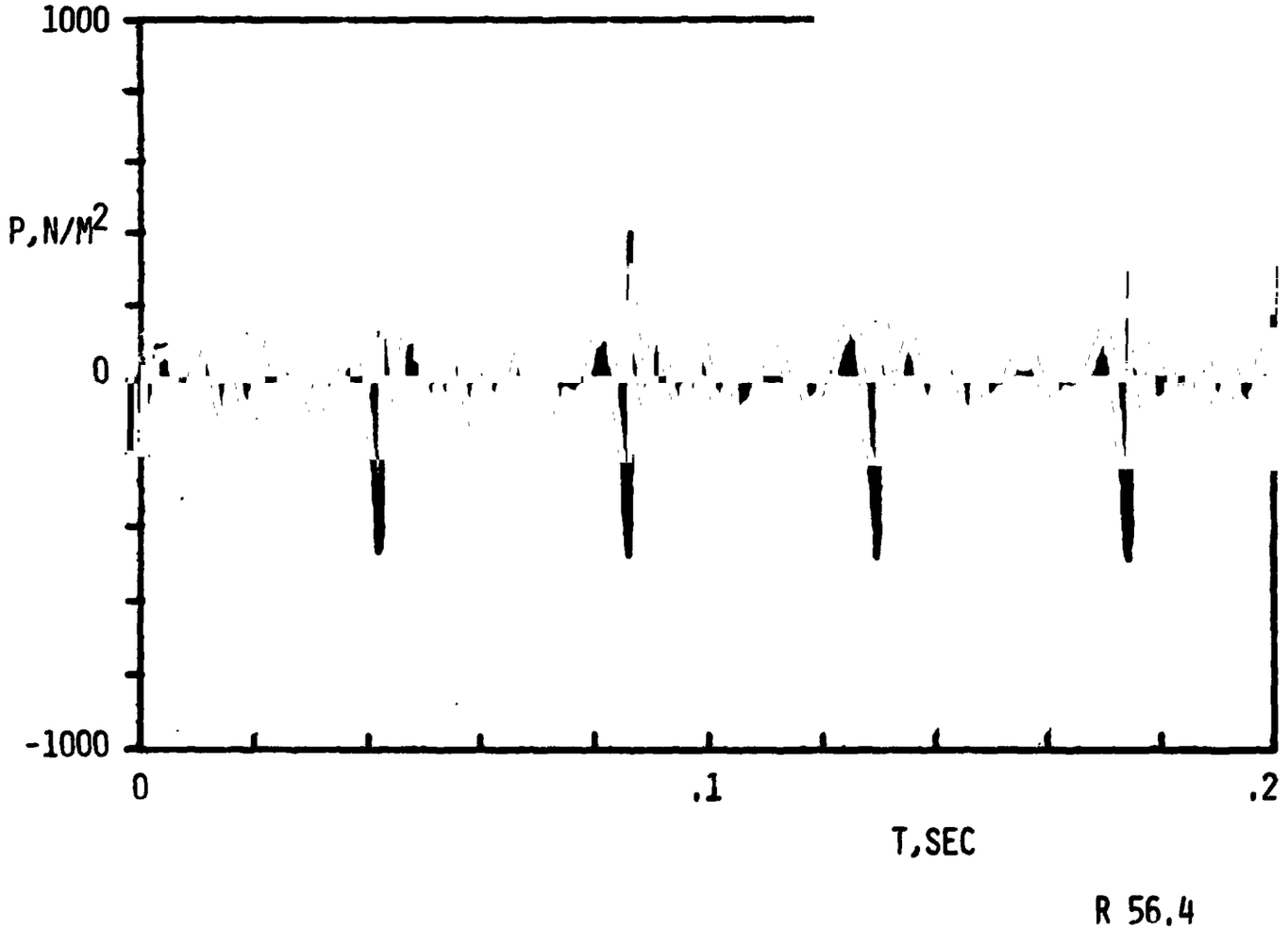

Figure 37 (b) - 25 Hz high pass digitally filtered

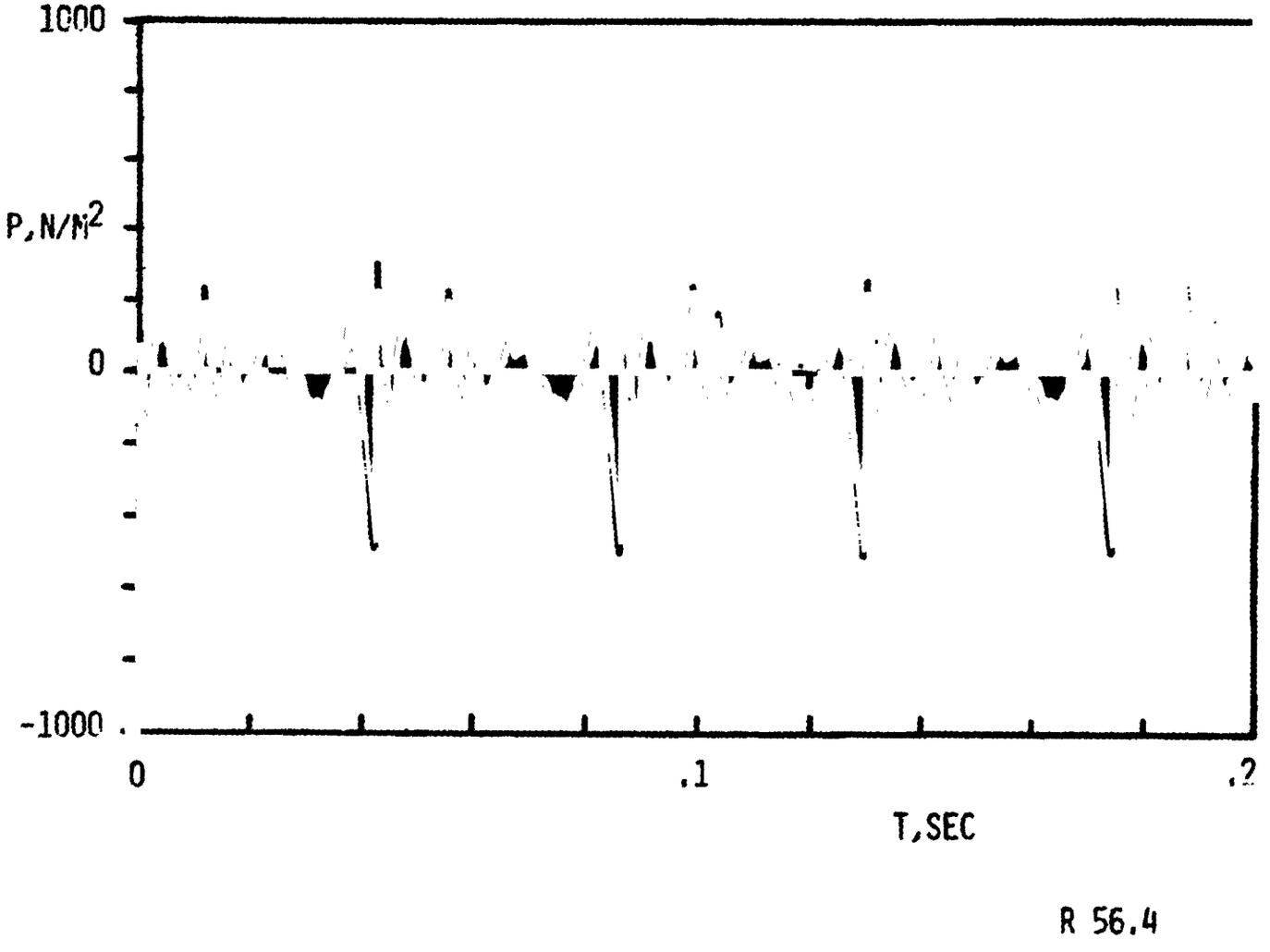

Figure 37 (c) - 50-ensemble averaged, no filtering

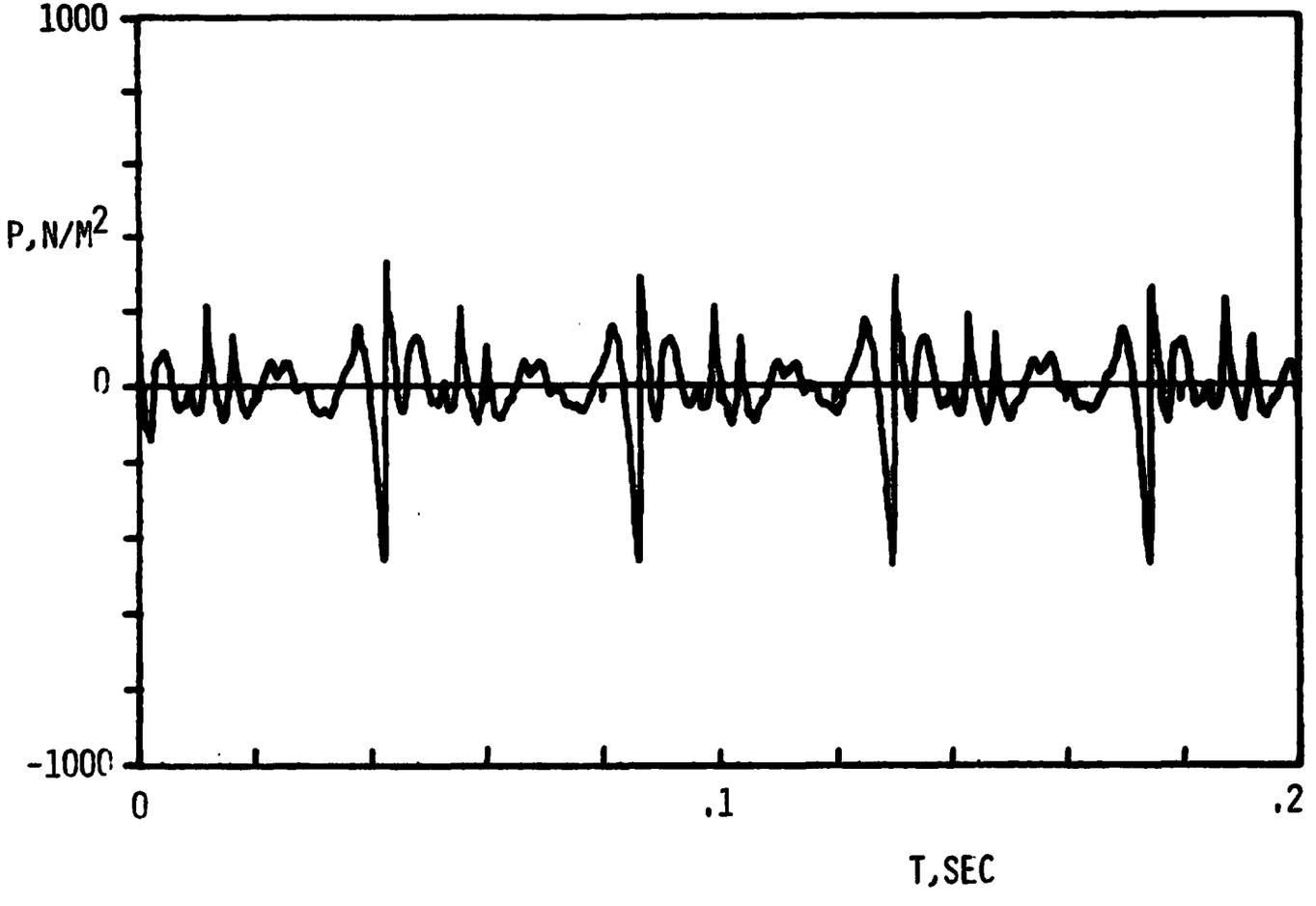

Figure 37 (d) - 50-ensemble averaged, 25 Hz high pass digitally filtered

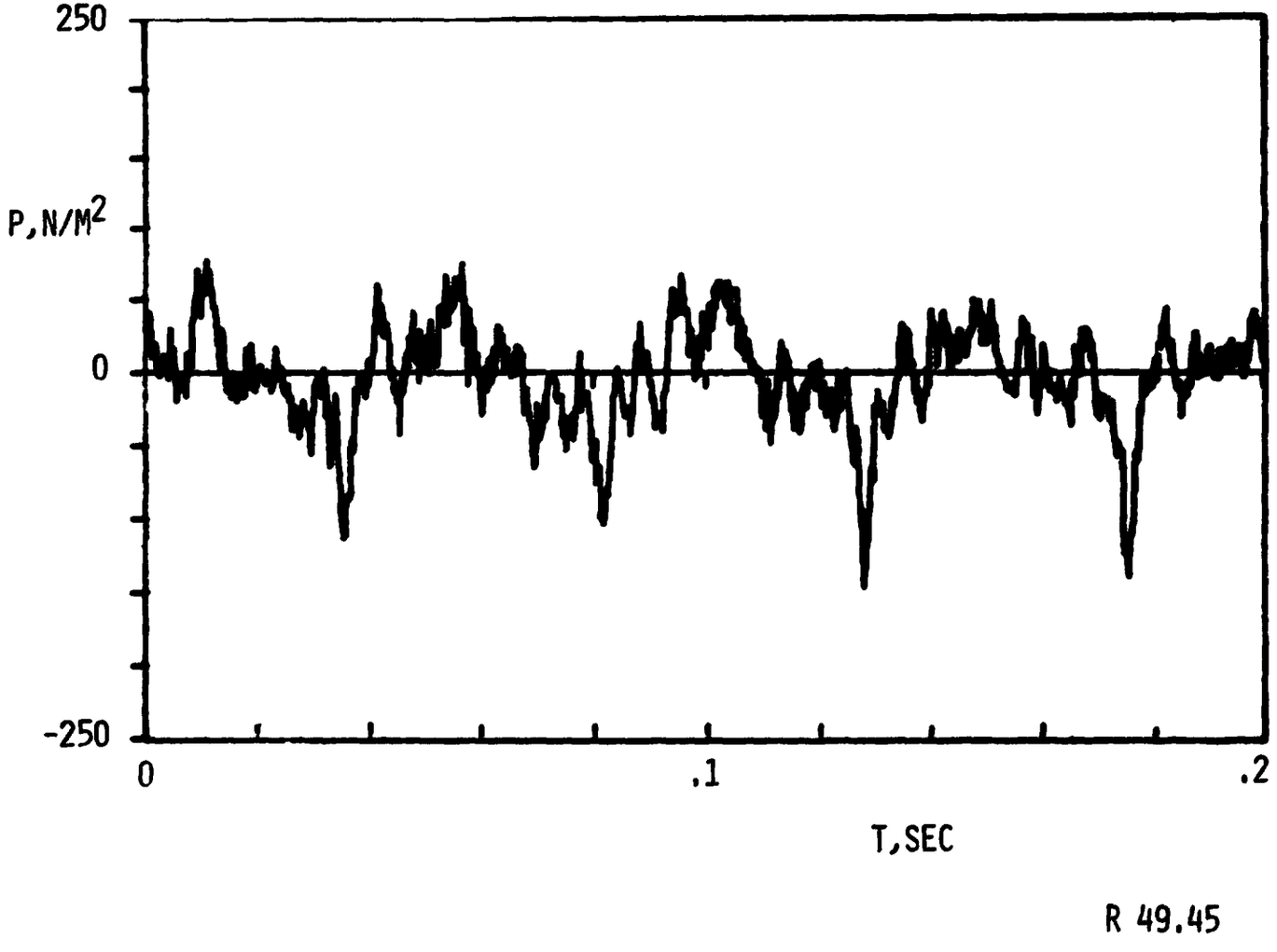

(a) Raw Data

Figure 38 - Acoustical Waveform from swept tip blades, Mic 3, $M_{1,\ 90} = 0.896$

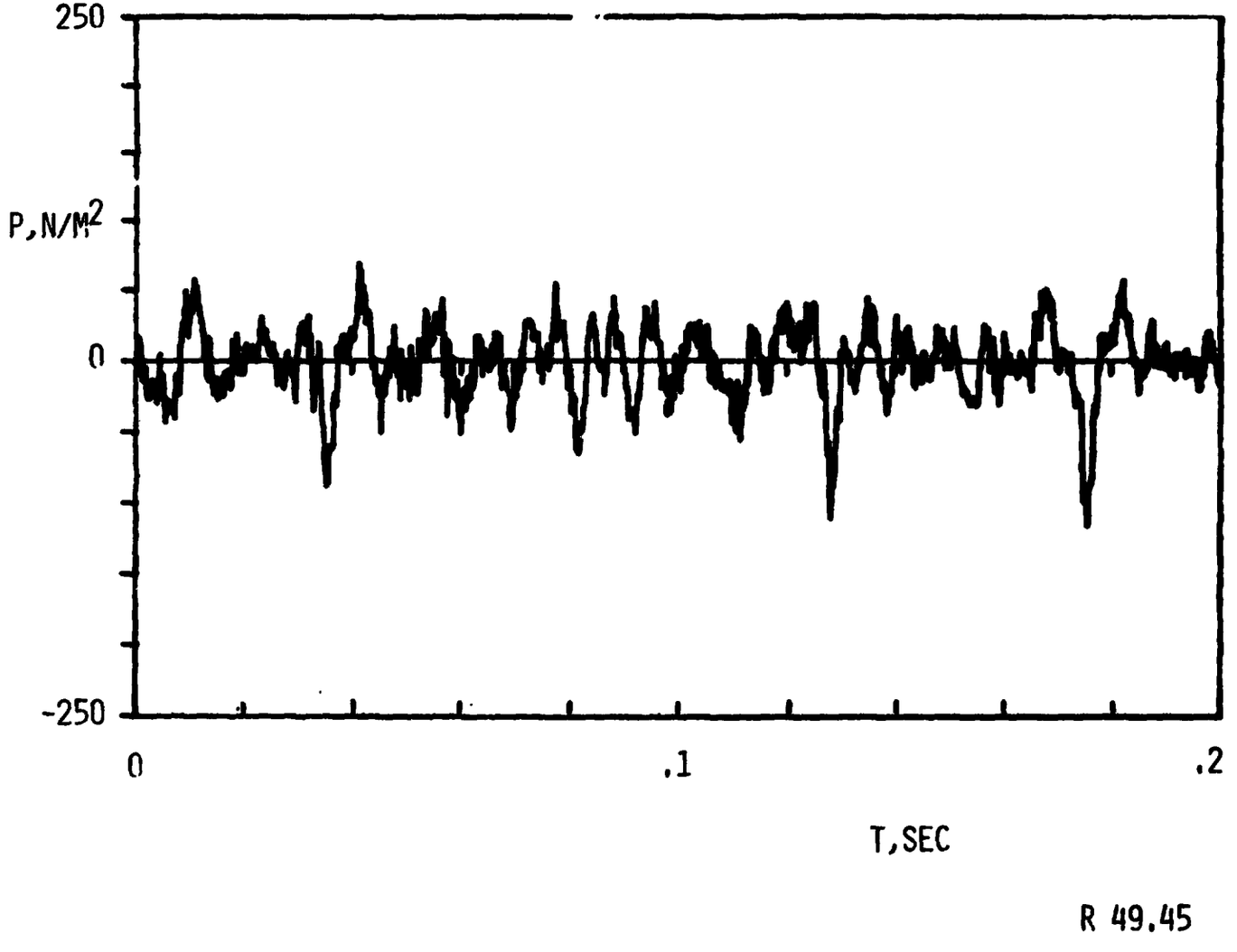

Figure 38 (b) - 25 Hz high pass digitally filtered

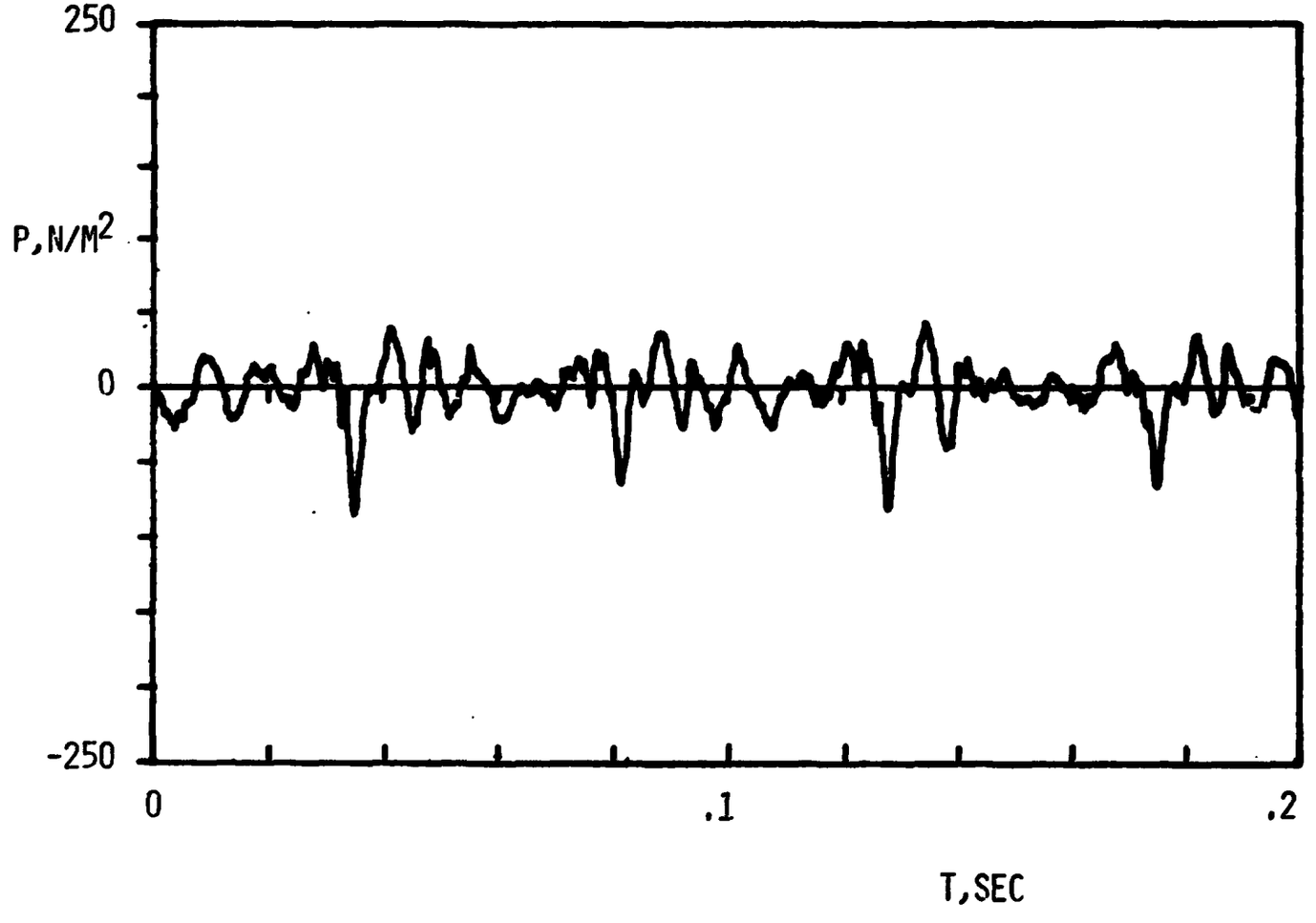

Figure 38 (c) - 50-ensemble averaged, no filtering

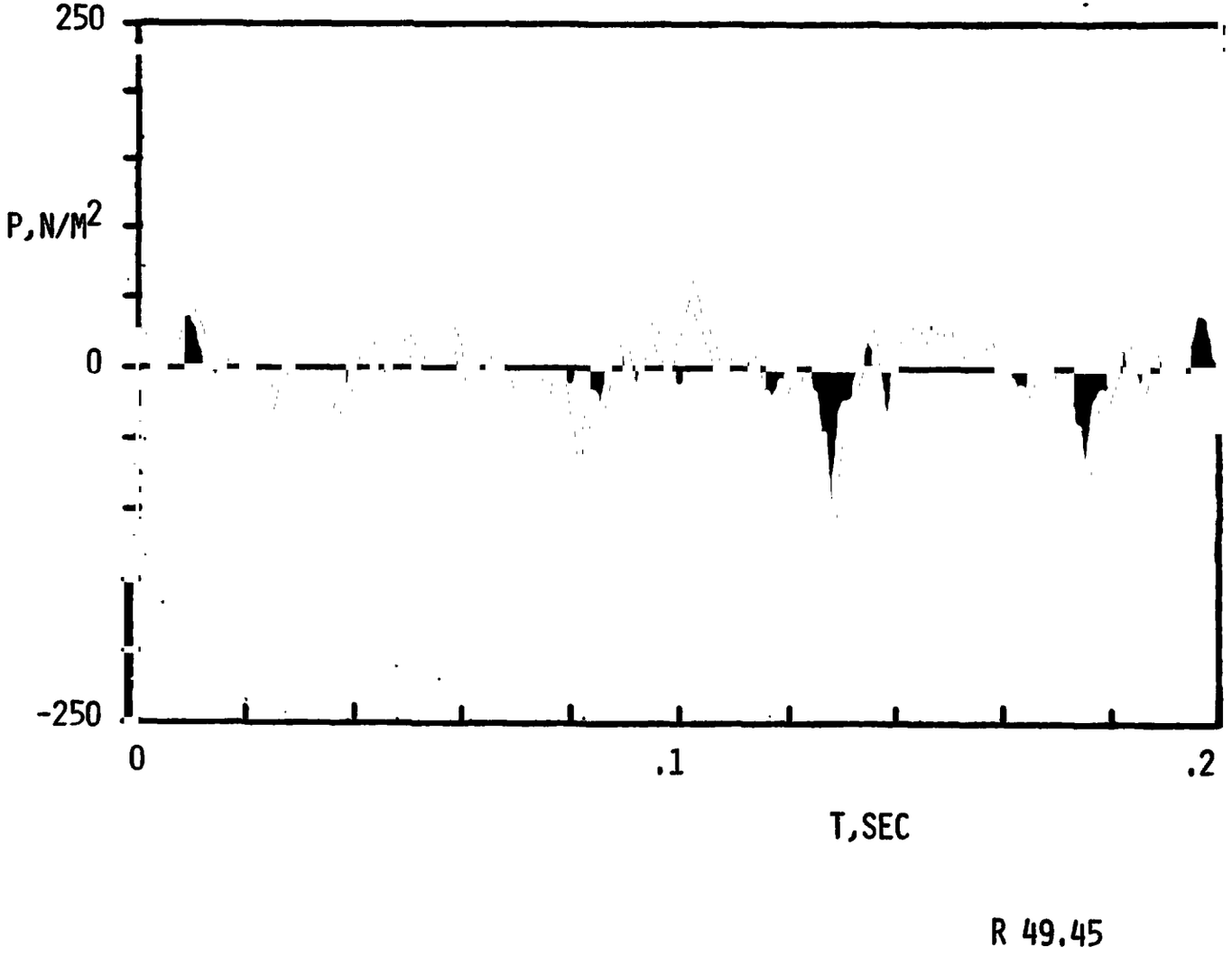

Figure 38 (d) - 50-ensemble averaged, 25 Hz high pass digitally filtered

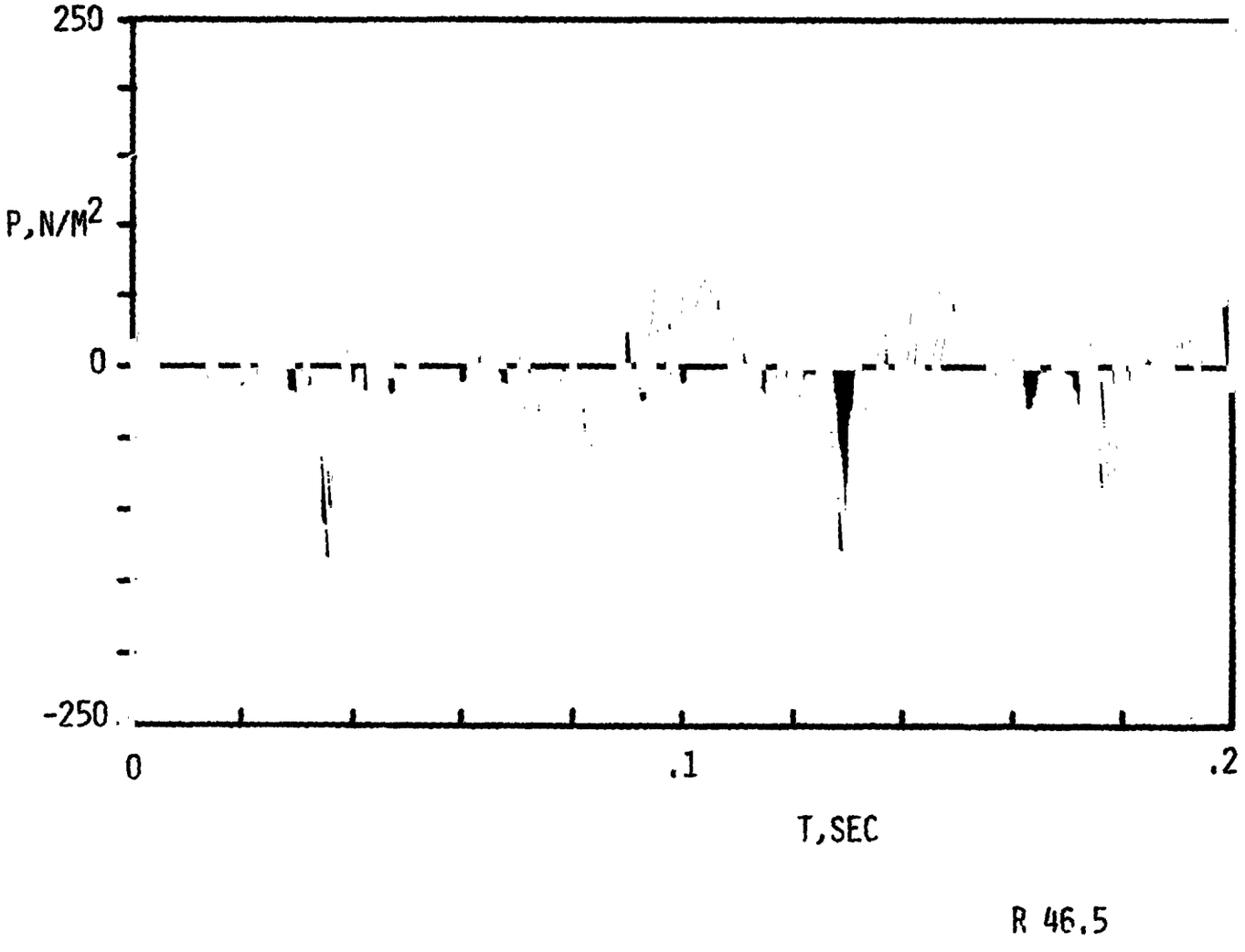

(a) Raw Data

Figure 39 - Acoustical Waveform from rectangular tip blades, Mic 3, $M_{1,\ 90} = 0.898$

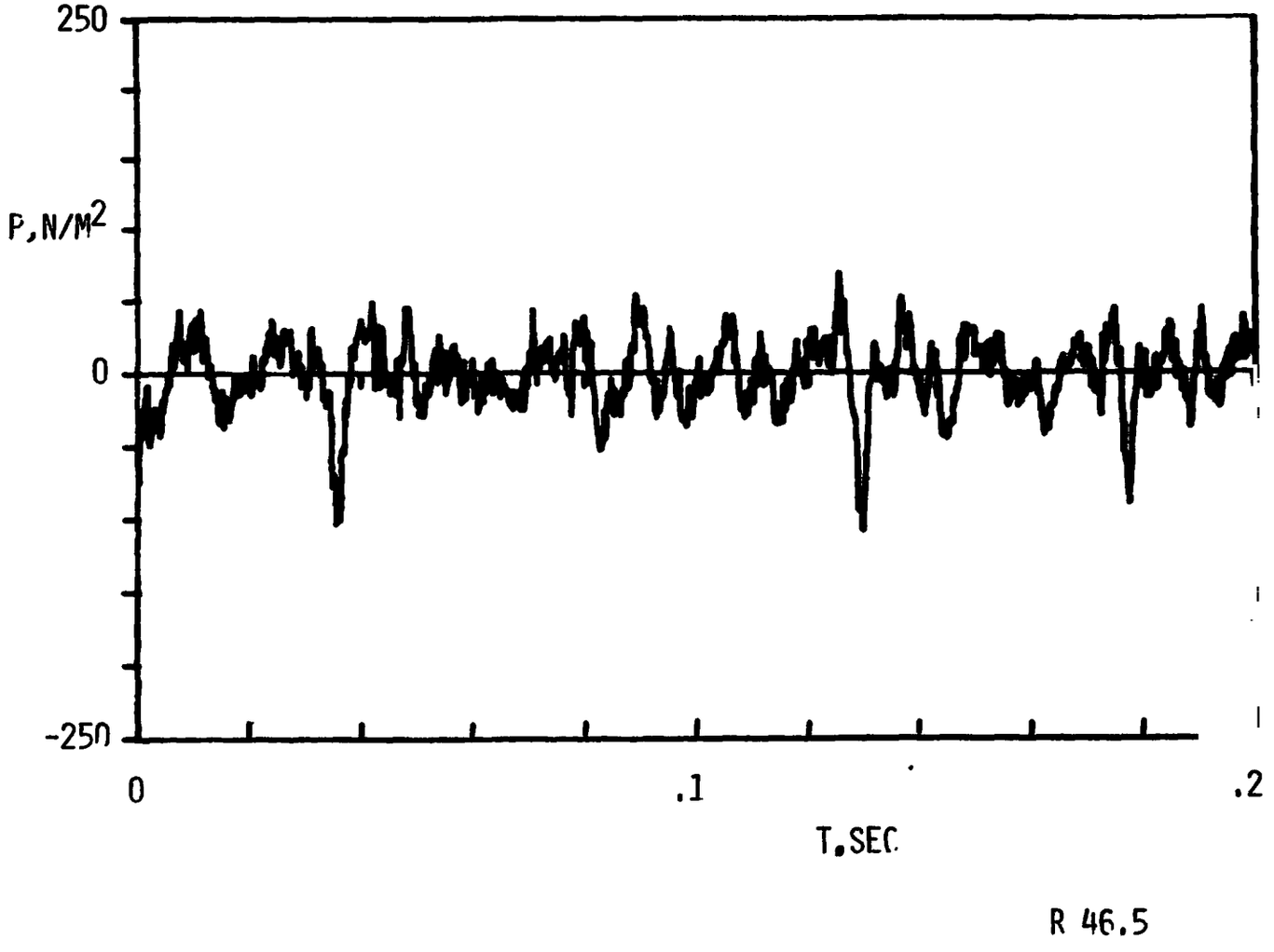

Figure 39 (b) - 25 Hz high pass digitally filtered

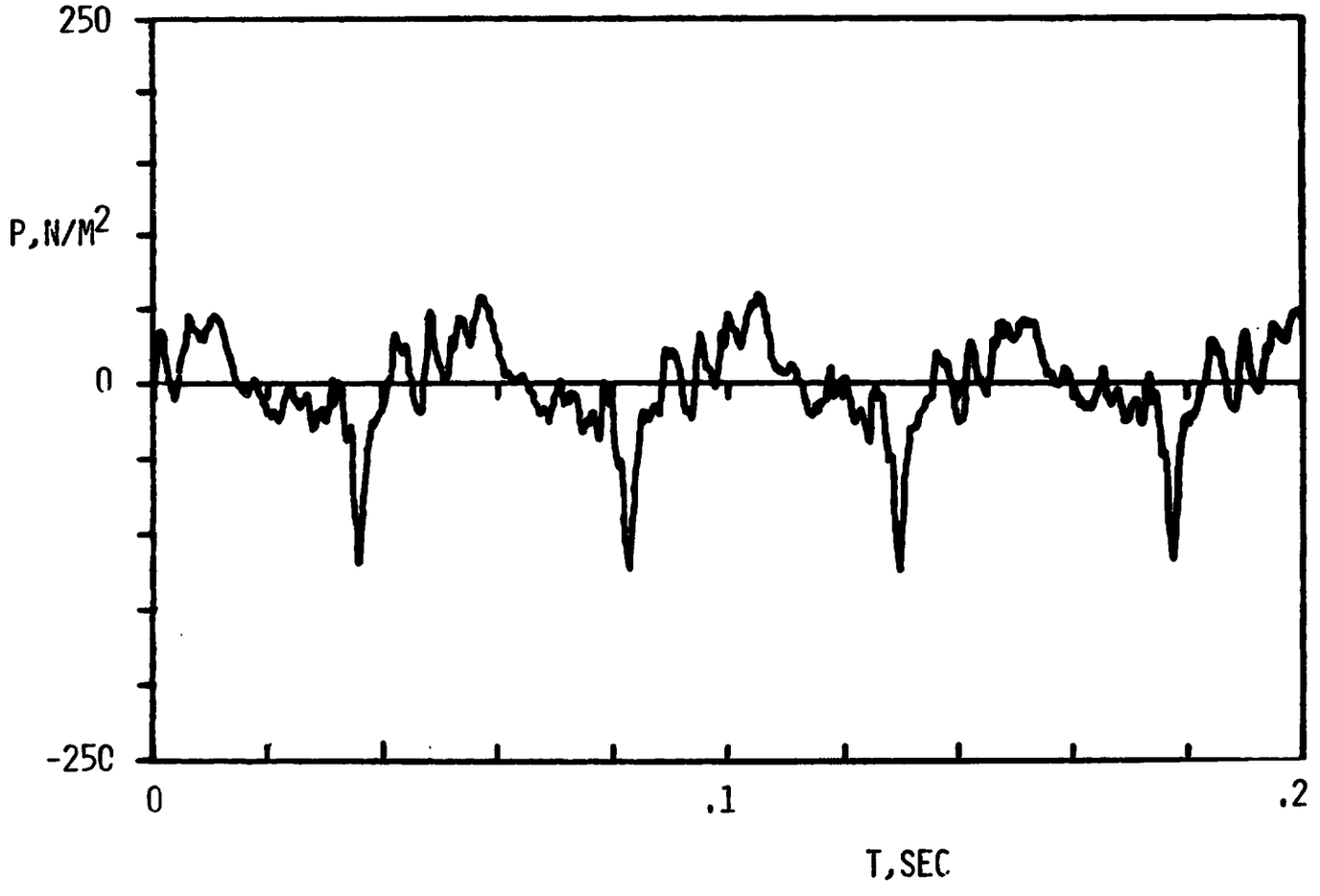

Figure 39 (c) - 50-ensemble averaged, no filtering

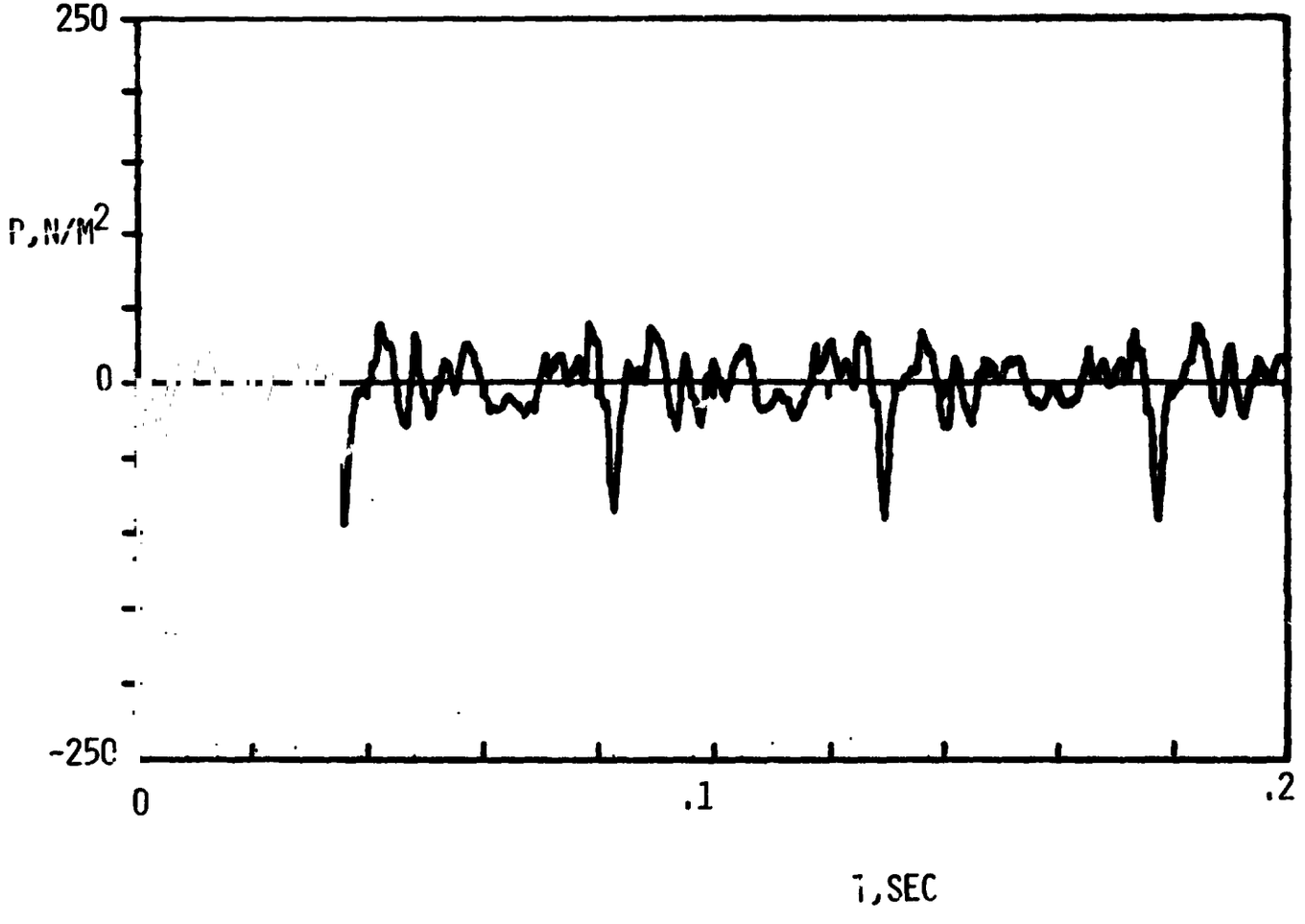

Figure 39 (d) - 50-ensemble averaged, 25 Hz high pass digitally filtered

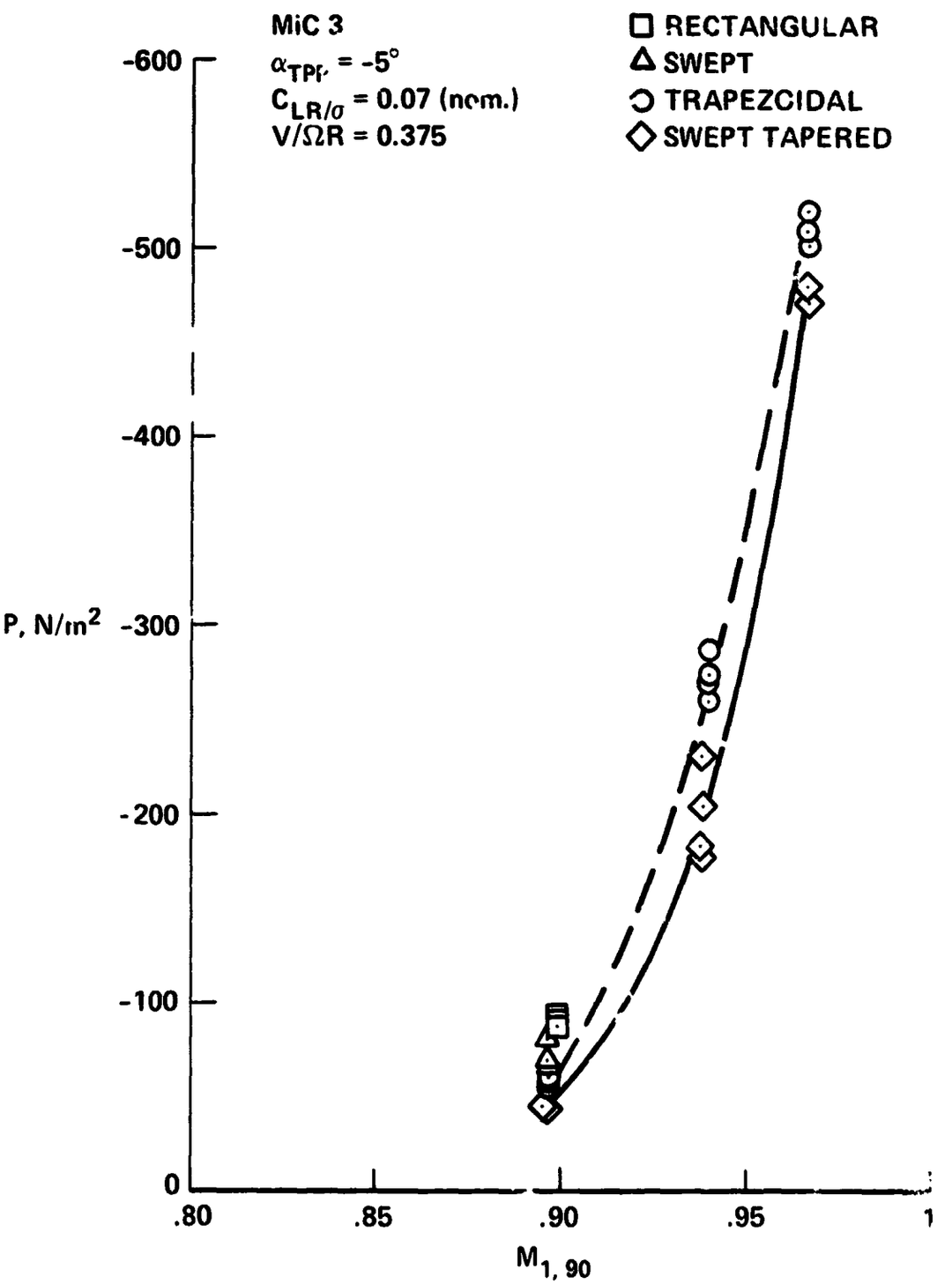

Figure 40 - The amplitude of rotor impulsive noise